Katholieke Universiteit Leuven
Group Biomedical Sciences
Faculty of Medicine
Department of Radiology

Minimal invasive imaging of the tumoral micro-environment in squamous cell carcinoma of the head and neck: value of diffusion-weighted and dynamic contrast-enhanced magnetic resonance imaging for tumour detection, regional staging and treatment follow-up

Vincent Vandecaveye

Katholieke Universiteit Leuven
Group Biomedical Sciences
Faculty of Medicine
Department of Radiology

Minimal invasive imaging of the tumoral micro-environment in squamous cell carcinoma of the head and neck: value of diffusion-weighted and dynamic contrast-enhanced magnetic resonance imaging for tumour detection, regional staging and treatment follow-up

Vincent Vandecaveye

Promotor: Prof. Dr. R. Hermans ((K.U.Leuven, Leuven, Belgium)
Co-promotor: Prof. Dr. S. Nuyts (K.U.Leuven, Leuven, Belgium)
Chair: Prof. Dr. P. Demaerel (K.U.Leuven, Leuven, Belgium)
Secretary: Prof. Dr. R. Sciot (K.U.Leuven, Leuven, Belgium)
Jury members:
Prof. Dr. R. Sciot (K.U.Leuven, Leuven, Belgium)
Prof. Dr. P. Schöffski (K.U.Leuven, Leuven, Belgium)
Prof. Dr. A. King (The Chinese University of Hong Kong, Hong Kong Special Administrative Region, China)
Prof. Dr. W. De Neve (UGent, Ghent, Belgium)

TO MY BELOVED MINA

EEN WOORD VAN DANK

Vooreerst dank ik Prof. Dr. Mark Waer, rector van deze universiteit, en zijn voorganger Prof. Dr. Marc Vervenne voor de kansen die ze bieden om wetenschappelijk onderzoek te doen aan deze instelling. In het bijzonder zou ik mijn diensthoofd, Prof. Dr. Guy Marchal, willen danken voor de mogelijkheid om dit doctoraatsproject te combineren met mijn opleiding. Ook gaat mijn dank uit naar de begeleider van de doctoraatscommissie, Prof. Dr. Raymond Oyen, en naar de leden van de jury, Prof. Dr. Patrick Schöffski, Prof. Dr. Wilfried De Neve, Prof. Dr. Ann King en Prof. Dr. Raf Sciot, voor de geïnvesteerde tijd en inspanningen die de jurering met zich meebrengt.

Mijn meest oprechte dank gaat uit naar mijn promotor, Prof. Dr. Hermans. Bob, bedankt voor het vertrouwen en de steun die je me van meet af aan hebt gegeven en ook voor het bijbrengen van rust en geduld. Het voelde enorm geruststellend aan om te kunnen werken in een omgeving waarin ik rustig kon groeien en waarin een snel resultaat of haastige publicatie ondergeschikt waren aan het opbouwen van een gedegen project dat nu stilaan zijn weg in de kliniek aan het vinden is. Bedankt om mee te mogen delen in je ervaring en expertise, maar vooral bedankt voor het blijvend vertrouwen dat je in me stelt, in de huidige en toekomstige samenwerking.

Ook mijn co-promotor, Prof. Dr. Sandra Nuyts, wil ik heel graag bedanken voor de prachtige samenwerking, de opbouwende discussies, de bemoedigende woorden en de ondersteuning van dit project. Deze samenwerking tussen radiologie en radiotherapie toont nogmaals aan dat twee sterker staan dan één.

Een bijzondere dankjewel gaat uit naar de ‘partners in crime’ Frederik De Keyzer, Piet Dirix en Maarten Lambrecht. Uit onze samenwerking is een hechte vriendschappelijke band gegroeid. Frederik, jouw inbreng als ingenieur is zonder enige twijfel van enorm belang geweest in dit project, en ik hoop dat we nog lang kunnen samenwerken in een zeer vriendschappelijk sfeer. Piet, benevens je vriendschap en werklust was het je karakter en – positief bedoeld - verbetenheid die ons op volle snelheid vooruit brachten. Ik mag hopen dat onze wetenschappelijke paden elkaar weer zullen kruisen na het beëindigen van je klinische opleiding. Maarten, we zullen er een ‘goeie lap’ op geven de komende 4 jaar en hard verder werken aan de basis die reeds gelegd is.

Graag zou ik ook de collega’s van de dienst radiologie willen bedanken voor mijn opleiding en de dagelijkse samenwerking, in het bijzonder Prof. Dr. Steven Dymarkowski, Prof. Dr. Stefan Sunaert, Prof. Dr. Didier Bielen, Prof. Dr. Filip Claus, Dr. Dirk Vanbeckevoort, Dr. Steven Pans, Dr. Marleen Thijs, Dr. Ragna Vanslembrouck en Dr. Katya Op de beeck.

Een warm woord van dank gaat uit naar Ilse Roebben die zorgt voor alle afspraken en praktische beslommeringen, en ook naar de studieverpleegkundigen Stefan Ghysels, Guido Putzeys en Kris Byloos. Ook een heel dikke dankjewel voor Linda Meersman voor de finale editing van de tekst.
Eveneens wens ik Prof. Dr. Vincent Vander Poorten en Prof. Dr. Pierre Delaere, de (toenmalige) co-assistenten en assistenten van neus-keel-oorziekten en het verplegend personeel van E450 te bedanken voor de (vaak enthousiaste) hulp en begeleiding van de studiepatiënten. Ook Prof. Dr. Erik Verbeken en de laborantes van pathologische ontleedkunde in het vriescoupelokaal wens ik te bedanken voor de geboden ondersteuning en hulp in de correlatieve studies.
Uiteraard zou deze thesis nooit tot een goed einde zijn gebracht zonder het duwtje in de rug, de sympathie, bijstand en vooral veel geduld van mijn familie, vrienden en Mina. Mina, it is so joyful to come home and see the sweet and loving smile on your face, and to know what a wonderful life we have together. Thank you for all the support and patience on my way to the finishing line of this thesis.
Mama en papa, dankjewel voor het heerlijke leven dat ik van jullie heb gekregen en voor de kansen om dit project te volbrengen. Wie had dit gedacht toen ik voor mijn volledige tweede zit stond in eerste kan? Sonja en Christophe, merci voor de vriendschap, de steun en gewoon om (schoon)familie te zijn. Broer, 't waren plezante studentenuitjes tot in de vroege uren in Leuven en soms misschien wel iets te dicht bij de examens, maar soit, om in de geest van deze thesis te blijven: dat heeft het uiteindelijke resultaat niet significant beïnvloed. MERCI!
Ook wil ik Dr. Marc Bruneel en Willy Landuyt bedanken. Jullie hebben mij, zij het op verschillende gelegenheden, een klein duwtje in de juiste richting van mijn carrière gegeven. In die zin zal ik jullie altijd een beetje als mijn mentor blijven beschouwen.
Ook wil ik graag al mijn vrienden bedanken voor de steun (en ontspanningsmomenten) door de jaren heen en dan in het bijzonder Evelyne, Pieter, Leentje, James, Eva, Kristof, Els, Marc, Isabel, Griet, Heleen, Dieter, Corine, Steven en Mehrnaz, en Stijn en Polien.
Een laatste woord van dank gaat uit naar de vrienden en collega's-dansers van 'DSC Dance Connection' voor de vele mooie dansjaren. Ook een welgemeende dankjewel voor de radiologen en verpleging van de dienst radiologie van het ZOL in Genk. Uiteindelijk heb ik bij jullie twee prachtige opleidingsjaren kunnen meemaken die ik nooit zal vergeten.
Mijn grote dank gaat tenslotte uit naar alle patiënten die belangeloos aan de studies in dit boek hebben meegewerkt.

Vincent Vandecaveye
7 mei 2010

TABLE OF CONTENTS

List of abbreviations

(18)F-MISO	(18)F-fluoromisonidazole
ΔADC	change of apparent diffusion coefficient
ΔPERF	change of perfusion parameter
ΔV	change of volume
AAO-HNS	American Academy of Otolaryngology Head and Neck Surgery classification
ADC	apparent diffusion coefficient
AIF	arterial input function
AS	arterial slope
AUC	area under the curve
$_B$	baseline time point of imaging prior to treatment
cm^2	square centimetre
c-peak	contrast-peak
CR	complete remission
CRT	chemoradiotherapy
CT	computed tomography
CT_{3m}	computed tomography 3 months after end of chemoradiation
DCE-MRI	dynamic contrast-enhanced magnetic resonance imaging
DWI	diffusion weighted imaging
EES	extravascular extracellular space
EPI	echo planar imaging
FDG-PET	Fluoro-deoxy-glucose positron emission tomography
FLT	fluorothymidine
FN	false negative
FoV	field of view
FP	false positive
Gd-BOPTA	Gadolinium-benzyloxypropionictetra-acetate
Gy	Gray
HE	haematoxylin and eosin
HNSCC	head and neck squamous cell carcinoma
Hz	Hertz
IAUC	initial area under the signal intensity curve
IMRT	intensity modulated radiotherapy
IQR	interquartile range
IS	interstitial space
IVS	intravascular space
k_{ep}	rate constant (extracellular extravascular space to blood plasma)
KI-67	antigen identified by monoclonal antibody Ki-67
K^{trans}	volume transfer constant (blood plasma to extracellular extravascular space)
kV	tube voltage

LRC	locoregional control
mAS	tube current time product
mBq	millibecquerel
mg	milligram
ml	millilitre
mm	millimetre
mm^2/s	square millimetre per second
mm^3	cubic millimetre
MRI	magnetic resonance imaging
MRI_{3w}	magnetic resonance imaging 3 weeks after end of chemoradiation
ms	milliseconds
M-stage	extent of distant metastases
MVD	microvessel density
µm	micrometre
N	given time point of imaging during or after treatment
NPV	negative predictive value
N-stage	regional nodal metastatic extent
PACS	picture archiving and communication system
PPV	positive predictive value
ROC	receiver-operator-characteristics
ROI	region of interest
RT	radiotherapy
s/mm^2	seconds per square millimetre
SCC	squamous cell carcinoma
SD	standard deviation
SE	spin-echo
SI	signal intensity
SNR	signal to noise ratio
STIR	short tau inversion recovery
SUV	standard value uptake
TE	echo time
TN	Ttrue negative
TNM	tumour-nodes-metastases classification
TP	true positive
TR	repetition time
TSE	turbo spin-echo
T-stage	primary tumour extent
TTP	time to peak
US	ultrasound
US-FNAB	ultrasound guided fine needle aspiration biopsy
USPIO	ultrasmall superparamagnetic iron oxide
V_e	leakage space
VEGF	vascular endothelial growth factor

Research team and co-operators

Vincent Vandecaveye, MD, Department of Radiology: study design, patient recruiting and selection, scanning of patients, functional image analysis, historadiological correlation, data analysis and interpretation, statistical analysis, literature research, manuscript drafting and revision

Frederik De Keyzer, MSc, Department of Radiology: study design, sequence optimization, phantom scanning, data analysis, statistical analysis, data interpretation, manuscript revision

Ilse Roebben, MSc, Department of Radiology: patient appointments, patient communication, contact person with clinical services, data analysis

Katya Op de beeck, MD, Department of Radiology: conventional imaging analysis

Robert Hermans, MD, PhD, department of radiology: study design, image analysis, data analysis and interpretation, manuscript revision, Phd promotor

Pascal Hamaeckers (2004-2006), Stefan Ghysels, Kris Byloos, Guido Putzeys, research technologists at the Department of Radiology: patient scanning

Piet Dirix, MD, Department of Radiation Oncology: study design, patient recruiting and selection, volumetric imaging assessment, historadiological correlation, data analysis and interpretation, manuscript revision

Sandra Nuyts, MD, PhD, Department of Radiation Oncology: study design, patient recruiting and selection, data analysis and interpretation, manuscript revision, Phd co-promotor

Vincent Vander Poorten, MD, PhD, Department of Otolaryngology and Head and Neck Surgery:

preparation of surgical specimens for histopathological analysis, statistical analysis, manuscript revision

Pierre Delaere, MD, PhD, Department of Otolaryngology and Head and Neck Surgery: preparation of surgical specimens for histopathological analysis

Erik Verbeken, MD, PhD, Department of Pathology: histopathological analysis, immuno-histochemistry

Chapter 1:
General introduction

1.1. Definition and epidemiology of head and neck cancer

Head and neck cancer is an anatomically based term defined to describe malignant tumours that originate from the upper aerodigestive tract and are located between the thoracic outlet and the skull base. These regions include the sinonasal region, oral cavity, the naso-, oro-, and hypopharynx and larynx. The majority of head and neck tumours consist of squamous cell carcinomas (SCC) which usually occur in the oral cavity, the pharynx, the larynx and sinonasal cavity. Other, but less frequent, types of malignant tumours are adenocarcinomas originating from the sinonasal cavities, nasopharyngeal carcinoma, salivary gland carcinoma, several subtypes of thyroid carcinoma and skin tumours. Finally, other malignant tumours that can occur in this region include sarcomas and lymphomas.

Although relatively uncommon, the incidence of head and neck SCC (HNSCC) is increasing. In 2002, HNSCC was, according to the World Cancer Report of 2002, the 8th most common cancer worldwide accounting for 390000 cases annually (1). In a recent report by Jemal et al, this number has increased to 500000 (2).

In Belgium, HNSCC took the 4th place in 2005 of most frequent tumours in men with 6% or 1806 cases. In women, the incidence HNSCC was roughly 3 times lower than in men with 2% or 553 cases. In men, HNSCC is the fifth most frequent cause of cancer related death. Notably, the incidence of HNSCC in Belgium is amongst the highest in Europe and for women the incidence is even the highest among selected European data (3). The tumours start to occur at the age of 35-40 years with a peak incidence at the age of 55-60 years. The anatomical subsite most frequently involved in head and neck cancer may vary per country, region and sex and relate in part to the underlying carcinogenic factors. For instance, oral cancer is most frequent in India, while nasopharyngeal carcinoma most frequently occurs along the south-eastern coast of China. In our country, men mostly suffer from laryngeal cancer while in women, the majority of tumours occur in the oral cavity. Overall, the most frequently affected subsites are oral cavity cancer (30%), pharyngeal cancer (29%) and laryngeal cancer (27%) (3).

Alcohol and tobacco are the most important risk factors for HNSCC and act synergistic in their carcinogenic effect. Other, be it less frequent, etiological factors include dietary imbalances and micronutrient deficiencies, occupational exposure to wood dust, nickel and asbestos for which the correlation with sinonasal cancer is well known. Wood dust and asbestos exposure also increase the risk for developing laryngeal cancer (4). Additionally, an association has been found between viral infections and the occurrence of head and neck cancer. Epstein-Barr virus has been associated with nasopharyngeal cancer while human papillomavirus has been associated with oral cavity and oropharyngeal cancer. However, the exact causal contribution of viral infections remain to be determined (5).

As smoking and alcohol abuse irritate the mucosa of the entire respiratory system and the upper digestive system, there is risk for the induction of a metachronous second primary tumour at the time of diagnosis of a primary head and neck cancer or in the post-treatment phase (6). Second primary tumours may impact patient prognosis more significantly than the primary head and neck cancer. A recent study showed that patients with a lung cancer as a second primary, had very poor chances for 5-years survival, while a second primary tumour in the head and neck offered better prognosis (7). The difference in prognosis is probably related to the better treatment options for obtaining local control and the lower propensity for developing distant metastases.

1.2 Histopathology of head and neck squamous cell carcinoma

1.2.1. Primary tumour

The normal mucosa of the upper aerodigestive tract consists of a thick stratified squamous epithelium with the lamina propria extending deep into the epithelium by numerous papillae. Next to striated fibres, the submucosal lamina propria contains blood and lymph vessels. Primary HNSCC usually arises from the superficial mucosal lining and its development can coincide with molecular alterations in tumour suppressor genes in the squamous epithelium (8). The development from hyperplasia over mild, moderate and severe dysplasia to carcinoma in situ is characterized by progressive microstructural alterations, compared to the normal epithelium. These microstructural changes include - like for many malignant tumours - an increase of cellular volume and cell density, cellular and nuclear polymorphism and a

chaotic instead of organized stratified microstructure. Further tumoral progression results in invasive carcinoma when the basal membrane of the epithelium is disrupted (Figure 1) .

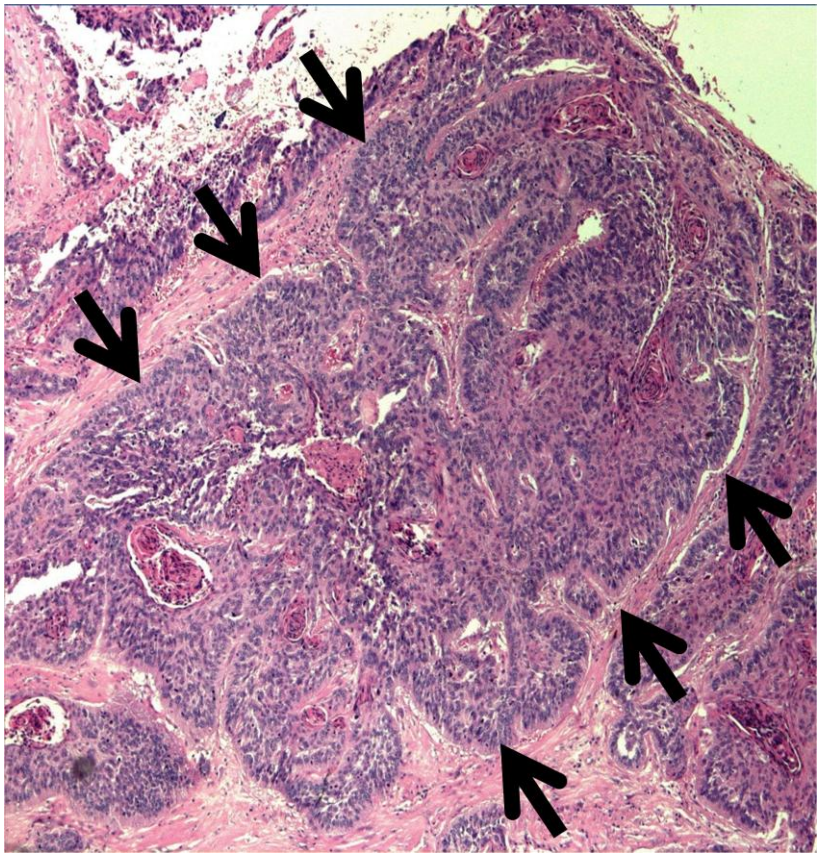

Figure 1: Histological appearance of primary location of head and neck squamous cell carcinoma (arrows). The tumour is composed of densely packed, large-sized pleomorphic cells and organized in a girdle-like microstructure (arrows)

At earlier stages only the submucosal fibrous tissue is invaded, although frequently, the underlying muscular tissue is also affected. Bone or cartilage invasion usually occurs at late stage. Perineural and/or intravascular spread is possible at all head and neck locations.

Next to progressive cellular changes, HNSCC is - similar as all malignant tumours - dependent of an angiogeneic network for locoregional growth and metastatic spread.

The tumoral vasculature shows a substantially different structure and altered function compared to normal blood vessels. The tumoral vasculature appears disorganized, with tortuous and variably sized vessels, excessive branching and shunting. The vessel wall is fragile and shows large gaps in the endothelial surface (9). These structural changes lead to a highly altered vascular functionality resulting in a heterogeneous and sometimes insufficient

transtumoral blood flow, increased capillary permeability and increased interstitial pressure (10,11).

1.2.2. Lymph node metastases

Normal lymph nodes are histologically divided in three regions, the cortex, the intermediate area or paracortex and the medulla. The cortex is composed of densely packed lymphocytes, organized in spheroid lymphoid follicles and the paracortex of migrating lymphocytes. The medulla is composed of three major areas: the medullary trabeculae, medullary cords and medullary sinuses (Figure 2).

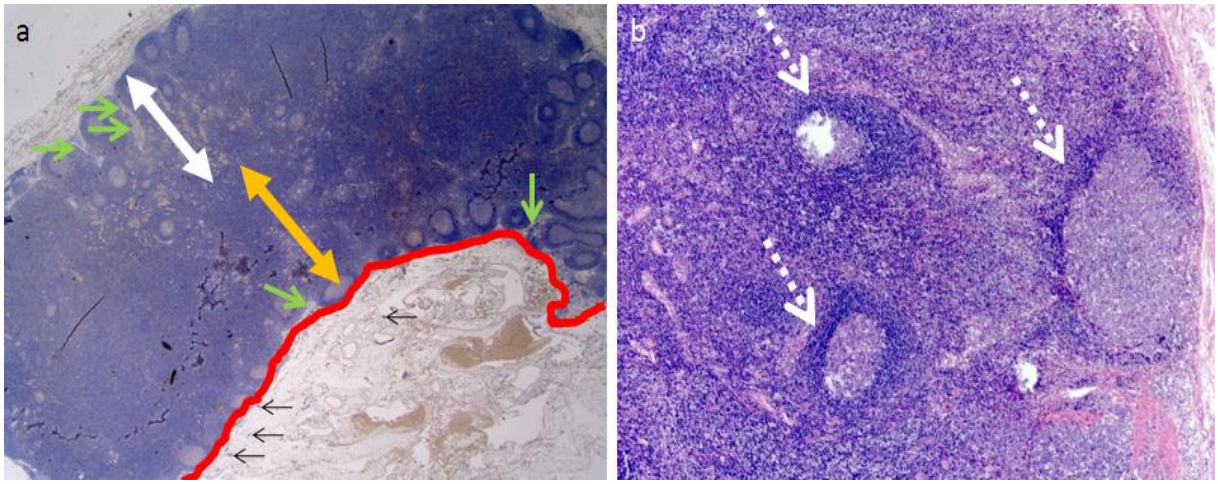

Figure 2: (a) Histological subdivision of normal lymph node in (white double arrow) cortex, (yellow double arrow) paracortex, (red margin) medullar sinus, (green arrows) medullar trabeculae and (black arrows) medullar cords. (b) Detailed histological image of cortex shows densely packed lymphocytes, partially organized in (arrows) lymphoid follicles.

The medullary trabeculae are composed of dense connective tissue and provide a way for the blood vessels. The medullary cords are ordered in a parallel pattern and contain mainly small lymphocytes and plasma cells (Figure 2). The medullary sinuses are filled with lymph. Lymph nodes show a rich vascularity which shows a central or hilar distribution prior to branching in the more peripheral areas of the lymph node.

The likelihood for developing locoregional nodal metastases is dependent of tumour location (12). For instance, nasopharyngeal and oropharyngeal carcinoma are associated with a high incidence of nodal metastases while glottic carcinoma rarely shows nodal metastatic spread. The development of nodal metastases disrupts the normal nodal lymphoid microstructure.

Metastatic HNSCC will disrupt the normal follicular structure, increase cell size and lead to an increased number of cellular boundaries compared to the normal lymphocytes (Figure 3).

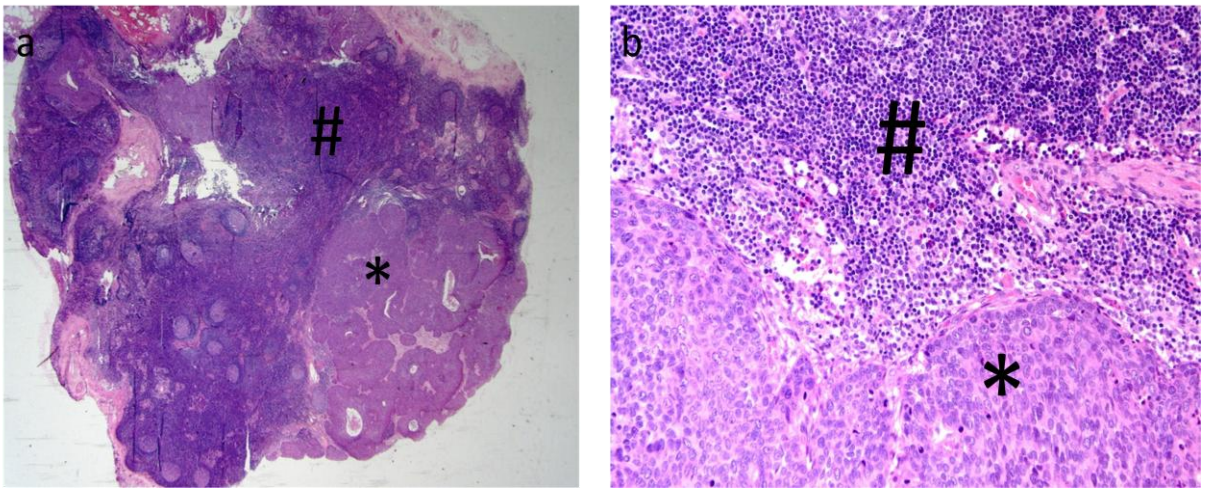

Figure 3: (a) Histological slide of metastatic lymph node showing metastatic deposit (*) and reactive lymphoid tissue (#). (b) Magnified histological image shows clear microstructural contrast between the metastatic squamous cell carcinoma consisting of larger cells (*) compared to the lymphoid tissue (#).

Additionally, neovascularisation secondary to tumoral activity is characterized by a shift of the vascularisation from the centre to the periphery of the lymph node (13) (Figure 4).

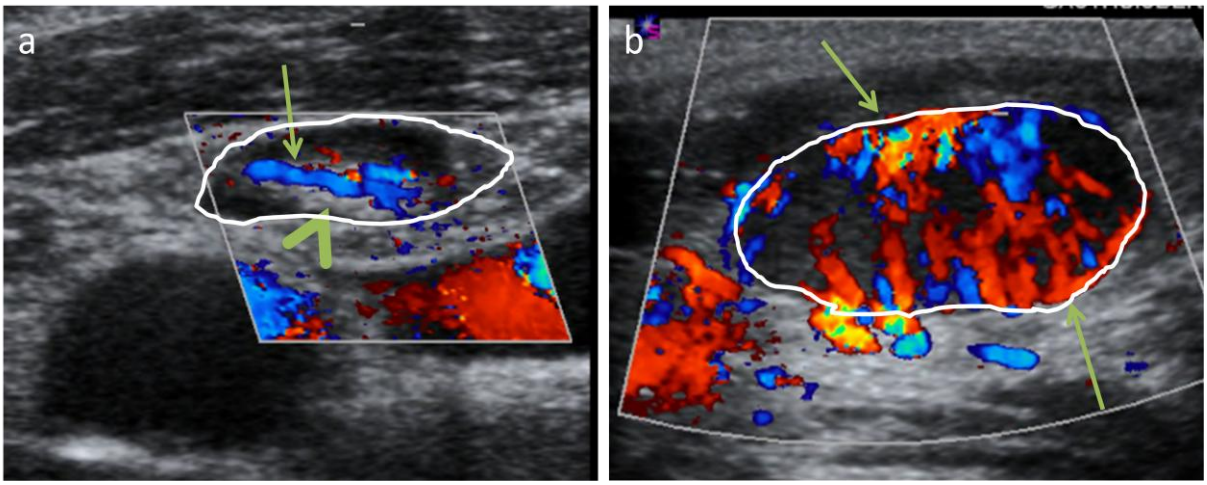

Figure 4: (a) Vascular assessment of normal lymph node (white contour) with color-doppler ultrasound, showing a centralized vascularisation (arrow) and fatty hilus (arrowhead). (b) vascular assessment in metastatic adenopathy (white contour) shows peripheral distribution of vascularity (arrows).

HNSCC shows tendency to develop micrometastatic deposits, especially in oral and pharyngeal carcinoma. These are usually defined as intranodal metastatic deposits smaller than 3 mm (14). Such small deposits can only be expected to create minimal cellular, morphologic, vascular or metabolic alterations to the lymph node environment which makes them very difficult to detect prior to treatment. The presence of micrometastases may correlate to an increased risk for recurrence and indicate poorer prognosis.

Extranodular spread is another histological feature that adversely affects prognosis, where the tumoral tissue extends through the capsule of the lymph node into the soft tissue of the neck. This feature is associated with a high risk for developing distant metastases (15).

1.3 Tumour classification

HNSCC is staged according to the Tumour-Nodes-Metastasis (TNM) classification of the Union Against Cancer and the American Joint Committee on Cancer (seventh edition, 2010). The TNM-classification is an anatomical classification system that describes the anatomic extent of the primary tumour (T-stage), spread of nodal metastases (N-stage) and presence of distant metastases (M-stage).

The criteria used for T-stage are site-specific. For oral and oropharyngeal tumours, tumour diameter is important to determine the T-stage while in the larynx, invasion of laryngeal subsites and vocal cord impairment and invasion of the paraglottic space are important criteria. Furthermore, the extent of nodal metastases is an important prognostic factor. For HNSCC, N-staging of the neck is based on uniform criteria including the size and anatomical spread of metastatic lymph nodes. However, in the current classification morphological criteria that also hold prognostic value, like extranodal spread, are not included.

Neck nodal metastases are topographically classified according to the American Academy of Otolaryngology Head and Neck Surgery classification (AAO-HNS) (16), where the neck is divided in different anatomical levels for localization of nodal metastases. This classification bears the advantage that it allows for an accurate and reproducible topographical description of nodal disease. A number of specific nodal locations are referred to by their pathological name, e.g., supraclavicular, retropharyngeal, parotid, facial, occipital and postauricular.

1.4 Treatment

The most important treatment modalities for HNSCC consist of surgery, radiotherapy (RT) and systemic therapy. Recent developments in both treatment modalities aim at an improved locoregional control (LRC) with a maximal reduction of therapy-induced damage to the surrounding tissue, and maximal preservation of organ functionality (17,18,19).

For most early stage HNSCC, high cure rates can be achieved with definitive RT or surgery. In such patients, treatment choice will be largely influenced by the patient's condition, disease site, anticipated functional and aesthetic outcome and long-term quality of life.

For locally advanced HNSCC, further improvement of LRC has been established with the development of concurrent chemoradiotherapy (CRT), cetuximab-radiotherapy and altered fractionated radiation schemes (20,21,22). A recent advance, intensity modulated radiotherapy (IMRT), allows to shape the three-dimensional dose distribution by varying the beam intensity which results in steep dose gradients outside the target and thus a substantial dose reduction to the surrounding normal tissues (23). In order to do so, an accurate depiction of tumoral tissue at the primary site and lymph nodes is mandatory.

Recent progress in surgical treatment has also focussed on improved organ preservation. More conservative surgical approaches such as laser surgery may raise the question for improved nodal staging and risk assessment in order to obviate neck dissection.

Furthermore, surgery has an important role as a salvage procedure in case of persistent or recurrent cancer after CRT. However, a number of issues remain to be dealt with in the management of the post-RT head and neck. Depending on the stage and localization of the persistent or recurrent tumour, the optimal time window for successful salvage surgery may be limited. In hypo- or oropharyngeal cancer, only a limited number of patients with recurrent disease may be eligible for salvage surgery (24). This implies that tumour recurrence should preferably be detected at an early stage. Also, as modern CRT allows to eradicate nodal metastases, the need for a planned neck dissection is questioned. Although adding a planned neck dissection improves disease free survival after CRT in patients with extensive nodal dissemination at diagnosis, the post-CRT neck dissection often results in negative histopathology and may result in significant patient morbidity and mortality (25,26).

As such, diagnostic modalities should help in the assessment for potential presence of persistent nodal metastases to outweigh surgical benefit against its associated risk for the patient.

1.5 Imaging

1.5.1 Pre-treatment phase

As HNSCC usually develops as a superficial mucosal lesion, in most cases the primary lesion can easily be assessed by clinical examination and histopathology after lesion biopsy. As such, except for the detection of tumours of unknown origin or submucosal tumour localizations, imaging is rarely used for lesion detection or characterization. However, imaging is necessary to determine locoregional tumour or distant metastatic extent. Imaging allows to evaluate local tumoral extension into the deep tissue spaces of the head and neck, perineural or intravascular spread which are difficult to assess by clinical examination. This information is critical towards treatment management and may be predictive for increased risk of later tumour recurrence. Additionally, imaging clearly improves regional staging as it allows the identification of clinically non-palpable or non-accessible lymph nodes.

Computed tomography (CT), and to a lesser extent, magnetic resonance imaging (MRI) are predominantly used in the initial assessment of patients with HNSCC as they simultaneously provide detailed information on the anatomical extent of the primary tumour and extent of locoregional nodal metastases (27). In laryngeal carcinoma, studies have shown that both CT and MRI improved local staging compared to clinical/endoscopic examination alone, more specifically in the assessment of invasion of the paraglottic space, the pre-epiglottic space and invasion of the laryngeal cartilage and extralaryngeal soft tissues (28,29). The combination of clinical/endoscopic examination with CT, respectively MRI reached an accuracy for local staging of 80% and 87% compared to 57% for clinical/endoscopic examination alone (29). Furthermore, although MRI shows higher sensitivity in detecting neoplastic cartilage invasion, it is less specific than CT and tends to overestimate tumoral cartilage invasion (30). However, recent reassessment of MRI criteria have significantly improved the specificity of the technique for identification of tumoral cartilage invasion (31).

For detection of nodal metastases, CT and MRI rely on size-related and morphologic criteria with overall sensitivities ranging from 54 to 88% and specificities ranging from 39 to 100% (32). The main advantage of CT and MRI is that they are routinely available and that morphological criteria are highly reproducible. Several size criteria for detecting neck nodal metastases have been reported with each cut-off value constituting a compromise between sensitivity and specificity. The criterion of 10 mm for short axis diameter, as proposed by van den Brekel et al, has now gained widespread acceptance (33). Morphological malignant

criteria like necrosis and indistinct margins can improve the detection of nodal metastases. However, as these features are rather infrequent in subcentimetric nodal metastases, they often fail to provide additional clinically relevant information (34). Therefore, the most important shortcoming of anatomical imaging modalities lies in the differentiation of subcentimetric lymph nodes.

Ultrasound (US) may be of additional value for nodal staging in HNSCC. Studies have described variable results for US compared to CT and MRI showing respectively higher and similar accuracy (32). The main advantages of US are the low cost and widespread availability, but as the technique does not allow for evaluation of the primary tumour and retropharyngeal lymph nodes, it should be considered as an additional diagnostic imaging modality. The potential advantage of US over CT and MRI lays in the higher spatial and contrast resolution which allows for a better evaluation of internal lymph node structural, abnormalities related to metastatic involvement and the ability to depict tumoral vascular alterations (35). However, as these features may be relatively infrequent in subcentimetric adenopathies, their added value for discrimination of subcentimetric lymph nodes may be variable in HNSCC.

The accuracy of ultrasonographic nodal evaluation can be increased by adding US-guided fine needle aspiration biopsy (US-FNAB). In experienced hands, specificities of 100% can be obtained while reported sensitivities range from 42% to 73% in the clinically negative neck (32,36). However, it is not clear to what extent US-FNAB may significantly improve nodal staging when the head and neck is already evaluated with CT (37). Moreover, as the technique is invasive, and the results are observer-dependent, US-FNAB has not gained widespread use in the routine evaluation of the patient with HNSCC.

Fluoro-deoxy-glucose positron emission tomography (FDG-PET) has gained broad attention in the pre-treatment evaluation of patients with HNSCC both for the evaluation of primary tumour, nodal staging and detection of distant metastases. For evaluation of primary tumours, FDG-PET is mainly employed for the detection of unknown primary tumours as prior studies have shown that FDG-PET has the ability to supplement clinical examination and anatomical imaging in patients with metastatic neck adenopathies of unknown origin (38). For nodal staging, FDG-PET has shown superior accuracy compared to CT and MRI (39,40). Despite the higher accuracy, the added clinical value for regional staging has not been unambiguously shown (41,42). An increased accuracy for detection of nodal metastases will not necessarily to higher accuracy on a per patient basis, while the inability to detect micrometastases does not allow to omit elective neck dissection. Also, the difficult anatomy of the head and neck,

where tumours may arise in areas with high physiological glucose uptake, the rather frequent presence of inflammatory lesions or nodal reactivity and the limited spatial resolution of FDG-PET may decrease overall accuracy of the technique for locoregional staging. The detection of small volume disease remains difficult and is not likely to be obviated by an improved anatomical correlation with PET-CT . Nevertheless, PET-CT has been shown to improve detection of distant metastases compared to whole-body CT alone and should be considered in patients with increased risk for distant metastatic spread (15).

A relatively new approach for nodal staging consists of ultra small particle iron-oxide (USPIO), a novel contrast agent for MRI. USPIO is phagocytised by lymphocytes in normal lymph nodes and lack uptake in metastatic intranodal tumoral tissue and therefore allows differentiation of benign and metastatic lymph nodes. USPIO-MRI has shown variable accuracy for nodal staging in the head and neck (43,44,45). Nevertheless, the increased sensitivity compared to anatomical imaging and repeatedly demonstrated high negative predictive value (NPV), may improve the diagnostic value for nodal staging and may have an impact on therapeutic management. However, currently, USPIO is unavailable for clinical routine practice. Also, as the contrast agent needs to be injected 24 hours prior to imaging, and thus faces potential logistical problems regarding outpatient management.

1.5.2 Post-treatment phase

The clinical evaluation of the post-CRT head and neck is difficult due to the presence of varying degrees of inflammation, oedema, necrosis and soft tissue swelling or distortion. Moreover, post-CRT tumour recurrence and complication like necrosis may show clinically a similar presentation. Definite diagnosis based on histopathological examination of biopsies may be difficult as a result of sampling error due to the general soft tissue swelling which may make the choice of biopsy sites non-straightforward but also because of the difficult interpretation of the biopsy specimen as the histological background of post-CRT normal tissue may show multiple cellular abnormalities. Moreover, as taking a biopsy may aggravate post-CRT necrosis and inflammation; patients should be carefully selected for such procedure. Therefore, contrary to the pre-treatment phase, imaging plays a more prominent role for lesion characterization next to locoregional staging.

Similarly as in the pre-treatment setting, anatomical imaging modalities like CT and MRI use size-related and morphological criteria for the differentiation of tumour recurrence and a post-CRT complication in lymph nodes are characterized and primary tumour site. CT has been

shown to detect tumour recurrence earlier than clinical examination alone (46). For follow-up CT, four months after the end of radiotherapy, an estimated tumour reduction of less than 50%, recurrent or persistent focal mass with a diameter of more than 1 cm after definitive radiotherapy for laryngeal or hypopharyngeal carcinoma indicates a high probability of local failure (46).

Similarly, in the follow-up of treated metastatic lymph nodes, a decrease ratio of more than 50% measured on CT-imaging at 4 weeks after the end of CRT tends to result in a negative hemineck, while a recent report has shown high negative predictive value (NPV) up to 95% if a nodal diameter of 1.5 cm and absence of focal lucency were taken into account (47,48).

However, anatomical imaging criteria are potentially hampered by the CRT-induced swelling and distortion of the normal tissue (46,49). For instance, post-CRT necrosis of the normal tissue may also present as an ulceration, difficult to differentiate from tumoral recurrence. Also, due to the dependence of size-related criteria for nodal staging, anatomical imaging modalities are limited in the detection of residual subcentimetric nodal disease or for the exclusion of residual disease in persistently enlarged lymph nodes.

FDG-PET has been shown to provide additional value for detection of post-CRT tumour recurrence and higher accuracy for detection of tumour recurrence than anatomical imaging modalities, both for the evaluation of the primary tumour site and neck nodes. Sensitivities ranging from 50 to 100% and specificities from 67 to 100% have been reported (50). In the post-CRT setting, FDG-PET is hampered by the susceptibility to inflammatory changes and low spatial resolution. This may respectively cause false positive and false negative results, and diminish the accuracy of the technique, especially in the early post-CRT phase (51). Therefore, in the follow-up of head and neck cancer in the post-CRT phase, FDG-PET imaging appears less reliable during the first 4 months post-CRT, potentially decreasing its value as an early response marker after completion of CRT (50).

The advent of IMRT, which allows for adaptive irradiation during the treatment, has increased the need for predictive imaging during CRT, as this may potentially help to tailor treatment regimens to the individual requirements of the patient. In this early response model, anatomical imaging modalities are likely to fall short as changes in dimension are usually a late treatment effect or do not necessarily show a straightforward relationship with tumour response to treatment. Until now, only a limited number of studies have addressed the use of FDG-PET imaging during (C)RT and the possibility to use FDG-PET during radiotherapy is not entirely clear. Brun et al found that the metabolic response on FDG-PET early during CRT for HNSCC correlated with treatment outcome (52). However, the possible induction of

tumour hypoxia and inflammation during CRT may interfere with the FDG-uptake in tumoral and non-tumoral tissue and decrease the accuracy of FDG-PET during fractionated RT (53,54) and potentially inhibits reliable use of the technique. Further research is required, possibly by use of dynamic FDG-PET studies, using differences in time activity curves between the normal and tumoral tissue. Other traces like (18)F-fluoromisonidazole (18)F-MISO have currently not clearly shown clinical value for prediction of treatment outcome when employed during CRT (55). As a result, until now, no adequate imaging technique is available for early response assessment during CRT.

1.6 References

1. The world health report 2002; Reducing risks, promoting healthy life.
2. Jemal A, Siegel R, Ward E, et al. Cancer statistics *Cancer J Clin* 2008;58:71-96
3. Belgian Cancer Registry. Cancer incidence in Belgium 2004-2005:38-44
4. Burch JD, Howe GR, Miller AB, Semenciw R. Tobacco, alcohol, asbestos, and nickel in the etiology of cancer of the larynx: a case-control study. *J Natl Cancer Inst* 1981;67:1219-1224
5. de Martel C, Franceschi S. Infections and cancer: established associations and new hypotheses. *Crit Rev Oncol Hematol* 2009;70:183-194
6. Pai SI, Westra WH. Molecular pathology of head and neck cancer: implications for diagnosis, prognosis, and treatment. *Annu Rev Pathol* 2009;4:49-70
7. Schwartz LH, Ozsahin M, Zhang GN, et al. Synchronous and metachronous head and neck carcinomas. *Cancer* 1994;74:1933-1938
8. Ghosh S, Ghosh A, Maiti GP, et al. Alterations of ROBO1/DUTT1 and ROBO2 loci in early dysplastic lesions of head and neck: clinical and prognostic implications. *Hum Genet* 2009;125:189-198
9. Carmeliet P, Jain RK. Angiogenesis in cancer and other diseases. *Nature* 2000;407:249-257
10. Hashizume H, Baluk P, Morikawa S, et al. Openings between defective endothelial cell explains tumourvessel leakiness. *Am J Pathol* 2000;156:1363-1680
11. Dvorak HF, Nagy JA, Feng D, Brown LF, Dvorak AM. Vascular permeability factor/vascular endothelial growth factor and the significance of microvascular hyperpermeability in angiogenesis. *Curr Top Microbiol Immunol* 1999;237:97-132
12. Werner JA, Dünne AA, Myers JN. Functional anatomy of the lymphatic drainage system of the upper aerodigestive tract and its role in metastasis of squamous cell carcinoma. *Head Neck* 2003;25:322-332
13. Ahuja AT, Ying M, Ho SY. Ultrasound of malignant cervical lymph nodes. *Cancer Imaging* 2008;8:48-56
14. van den Brekel MW, van der Waal I, Meijer CJ, Freeman JL, Castelijns JA, Snow GB. The incidence of micrometastases in neck dissection specimens obtained from elective neck dissections. *Laryngoscope* 1996;106:987-991

15. Ljumanovic R, Langendijk JA, Hoekstra OS, Leemans CR, Castelijns JA. Distant metastases in head and neck carcinoma: identification of prognostic groups with MR imaging. *Eur J Radiol* 2006;60:58-66
16. Robbins KT, Medina JE, Wolfe GT, et al. Standardizing neck dissection terminology. Official report of the Academy's Committee for Head and Neck Surgery and Oncology. *Arch Otolaryngol Head Neck Surg* 1991;117:601-605
17. Ang KK, Harris J, Garden AS, et al. Concomitant boost radiation plus concurrent cisplatinum for advanced head and neck carcinomas: Radiation Therapy Oncology Group phase II trial 99-14. *J Clin Oncol* 2005; 23:3008-3015
18. Kaanders JH, Pop LA, Marres HA, et al. ARCON: experience in 215 patients with advanced head-and-neck cancer. *Int J Radiat Oncol Biol Phys* 2002;52:769-778
19. El-Deiry M, Funk GF, Nalwa S, et al. Long-term quality of life for surgical and nonsurgical treatment of head and neck cancer. *Arch Otolaryngol Head Neck Surg* 2005;131:879-885
20. Fu KK, Pajak TJ, Trotti A, et al. A radiation therapy oncology group (RTOG) phase III randomized study to compare hyperfractionation and two variants of accelerated fractionation to standard fractionation therapy for head and neck squamous cell carcinomas: first report of RTOG 9003. *Int J Radiat Oncol Biol Physics* 2000;48:7-16
21. Cooper JS, Ang K.K. Concomitant chemotherapy and radiation therapy certainly improves local control. *Int J Radiat Oncol Biol Phys* 2005;61:7–9
22. Budach W, Hehr T, Budach V, et al. A meta-analysis of hyperfractionated and accelerated radiotherapy and combined chemotherapy and radiotherapy regimens in unresected locally advanced squamous cell carcinoma of the head and neck. *BMC Cancer* 2006;6:28
23. Gregoire V, De Neve W, Eisbruch A, Lee N, Van den Weyngaert D, Van Gestel D. Intensity-modulated radiation therapy for head and neck carcinoma. *Oncologist* 2007;12:555-564
24. Yom SS, Machtay M, Biel MA, et al. Survival impact of planned restaging and early surgical salvage following definitive chemoradiation for locally advanced squamous cell carcinomas of the oropharynx and hypopharynx. *Am J Clin Oncol* 2005;28:385-392
25. Brizel DM, Prosnitz RG, Hunter S, et al. Necessity for adjuvant neck dissection in setting of concurrent chemoradiation for advanced head-and-neck cancer. *Int J Radiation Oncology Biol Phys* 2004;58:1418-1423

26. Machtay M, Moughan J, Trotti A, et al. Factors associated with severe late toxicity after concurrent chemoradiation for locally advanced head and neck cancer: an RTOG analysis. *J Clin Oncol* 2008;26:2582-2589
27. Castelijns JA, van den Brekel MW. Imaging of lymphadenopathy in the neck. *Eur Radiol* 2002;12:727-738
28. Zbären P, Becker M, Läng H. Staging of laryngeal cancer: endoscopy, computed tomography and magnetic resonance versus histopathology. *Eur Arch Otorhinolaryngol* 1997;254:S117-122
29. Zbären P, Becker M, Läng H. Pretherapeutic staging of laryngeal carcinoma. Clinical findings, computed tomography, and magnetic resonance imaging compared with histopathology. *Cancer* 1996;77:1263-1273
30. Becker M, Zbären P, Laeng H, Stoupis C, Porcelinni B, Vock P. Neoplastic invasion of the laryngeal cartilage: comparison of MR imaging and CT with histopathologic correlation. *Radiology* 1995;194:661-669
31. Becker M, Zbären P, Casselman J, Kohler R, Dulguerov P, Becker CD. Neoplastic invasion of laryngeal cartilage: reassessment of criteria for diagnosis at MR imaging. *Radiology* 2008;249:551-559
32. de Bondt RB, Nelemans PJ, Hofman PA, et al. Detection of lymph node metastases in head and neck cancer: a meta-analysis comparing US, USgFNAC, CT and MR imaging. *Eur J Radiol* 2007;64:266-272
33. van den Brekel MW, Stel HV, Castelijns JA, et al. Cervical lymph node metastasis: assessment of Radiologic criteria. *Radiology* 1990;380:379-384.
34. King AD, Tse GM, Ahuja AT, et al. Necrosis in metastatic neck nodes: Diagnostic accuracy of CT, MR imaging and US. *Radiology* 2004;230:720-726
35. Richards PS, Peacock TE. The role of ultrasound in the detection of cervical lymph node metastases in clinically N0 squamous cell carcinoma of the head and neck. *Cancer Imaging* 2007;7:167-178
36. van den Brekel MW, Castelijns JA, Stel HV. Occult metastatic neck disease: detection with US and US-guided fine-needle aspiration cytology. *Radiology* 1991;182:457-461
37. Takes RP, Righi P, Meeuwis CA. The value of ultrasound with ultrasound-guided fine-needle aspiration biopsy compared to computed tomography in the detection of regional metastases in the clinically negative neck. *Int J Radiation Oncology Biol Phys* 1998;40:1027-1032

38. Lonneux M, Haloir M, Reychler H, et al. Positron emission tomography with [18F]fluorodeoxyglucose improves staging and patient management in patients with head and neck squamous cell carcinoma: a multicenter prospective study. *J Clin Oncol* 2010;28:1190-1195
39. Goerres GW, Schmid DT, Grätz KW, von Schultess GK, Eyrich GK. Impact of whole body positron emission tomography on initial staging and therapy in patients with squamous cell carcinoma of the oral cavity. *Oral Oncol* 2003;39:547-551
40. Wong RJ. Current status of FDG-PET for head and neck cancer. *J Surg Oncol* 2008;97:649-652
41. Ng SH, Yen TC, Chang JT, et al. Prospective study of [18]fluorodeoxyglucose positron emission tomography and computed tomography and magnetic resonance imaging in oral cavity squamous cell carcinoma with palpably negative neck. *J Clin Oncol* 2006;24:4371-4376
42. Roh JL, Yeo NK, Kim JS, et al. Utility of 2-[18F] fluoro-2-deoxy-D-glucose positron emission tomography and positron emission tomography/computed tomography in the management of patients with head and neck cancer. *Oral Oncol* 2007;43:887-893
43. Sigal R, Vogl T, Casselman J, et al. Lymph node metastases from head and neck squamous carcinoma: MR imaging with ultrasmall superparamagnetic iron oxide particles (Sinerem MR) – results of a phase-III multicenter clinical trial. *Eur Radiol* 2002;12:1104-1113
44. Hoffman HT, Quets J, Toshiaki T, et al. Functional magnetic resonance imaging using iron oxide particles in characterizing head and neck adenopathy. *The Laryngoscope* 2000;110:1425-1430
45. Mack MG, Balzer JO, Straub R, Vogl TJ. Superparamagnetic iron oxide-enhanced MR imaging of head and neck lymph nodes. *Radiology* 2002;222:239-244
46. Hermans R, Pameijer FA, Mancuso AA, et al. Laryngeal or hypopharyngeal squamous cell carcinoma: can follow-up CT after definitive radiotherapy be used to detect local failure earlier than clinical examination alone? *Radiology* 2000;214:683-687
47. Ojiri H, Mendenhall WM, Stringer SP, Johnson PL, Mancuso AA. Post-RT CT results as a predictive model for the necessity of planned post-RT neck dissection in patients with cervical metastatic disease from squamous cell carcinoma. *Int J Radiat Oncol Biol Phys* 2002;52:420-428

48. Liauw SL, Mancuso AA, Amdur RJ, et al. Postradiotherapy neck dissection for lymph node-positive head and neck cancer: the use of computed tomography to manage the neck. *J Clin Oncol* 2006;24:1421-1427
49. Nomayr A, Lell M, Sweeney R, et al. MRI appearance of radiation-induced changes of normal cervical tissues. *Eur Radiol* 2001;11:1807-1817
50. Kostakoglu L, Goldsmith SJ. PET in the assessment of therapy response in patients with carcinoma of the head and neck and of the esophagus. *J Nucl Med* 2004;45:56-68
51. McCollum AD, Burrell SC, Haddad RI, et al. Positron emission tomography with 18F-fluorodeoxyglucose to predict pathologic response after induction chemotherapy and definitive chemoradiotherapy in head and neck cancer. *Head Neck* 2004;26:890-896
52. Brun E, Kjellén E, Tennvall J, et al. FDG PET studies during treatment: prediction of therapy outcome in head and neck squamous cell carcinoma. *Head Neck* 2002;24:127-135
53. Geets X, Tomsej M, Lee JA, et al. Adaptive biological image-guided IMRT with anatomic and functional imaging in pharyngo-laryngeal tumors: impact on target volume delineation and dose distribution using helical tomotherapy. *Radiother Oncol* 2007;85:105-115
54. Madani I, Duthoy W, Derie C, et al. Positron emission tomography-guided, focal-dose escalation using intensity-modulated radiotherapy for head and neck cancer. *Int J Radiat Oncol Biol Phys* 2007;68:126-135
55. Lee N, Nehmeh S, Schöder H, et al. Prospective Trial Incorporating Pre-/Mid-Treatment [(18)F]-Misonidazole Positron Emission Tomography for Head-and-Neck Cancer Patients Undergoing Concurrent Chemoradiotherapy. *Int J Radiat Oncol Biol Phys* 2009;75:101-108

1.7 Aims of the study

The aim of this thesis project is to evaluate whether diffusion-weighted imaging (DWI) and dynamic contrast-enhanced (DCE)-MRI, respectively by measuring differences in tissue microstructure and tissue perfusion, can be used for tissue characterization, early response assessment and post-treatment follow-up in HNSCC.

In solid malignant lesions, the high microstructural density, leads to a restriction of the Brownian or random water molecule movement. Contrary, in benign tissue and necrosis, the low or absent microstructural density leads to a facilitation of the random water movement due to the lesser interaction with cellular membranes.

Additionally, the angiogenesis related to tumoral development leads to an altered vascular structure and functionality, different from normal tissue or treatment-induced necrosis, in the aspect of transtumoral blood flow, capillary permeability and interstitial pressure.

The project will be divided in 4 major projects:

Project 1: In HNSCC, accurate nodal staging is of utmost importance as it has major impact on treatment planning and determines patient prognosis. DWI has already been researched in a limited number for differentiation of benign and metastatic lymph nodes, be it only in enlarged lymph nodes. Until now, results of DWI have not been compared with other imaging modalities used for nodal staging of HNSCC.

The aim of this study is to evaluate DWI for the differentiation of metastatic and benign lymph nodes in patients with HNSCC and to determine the added value of DWI in the characterization of subcentimetric lymph nodes in comparison to conventional MRI and FDG-PET.

Project 2: CT is often applied as surveillance imaging modality after CRT for HNSCC. Although CT improves the detection of a tumoral recurrence in comparison to clinical examination alone, CRT-induced tissue distortions are the cause of false positive en false negative findings. This cannot be resolved by conventional MRI as T2- or T1-signal intensity (SI) do not show additional value in the differentiation of tumoral tissue. Although FDG-PET, has additional value in the differentiation of tumoral recurrence from post-CR inflammation, post-CRT inflammation and the low spatial resolution of the technique limit its diagnostic accuracy in the post-CRT setting. The aim of this study is to evaluate DWI and DCE-MRI for

the differentiation of post-radiotherapeutic tumour recurrence from inflammation and necrosis at the time of clinical presentation. To determine the potential added value, DW- and DCE-MRI will be compared to CT and FDG-PET.

Project 3: DW- and DCE-MRI will be evaluated as potential biomarkers for predictive imaging during and early after CRT for HNSCC. The project aims to determine the most optimal strategy for treatment prediction by comparing both techniques to volumetric measurements or morphological criteria.
The predictive value of DW- and DCE-criteria at these early time points will be correlated to LRC, and compared with known predictive parameters, such as initial tumour stage and tumour volume.

Project 4: DW- and DCE-MRI rely on quantitative measurements based on manually drawn regions of interest (ROI) for differentiation of tissue composition, respectively vascularity. Variability of measurements between different readers may thus influence imaging results which may be highly dependent of observer training.
The aim of this study is to determine the inter- and intra-observer variability in quantitative analysis of DWI.

Chapter 2:
Rationale for using functional magnetic resonance imaging: probing the tumoral microenvironment

2.1 Diffusion-weighted MRI

Water molecules are in constant motion, also called Brownian motion (Figure 1). These thermal motions lead to random rotations of the water molecules that produce fluctuations of the magnetic field. These fluctuations, felt by the hydrogen atoms, result in relaxation. Additionally to the random rotations of the molecules, these thermal motions also produce random molecule displacements or diffusion (1).

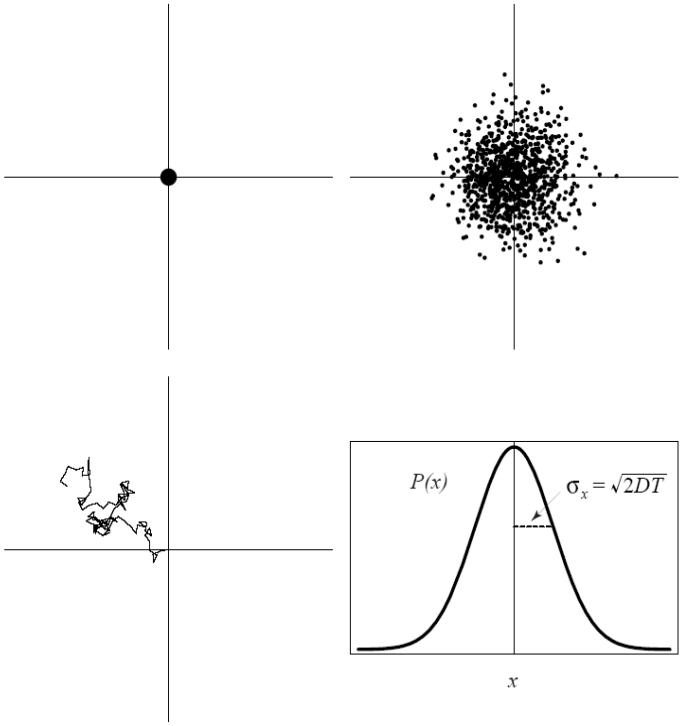

Figure 1: Illustration of process of diffusion. Considering a large number of protons in the centre at the start of the diffusion time (top left), the random Brownian motion will induce a spread out of the protons over time (top right). The bottom left image shows a random path of one proton, while the bottom right indicates the mathematical spread function induced by the diffusion in the given time T.

Contrary to water outside the body where the random movement is free, water molecules in biological tissues are variably restricted in their motion, inversely correlated to tissue cellularity and cell membrane integrity. In biological tissue water molecule displacements

occur in and between three major compartments: the intracellular space (IS), the extravascular extracellular space (EES) and the intravascular space (IVS). In solid malignant lesions, the EES will be relatively diminished compared to the IS, due to the high microstructural density, consisting of an increased number of cells, cellular pleomorphism, large cell volume and neo-angiogeneic vessels disorganized in a chaotic structure. This increased microstructural density will lead to a restriction of the Brownian or random water molecule movement, due to their interaction with the intact cellular membranes and macromolecules.

Contrary, tissue with low cellularity, like benign lesions or tissues with more pronounced necrosis, the EES will be relatively enlarged compared to the IS due to the lower density of cells and membranes, or in case of necrosis, the complete absence of any organized tissue structures. As such, the lesser interaction with cell membranes will lead to a facilitation of random water molecule movement (2) (Figure 2).

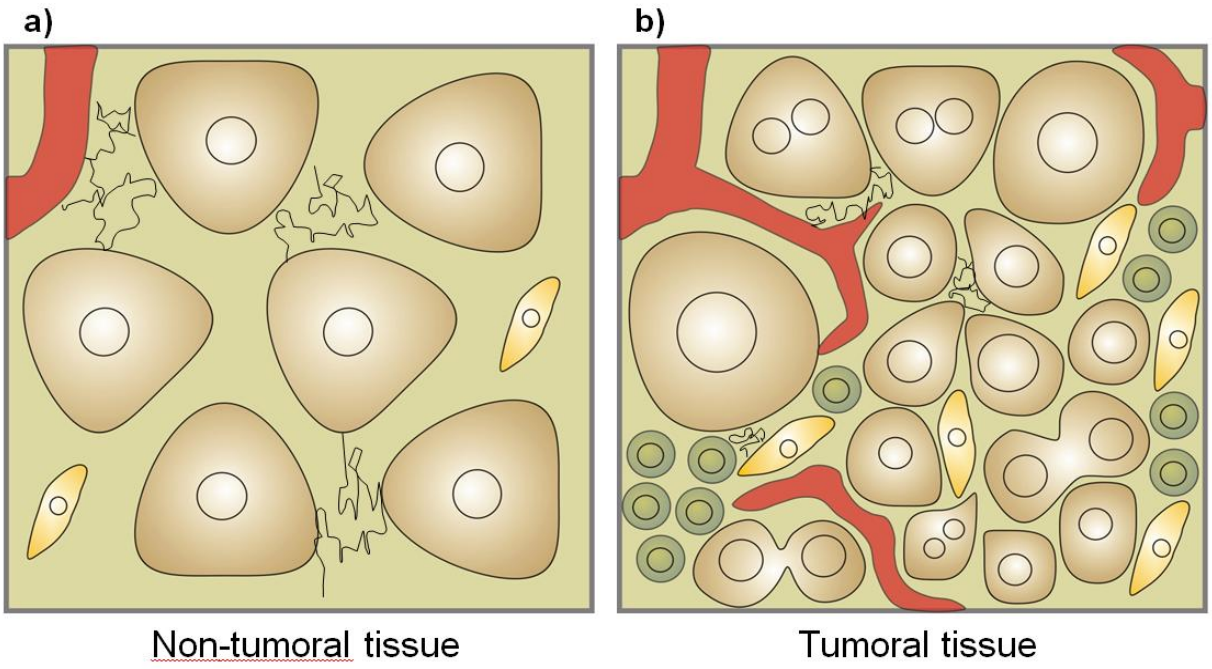

Figure 2: (a) Low cellularity allows for larger interstitial space, facilitating Brownian movement of water molecules (black line represent random trajectory of a water molecule). (b) High cellularity in tumoral tissue decreases the interstitial space and increases the surface of cell membranes for interaction with water molecules. This leads to a restriction of Brownian or random water molecule movement (black line represent random trajectory of a water molecule).

The DWI sequence is made susceptible to the differences in water mobility by pairing two equally large but opposite gradient pulses around the 180° refocusing gradient of a standard T2-weighted spin-echo (SE) sequence (Figure 3).

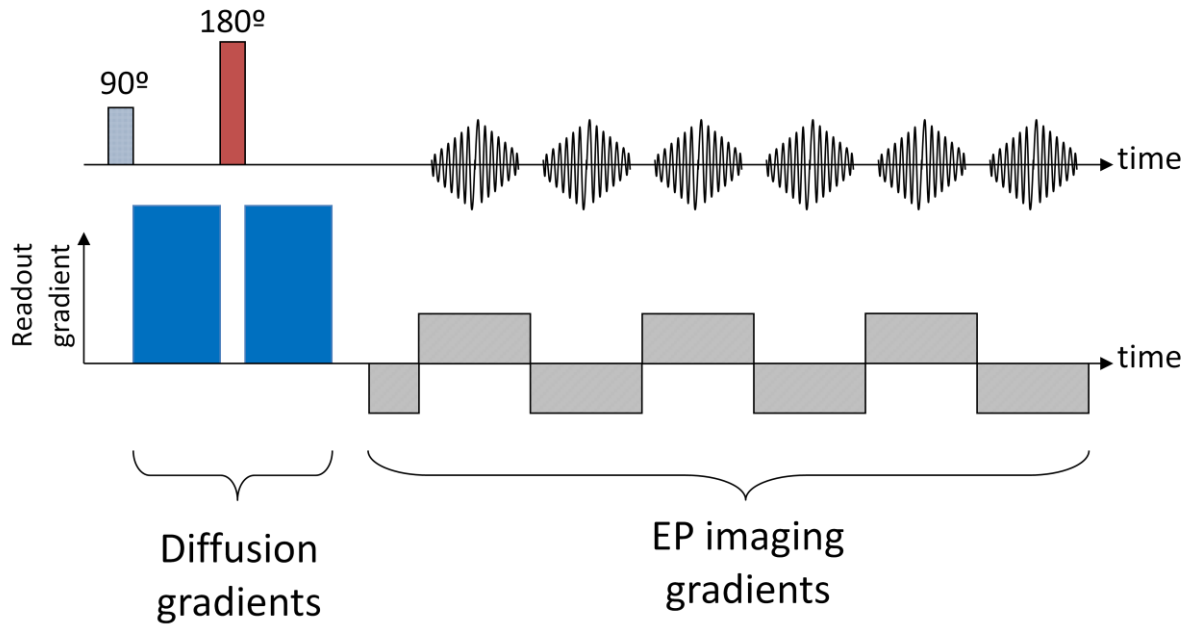

Figure 3: schematic drawing of echo-planar diffusion weighted sequence. The effects of the paired diffusion gradients (blue) are opposed to each other due to the application of a 180° refocusing gradient (red).

The first gradient pulse induces a phase shift of water molecules proportional to its initial location while the second gradient pulse rephases the water molecules. If water molecules would be static, the rephasing would be complete and not result in a significant loss of SI. However, due to the variable random water movement, the rephasing will always be incomplete in biological tissues and result in a net signal loss dependent of microstructural density and diffusion sensitivity (2). The diffusion sensitivity to water motion can be changed by modulating the gradient amplitude, the duration of the gradient or changing the duration between both gradients. However, in practice, the diffusion sensitivity is modulated by the b-value, which represents the effect of gradient strength on diffusion sensitivity (3). In standard DWI-sequences, consecutive native images with increasing b-values ranging from 0 to 1000 seconds per square millimetres (s/mm^2) are used.

When using low b-values, water molecules with a great diffusion distance are preferably depicted (mostly intravascular space), while the application of high b-values allows to perceive small diffusion distances and thus restricted water movement in the EES and IS (4).

By repeating the sequence with consecutive and increasing b-values, the progressive signal decay over the images with increasing b-value loss can be quantified using the apparent diffusion coefficient (ADC). By plotting the logarithm of the SI on the Y-axis relative to the

b-values on the x-axis a slope line can be fitted through the plots (exponential function) from which the ADC is calculated using a least squares solution of the following equation:

$$SI_i = SI_0 \text{ x } exp(-b_i \text{ x } ADC)$$

where SI_i is the signal intensity measured on the i'th b-value image and b_i is the corresponding b-value. SI_0 is a variable that estimates the exact (without noise induced by the MR measurement) signal intensity for b = 0 s/mm^2. As such, the ADC indicates the amount of water molecule mobility present in the tissue and in a simplified model shows an inverse correlation with tissue cellularity (5).

Hypercellular tissue, characterized by a limited EES and diffusion restriction, will only show limited signal decay with increasing b-value (more complete rephasing due to limited water mobility) with a persistent high SI on the native DWI images with high b-value (1000s/mm^2) resulting in a low ADC (Figure 4). Contrary, areas of low cellularity, showing a large EES and facilitation of water movement, will show rapid signal decay with increasing b-value (incomplete rephasing due to pronounced water mobility) with low or absent SI on the native DWI images with high b-value (1000s/mm^2) resulting in a high ADC (Figure 4). As such malignant tissue can potentially be differentiated from benign tissue, or in case of treatment follow-up, from necrosis or inflammation based on high b-value SI combined with ADC-calculation.

However, as low b-values (0-100 s/mm^2) are usually included in routine ADC-calculation, there will always be an additional but variable influence of microperfusion (flow-sensitive ADC) (1,4). A possible solution lies in excluding low b-values (0-300 s/mm$^{2)}$ from the calculation for which the non flow-sensitive ADC would more closely reflect true cellularity (6,7). However, the exclusion of low b-value factors may not go without penalty as a more unfavourable signal-to-noise ratio (SNR) would be introduced, which cannot always be sufficiently compensated on currently used clinical MRI-systems at 1.5 Tesla. As benign lesions usually show a lack of sufficient SI in the high b-value range, the resulting ADC will be decreased due to the low SNR, which is difficult to discriminate from a low ADC caused by diffusion restriction in malignancy. This is of particular importance for head and neck DWI where the high amount of air-tissue interfaces and movement may lead to suboptimal signal generation.

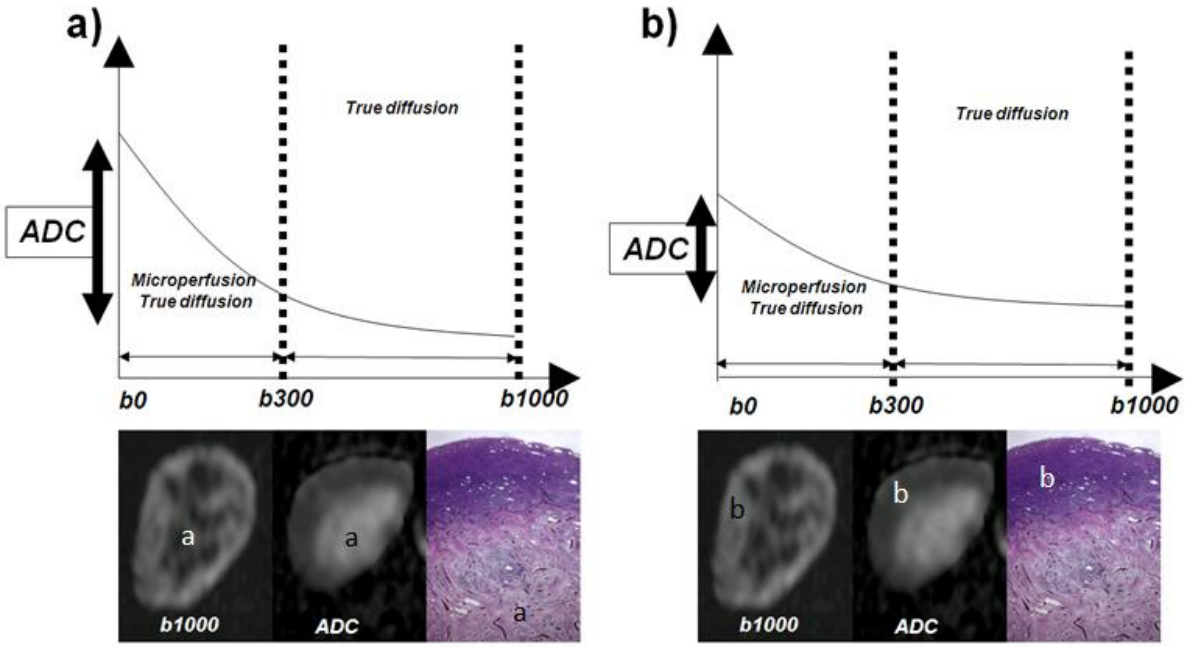

Figure 4: (a) Necrotic centre of rodent rabdomyosarcoma shows substantial loss of signal (logarithmic curve) over consecutive b-values correlating to a high apparent diffusion coefficient (represented by vertical double arrow). (b) Intact tumoral tissue in the peripheral area of the tumour shows only limited loss of signal over the consecutive b-values, correlating to a low apparent diffusion coefficient.

Furthermore, signal generation on DWI images does not solely depend on water diffusion but also on T2 relaxation time. An area with very long T2 - usually fluid, possibly in necrosis – may show persistent hyperintensity on high b-value images difficult to distinguish from hyperintensity related to diffusion restriction. This is called the T2 shine-through effect and can hamper qualitative interpretation of DWI images (8). As in head and neck imaging, image interpretation routinely consists of lesion detection on a high b-value image in combination to ADC quantification, this should hardly have any influence on diagnostic accuracy (9).

Potential limitations for application of DWI in the head and neck are artifacts related to physiological motion, susceptibility and chemical shift artifacting, which could restrict diagnostic accuracy. Improved echo-planar imaging (EPI) technology, use of dedicated coils and dedicated sequence optimization enables a maximal reduction of EPI-related artifacts. The reduction of these artifacts, in combination with high gradient strength available on current MRI-systems, substantially increases the SNR, necessary for the detection of small lesions (10).

A major advantage of DWI, compared to other biological imaging methods, is the lack of radiation exposure and the absent need for an extrinsic contrast agent.

2.2 Dynamic contrast-enhanced MRI

The vascular structural changes related to intratumoral angiogenesis lead to a highly altered vascular functionality resulting in a heterogeneous and sometimes insufficient transtumoral blood flow, increased capillary permeability and increased interstitial pressure compared to normal tissue (11). DCE-MRI is acquired by repetitive imaging with high temporal resolution over a predefined lesion or anatomical region prior to and during the injection of a low-molecular gadolinium-based contrast agent (Figure 5).

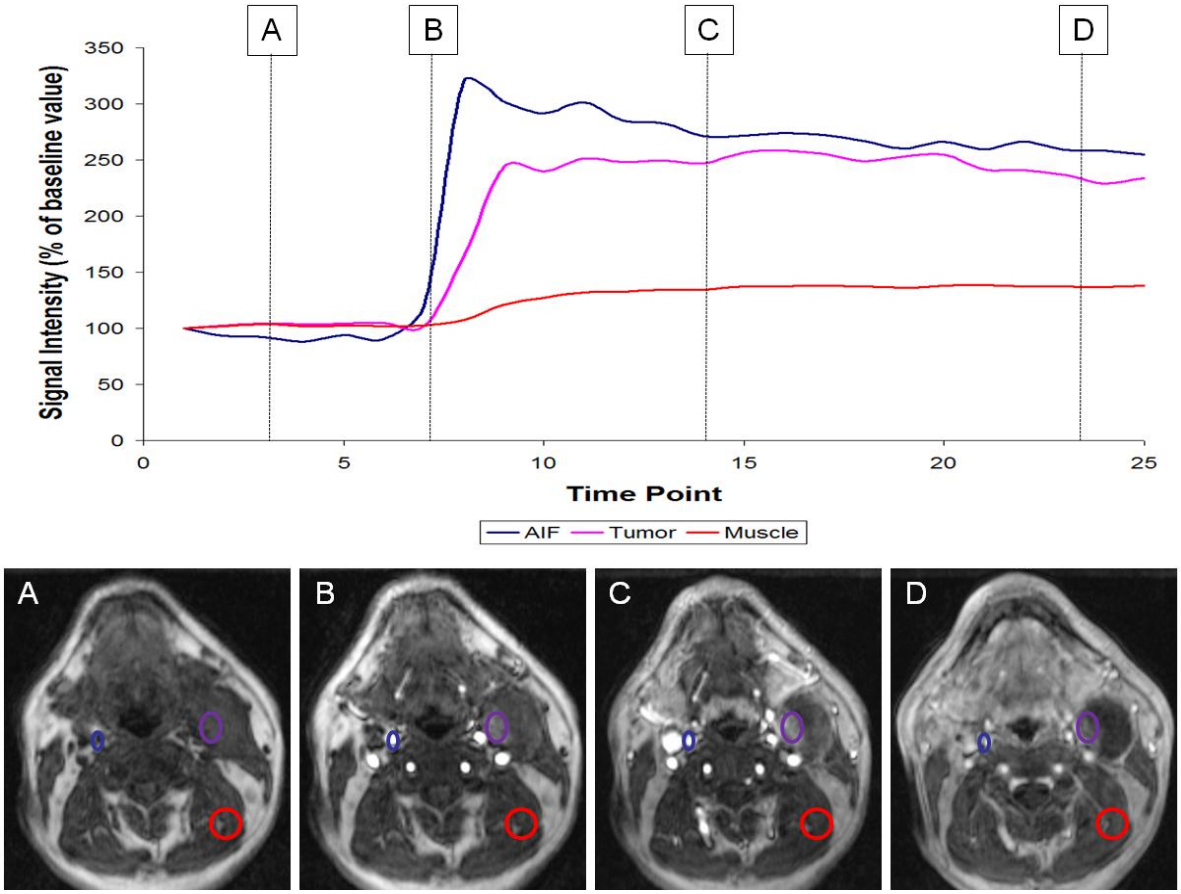

Figure 5: Time intensity curve respectively in artery (blue region of interest), metastatic adenopathy (purple region of interest) and muscle (red region of interest) at separate time points during the dynamic contrast-enhanced: (A) prior to contrast injection, (B) early arterial phase, (C) early washout phase, (D) late washout phase.

In the arteries, the concentration rises after contrast agent injection and falls back to a steady state value before being washed out by the kidneys. In normal tissue and tumoral lesions, the contrast agent will leak into the interstitial space at a variable rate and will only be washed out when the vessel concentration is very low. The rate of contrast agent leakage into the

interstitial space depends on tissue perfusion, vessel wall permeability and the total vessel surface area (12).

The resulting SI's acquired by the consecutive sequences over time, or the signal intensity curve, hold information about tissue perfusion, tracer uptake and blood volume. Typically, the signal intensity curve will show 3 distinct phases: the upslope or rapid arterial enhancement, the point of maximum enhancement and delayed washout (Figure 6).

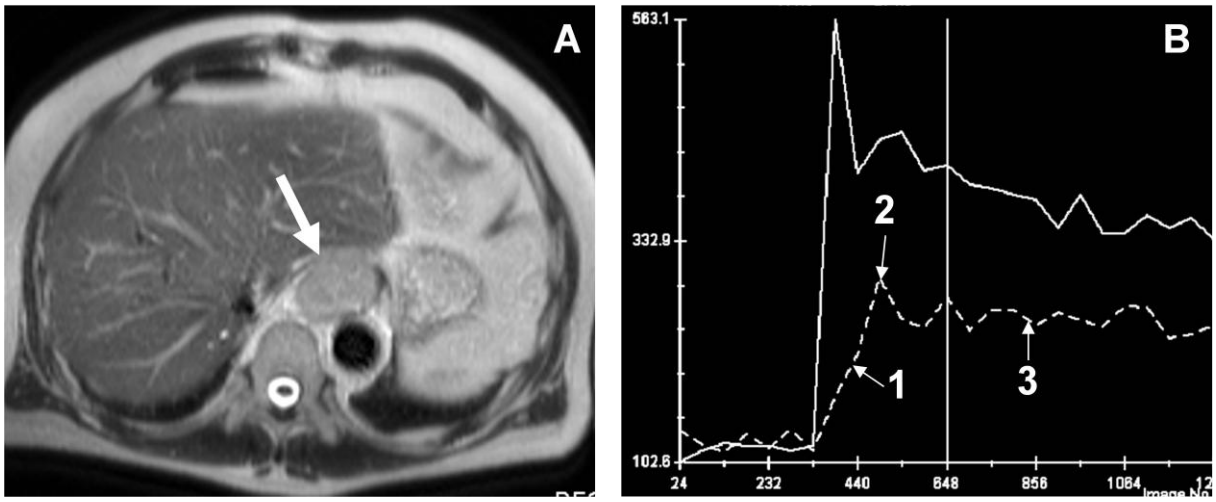

Figure 6: (A) Visualisation of tumoral mass (arrow) in the lower oesophagus consistent with biopsy-proven adenocarcinoma. (B) Concentration-time-curve for (full line) arterial input function (AIF) and (dotted line) tumour is shown. The typical components of the concentration-time-curve of the tumoral mass consist of (1) steep upslope indicating rapid arterial enhancement (initial slope), (2) high point of maximum enhancement (contrast-peak) and (3) rapid washout of contrast agent in the delayed phase.

In general, the rate of upslope will predominantly be influenced by tissue perfusion secondary to the high blood volume and high first pass extraction. The maximum enhancement will predominantly be influenced by the total uptake of contrast agent in the interstitial space and the washout will be largely determined by extraction of contrast agent out of the interstitial space and will be strongly related to vessel permeability and vessel surface area.

The dynamic signal enhancement on T1-weighted DCE-MRI can be assessed by semi-quantitative evaluation of the signal intensity curve or by quantification of the change of contrast agent concentration based on pharmacokinetic modelling techniques (13,14). Semi-quantitative parameters attempt to quantify a certain aspect of the signal intensity-curve, while ignoring the information in the rest of the curve. These parameters include the maximal contrast enhancement (contrast-peak/c-peak), time to maximal contrast enhancement (time to peak/TTP) and the speed of arterial contrast enhancement (arterial slope/AS). They are very

robust and easily implemented, facilitating their use in clinical routine. However, semi-quantitative parameters do not accurately reflect contrast agent concentration in tissues and may show variability due to scanner settings and differences in interpatient cardiovascular physiology (12). In order to decrease intra- and interpatient variability during treatment follow-up, normalization of contrast agent uptake is done by analyzing contrast enhancement in a feeding artery and normalizing the tissue measurements to this arterial input function (AIF) (15).

Quantitative analysis is performed on the contrast-time-curves instead of on the signal intensity curves. These contrast-time-curves are calculated from the signal intensity curves through normalization to the baseline signal intensity, keeping in mind the non-linearity of the signal intensity increase with increasing contrast agent concentration. For quantitative analysis, the entire contrast-time-curve is fitted by a curve model based on biological assumptions, such as blood volume, blood flow or permeability. In most cases, a modified two compartment model correlating the tissue tracer concentration to the difference between arterial plasma and interstitial fluid concentrations is used (16). Quantitative parameters that are increasingly researched include the volume transfer constant of the contrast agent (K^{trans}) and the rate constant (k_{ep}). These parameters provide information that can be linked to underlying biologic processes of the vasculature, such as the permeability surface area and flow (12). Thus, next to clinical applications, these parameters are more suited than semi-quantitative parameters for scientific or clinical evaluation of the efficacy of antivascular treatment (17).

However, quantified models are more complex to derive, less robust to noise and more susceptible to artifacting secondary to patient or physiological movement, making interpretation of the results more difficult. Also, the contribution of intravascular flow to the MRI-signal remains unclear and may have variable influence to the accuracy of the models depending on the tumour type. For a diffusible tracer, the contribution of the intravascular component may be neglected due to the low proportion compared to its distribution volume (18). However, this assumption is less accurate for an extracellular tracer as the distribution volume will be substantially lower and intravascular flow may possibly contribute more to the tissue signal. As such, estimates of kinetic parameters may be less reliable.

An intermediate solution to quantify perfusion is the use of the initial area under the signal intensity curve (IAUC) or contrast agent concentration curve (12). Using these semi-quantitative parameters, estimations can be made of the K^{trans} or the leakage space (v_e), without the difficult calculations inherently linked to fitting biophysical curve models to the data. This parameter combines the robustness of the semi-quantitative parameters with the easier inter- and intrapatient comparison and lower scanner hardware dependence of the quantitative parameters and is currently one of the more promising parameters for clinical routine (12,19,20)

Although DCE-MRI shows value in treatment follow-up and prognosis for several tumour types and different non-surgical treatment regimens (21,22,23), one of the major limitations of the technique is that it can only act as an indirect marker for tumour tissue viability and may have difficulties to depict small residual viable tumoral deposits early after the end of therapy (4).

For perfusion imaging with MRI, different sequences can be used and the type of sequence employed will influence the techniques' reliability and quality. In extracranial tumours, perfusion measurements are usually acquired using a T1-weighted gradient-echo sequence with injection of a low-molecular weight Gadolinium based contrast agent. This is in part attributable to its robustness, anatomical image quality and relative resistance to image artifacting compared to T2*-based perfusion-MRI, whose use is mostly limited to brain imaging (24,25). Although T2*-based perfusion imaging has the advantage that it allows absolute quantification of perfusion, its sensitivity to motion and susceptibility artifacts (e.g.: patient motion, air-tissue boundaries in the bowel) can decrease the reliability of the technique substantially for extracranial applications. Other advantages of T1-weighted DCE-MRI are the lower amount and injection-rate of contrast agent required and the possibility for coverage of sufficiently large scan volumes (such as the entire head and neck) in acceptable time resolution. Also, the positive contrast enhancement used in the T1-weighted DCE-MRI is more beneficial in the relatively low SNR areas outside of the brain, compared to the negative contrast enhancement of the T2*-weighted DCE-MRI.

2.3 References

1. Le Bihan D, Breton E, Lallemand D, Aubin ML, et al. Separation of diffusion and perfusion in intravoxel incoherent motion MR imaging. *Radiology* 1988;168:497-505
2. Ross BD, Moffat A, Lawrence TS, et al. Evaluation of cancer therapy using diffusion magnetic resonance imaging. *Mol Cancer Ther* 2003;2:581-587
3. Melhem ER, Itoh R, Jones L, et al. Diffusion tensor imaging of the brain: effect of diffusion weighting on trace and anisotropy measurements. *Am J Neuroradiol* 2000;21:1813-1820
4. Thoeny HC, De Keyzer F, Vandecaveye V. Effect of vascular targeting agent in rat tumourmodel: dynamic contrast-enhanced versus diffusion-weighted MR imaging. *Radiology* 2005;237:492-499
5. Chenevert TL, Meyer CR, Moffat BA, et al. Diffusion MRI: a new strategy for assessment of cancer therapeutic efficacy. *Mol Imag* 2002;1:336-343
6. Sun X, Wang H, Chen F, et al. Diffusion-weighted MRI of hepatic tumor in rats: comparison between in vivo and postmortem imaging acquisitions. *J Magn Reson Imaging* 2009;29:621-628
7. Roth Y, Tichler T, Kostenich G, et al. High-b-value diffusion-weighted MR-imaging for pre-treatment prediction and early monitoring of tumour response to therapy in mice. *Radiology* 2004;232:685-692
8. Koh DM, Collins DJ. Diffusion-weighted MRI in the body: applications and challenges in oncology. *Am J Neuroradiol* 2007;188:1622-1635
9. Wang J, Takashima S, Takayama F, et al. Head and Neck lesions: Characterization with Diffusion-weighted Echo-planar MR Imaging. *Radiology* 2001;220:621-630
10. Vandecaveye V, De Keyzer F, Hermans R. Diffusion-weighted magnetic resonance imaging in neck lymph adenopathy. *Cancer Imaging* 2008;8:173-180
11. Dvorak HF, Nagy JA, Feng D, Brown LF, Dvorak AM. Vascular permeability factor/vascular endothelial growth factor and the significance of microvascular hyperpermeability in angiogenesis. *Curr Top Microbiol Immunol* 1999;237:97-132
12. Padhani AR. MRI for assessing antivascular cancer treatments. *Br J Radiol* 2003;76:S60-S80

13. Kvistad K, Rydland J, Vainio J, et al. Breast lesions: evaluation with dynamic contrast-enhanced T1-weighted MR imaging and with T2*-weighted first-pass perfusion MR imaging *Radiology* 2000;216:545-553
14. Tofts PS, Buckley DL, Evelhoch JL. Estimating kinetic parameters from dynamic contrast-enhanced T(1)-weighted MRI of a diffusable tracer: standardized quantities and symbols. *J Magn Reson Imaging* 1999;10:223-232
15. Port RE, Knopp MV, Brix G. Dynamic contrast-enhanced MRI using Gd-DTPA: interindividual variability of the arterial input function and consequences for the assessment of kinetics in tumors. *Magn Reson Med* 2001;45:1030-1038
16. Tofts PS, Kermode AG. Measurement of the blood-brain barrier permeability and leakage space using dynamic MR imaging. 1. Fundamental concepts. *Magn Reson Med* 1991;17:357-367
17. Leach MO, Brindle KM, Evelhoch JL, et al. Assessment of anti-angiogenic and anti-vascular therapeutics using magnetic resonance imaging: recommendations for appropriate methodology for clinical trials. American Association for Cancer Research 2003. Washington, D.C. 504
18. Brix G, Bahner ML, Hoffmann U, Horvath A, Shreiber W. Regional blood flow, capillary permeability, and compartmental volumes: measurements with dynamic CT – initial experience. *Radiology* 1999;210:269-276
19. Leach MO, Brindle KM, Evelhoch JL, et al. The assessment of antiangiogenic and antivascular therapies in early-stage clinical trials using magnetic resonance imaging: issues and recommendations. *Br J Cancer* 2005;92:1599-1610
20. O'Connor JP, Jackson A, Parker GJ, Jayson GC. DCE-MRI biomarkers in the clinical evaluation of antiangiogenic and vascular disrupting agents. *Br J Cancer* 2007;29:189-195
21. DeVries AF, Kremser C, Hein PA, et al. Tumor microcirculation and diffusion predict outcome for primary rectal carcinoma. *Int J Radiat Oncol Biol Phys* 2003;56:958-965
22. Mayr NA, Yuh WT, Arnholt JC, et al. Pixel analysis of MR perfusion imaging in predicting radiation therapy outcome in cervical cancer. *J Magn Reson Imaging* 2001;12:1027-1033
23. van Laarhoven HW, Klomp DW, Rijpkema M, et al. Prediction of chemotherapeutic response of colorectal liver metastases with dynamic gadolinium-DTPA-enhanced MRI and localized 19F MRS pharmacokinetic studies of 5-fluorouracil. *NMR Biomed* 2007;20:128-140

24. Jenkinson MD, Plessis DG, Walker C, Smith TS. Advanced MRI in the management of adult gliomas. *Br J Neurosurg* 2007;21:550-561
25. Cha S, Lu S, Johnson G, Knopp EA. Dynamic susceptibility contrast MR imaging: correlation of signal intensity changes with cerebral blood volume measurements. *J Magn Reson Imaging* 2000;11:114-119

Chapter 3:
Standardized methodological aspects common to the consecutive studies

3.1 Imaging techniques

3.1.1 MRI

The studies were performed on a 1.5T SONATA Vision MRI-scanner (Siemens, Erlangen, Germany) combining a standard head coil and two-channel dedicated surface neck coil. All sequences covered the entire head and neck ranging from the skull base to the thoracic inlet in order to allow the evaluation of the primary tumour and all nodal stations. The anatomical, DCE- and DWI sequences were scanned with identical geometry to allow for identification and comparison of corresponding primary tumours and lymph nodes. A transverse T2-weighted Turbo Spin-Echo (TSE)-sequence was acquired with 44 slices, 4 millimetre (mm) slice thickness, 0.4 mm intersection gap, Field of View (FoV) of 20x25 square centimetre (cm^2), matrix of 291x512, repetition time/echo-time (TR/TE) = 3080 milliseconds (ms)/106 ms, 2 averages, an echo-train length of 19 and a pixel resolution of 0.7x0.5x4.0 cubic millimetre (mm^3). The acquisition time was 5’42”. A transverse T1-weighted TSE-sequence was acquired with 44 slices, 4 mm slice thickness, 0.4 mm intersection gap, FoV of 20x25 cm^2, matrix of 250x512, TR/TE = 775 ms/8.3 ms, 3 averages, an echo-train length of 9 and a pixel resolution of 0.8x0.5x4.0 mm^3. The acquisition time was 4’55”. EPI DWI was acquired prior to contrast-injection in the transverse plane with 44 slices, bandwidth of 1502 (Hertz) Hz/pixel, 4 mm slice thickness, 0.4 mm intersection gap, FoV 20x25 cm^2, matrix of 104x128, TR/TE = 7100 ms/84 ms, 3 averages and a pixel resolution of 2.0x2.0x4.0 mm^3. Six b-values were applied (b=0, 50, 100, 500, 750 and 1000 s/mm^2). The acquisition time was 5’19”. All diffusion-sensitizing gradients were applied in 3 orthogonal directions, combined to create a 3-scan trace. An ADC-map was calculated using the built-in manufacturer’s software.

Critical to optimize image quality of the DWI; manual shimming was applied in an identical way in all patients. The inclusion of moving or air containing anatomical structures within the shim box was obviated. As such, the shim box was placed over the spine and muscles of the neck (Figure 1).

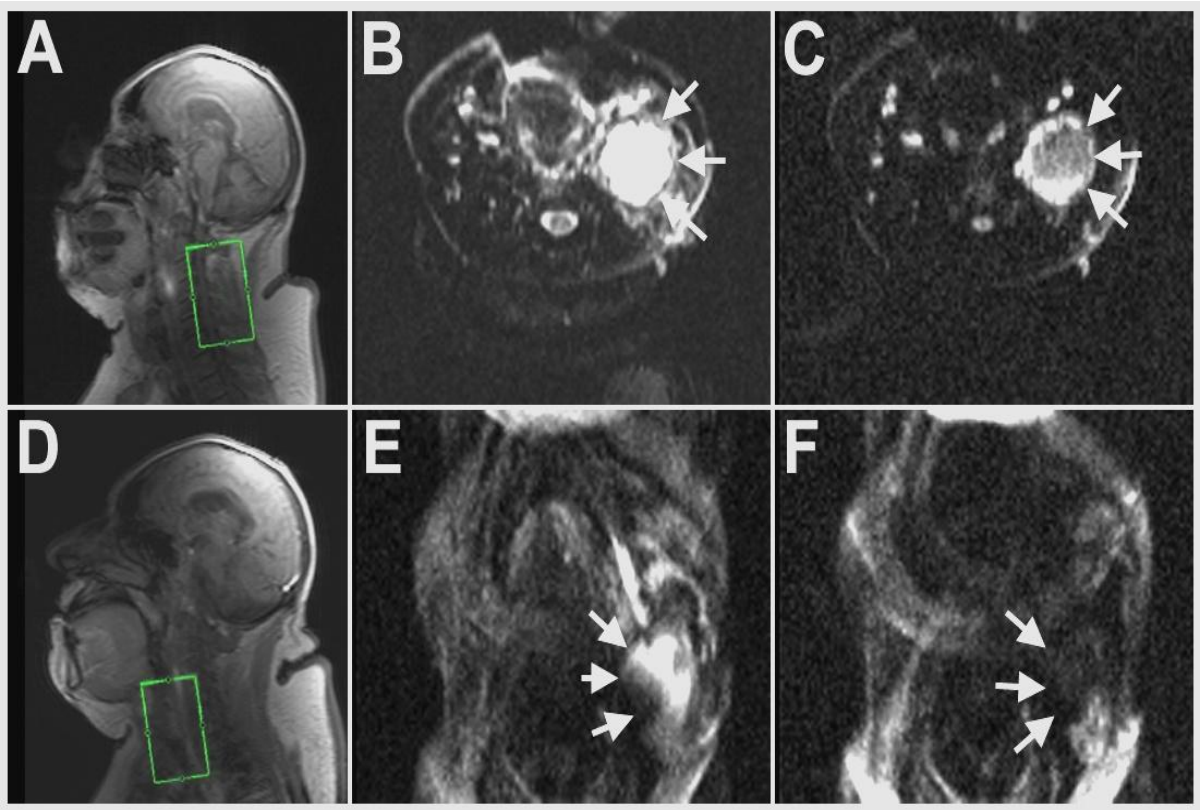

Figure 1: The effect of manual shim-optimization is shown in a representative patient with a large necrotic adenopathy in left level 2 (arrows): (A) the shim-box (green grid) is positioned in the area of the spine and posterior muscles of the neck, with (B,C) only limited artifacting visible on the b0 and b1000 images. (D) The shim-box is erroneously placed on the larynx, resulting in severe fat-shift and distortion artifacts. (E,F) The large necrotic adenopathy (arrows) is barely visible on the native b0 images and not visible on the b1000 images.

DCE-MRI was acquired using a three-dimensional T1-weighted gradient-echo sequence with fat saturation and consisted of 44 slices, 4 mm slice thickness, 0.4 mm intersection gap, 22.5x30 cm FoV, TR/TE of 4.3/1.6 ms. Twenty-five runs, each lasting 8.4 s were dynamically performed prior to, during and after the injection of a single-dose Gadolinium-benzyloxypropionictetra-acetate (Gd-BOPTA) (Multihance®, BRACCO, Milan, Italy). The T1-weighted sequence was repeated after intravenous administration in all patients with or without fat-suppression. Coronal and/or sagittal T1-weighted sequences with identical imaging parameters were applied after contrast agent administration, depending on the

localization of the primary tumour. All TSE-sequences were acquired by means of a partial Fourier factor of 5/8.

3.1.2 CT scan

Contrast-enhanced CT studies of the head and neck were performed, using a multidectector scanner (Sensation 16, Siemens, Erlangen, Germany). Collimation was 16x0.75 mm, feed/rotation 9.9 mm/s, tube voltage 120 (kilovolt) kV and output (mAs_{eff}) of 250. The effective slice thickness was 1.5 mm, the reconstruction interval 0.75 mm; adjacent axial and coronal slices were reformatted with a thickness of 3 mm parallel to and perpendicular on the true vocal cords.

3.1.3 FDG-PET/CT

Single-section, whole-body, spiral CT (85 mAs, 130 kV, slice thickness 5 mm, table feed 12 mm/rotation) was performed after intravenous injection of 120 millilitre (ml) of a contrast agent containing 300 milligram (mg) iodine/ml. PET-CT images were acquired 60 minutes after the intravenous administration of FDG at a dose of 305 millibecquerel (mBq). PET was performed with an in plane resolution of 4.6 mm and an axial field of view of 15.5 cm for each bed position. PET images were corrected for attenuation using the CT-data.

3.2 Image analysis

3.2.1 DWI

For all studies, DWI analysis was done on a PACS-workstation (Agfa-Gevaert, Mortsel, Belgium). The DWI images were analyzed in a first step by visual inspection of the native DWI-images with b-value 0 and 1000 s/mm² (b0- and b1000-images), in order to localize lesions at the primary site and lymph nodes. For quantitative assessment, regions of interest (ROI) were placed over lesions at the primary site and lymph nodes on the images with b-value of 0 s/mm² and automatically copied to the other b-value images by the software. As HNSCC has a high propensity for developing necrosis, quantitative assessment should be able to assess intralesional tissue heterogeneity. Therefore, ROI-delineation was guided by SI on the b1000 images. Native high b-value images allow to identify the separate tissue components. Currently, there is no agreement as to which b-value best delineates intact

tumoral tissue from necrosis or background tissue. Therefore, for this study, the native b1000 images were chosen to identify solid tumoral areas from background or necrosis as it is most likely that the suppression of T2 shine through effects in necrosis or fluid containing regions is most effective and that the volume of solid tumoral tissue cannot be overestimated due to remnant signal in necrotic areas.

For solid lesions at the primary site and solid sub- and supracentimetric lymph nodes, the ROIs were placed over the entire lesion (Figure 2). In the case of obvious solid and necrotic components on the DW images, ROIs were placed on the solid tumoral components according to their signal heterogeneity on the images acquired by a b-value of 1000 s/mm^2 (1,2) (Figure 3).

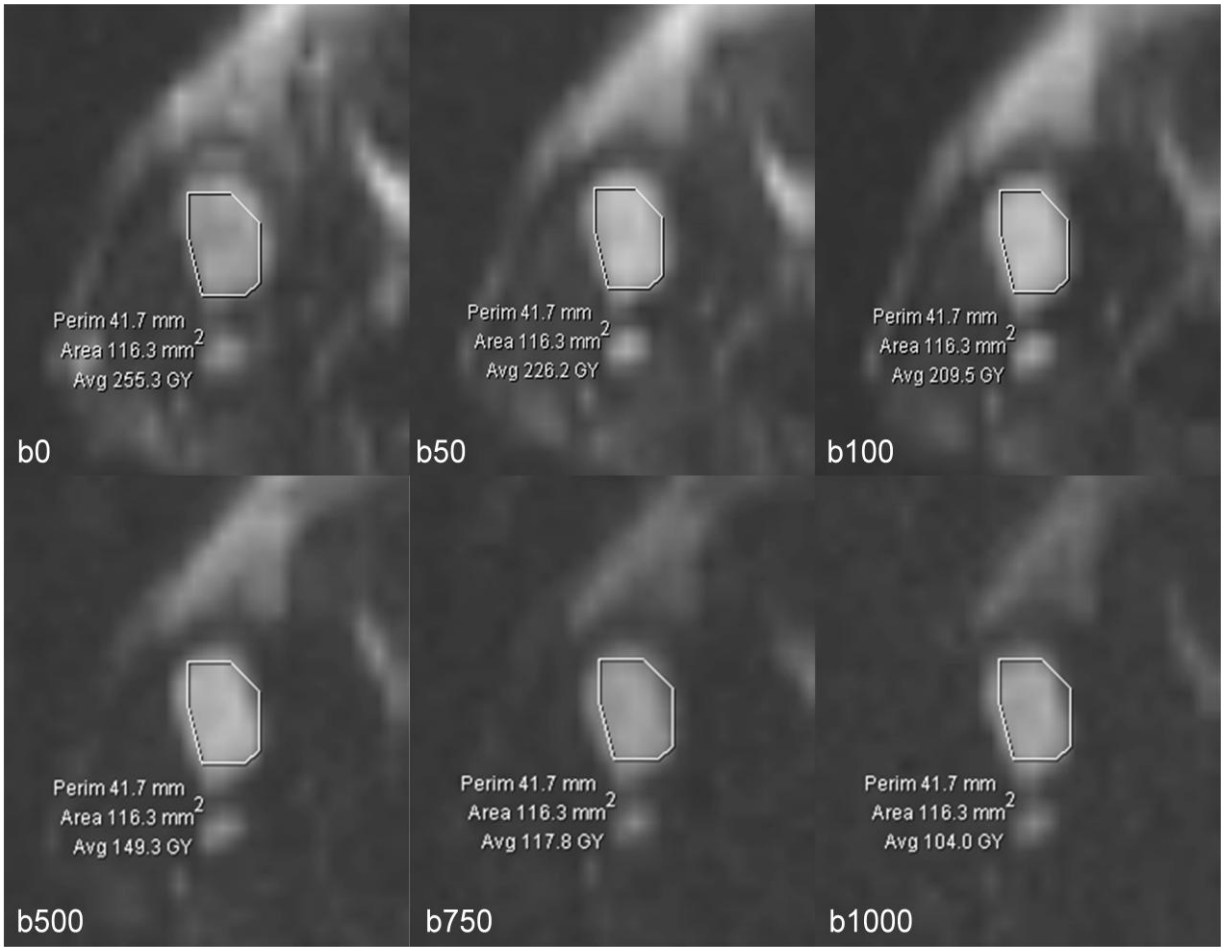

Figure 2: Regions of interest covers the entire lesion on the b0 image in a solid adenopathy and is automatically copied to the consecutive b-value images.

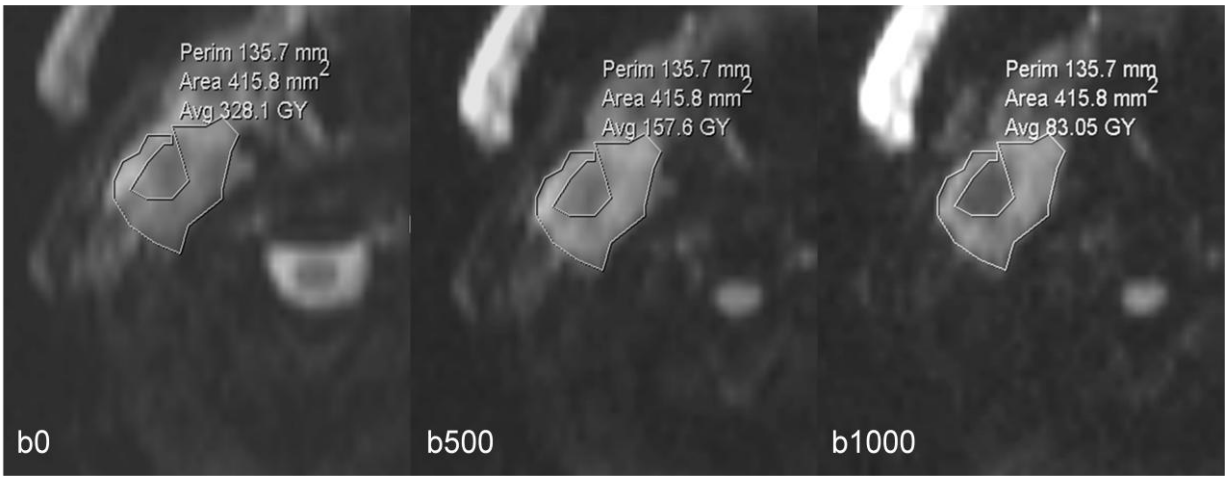

Figure 3: Region of interest covers the solid part of the lesion on the b0 image, guided by the hyperintensity on the b1000 image in a centrally necrotic adenopathy, and is automatically copied to the consecutive b-value images.

To reduce the effect of partial volume artifacts, the lowest size limit for ADC-calculation in a lesion was set to a minimal axial diameter of 4 mm. For each lesion, all ROIs were combined into a single ROI per lesion for each b-value and the average SI was then calculated for each b-value per delineated lesion (SI of *b*=0, 50, 100, 500, 750 and 1000 s/mm^2). The ADC was calculated from this range of b-values as described in paragraph 2.1 with an online calculator (Figure 4) developed in our department.

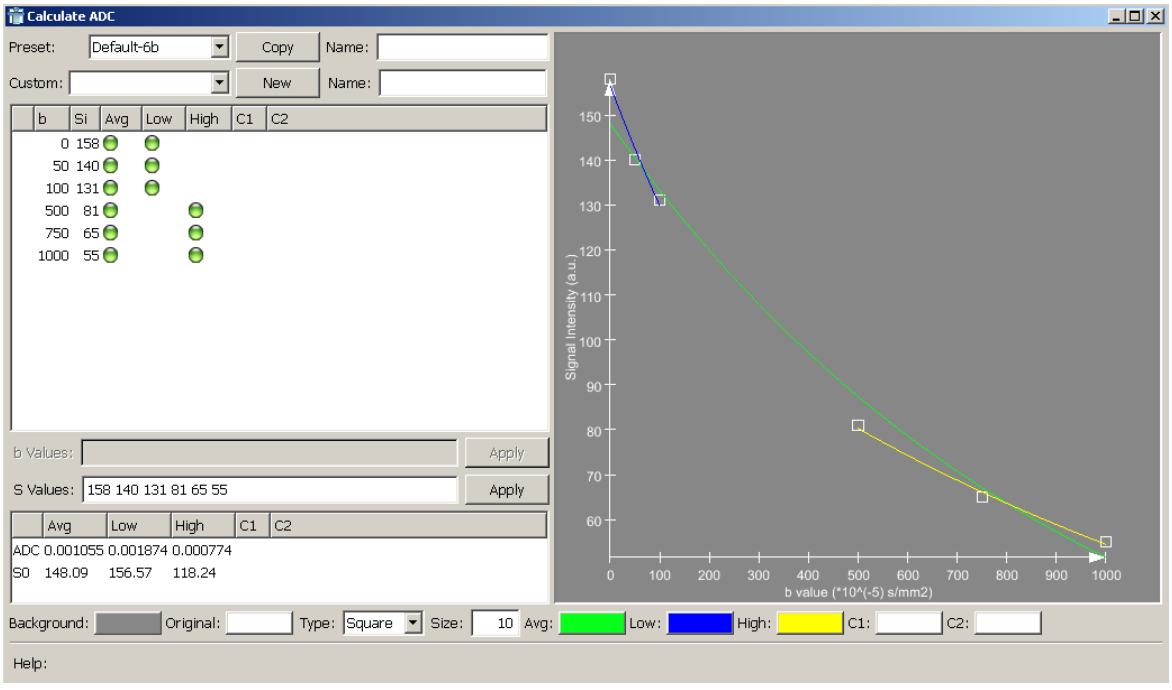

Figure 4: Online calculator used for standardized ADC-calculation in the study

3.2.2 DCE-MRI

The DCE-MRI was analyzed on an off-line workstation using dedicated software (BioMAP, Novartis Pharma AG, Basel, Switzerland).

DCE-MRI images were analyzed in a first step by visual inspection of the fifth scan run (arterial enhancement phase), in order to localize primary lesions and lymph nodes. For quantitative assessment, regions of interest (ROI) were placed over primary lesions and lymph nodes in these images and were automatically copied by the software to the other dynamic runs. Similar as for the DWI-images, in case of obvious solid and necrotic component identified by differences in contrast enhancement on the native DCE-MRI images, ROIs were placed on the separate tissue portions and the multiple ROIs were analyzed separately in order to study the influence of intralesional tissue heterogeneity on the acquired DCE-MRI signal.

Viable tumoral tissue was identified based on arterial enhancement on the native dynamic images. Solid tumoral parts were characterized as arterial enhancing tissue on the fifth scan run (arterial enhancement phase) while necrotic tumoral parts did not show early arterial enhancement. In case of solid lesions, ROIs were drawn over the entire lesion. For all ROIs, the SI on the separate dynamic runs were calculated and evaluated by semi-quantitative parameters: AS or wash-in ratio, washout ratio and c-peak or maximum enhancement. In order to normalize the data between the patients, the AIF was calculated out of a ROI on the common carotid artery.

3.2.3 CT scan – conventional MRI

In the studies involving lesion characterization, anatomical imaging data on CT studies and conventional MRI were interpreted by qualitative assessment. The CT scans were evaluated for tissue changes at the primary site such as tissue asymmetry, presence of a mass and/or pathologic contrast enhancement. The nodal status was determined using nodal diameter, nodal morphology and contour and the presence of intranodal in homogeneity (3).

In the studies involving per-treatment follow-up and –prediction, anatomical imaging data were analyzed by volumetric assessment. For each identified lesion, contours were drawn around the lesion border at each slice position (Figure 5). Subsequently, the volume of each lesion was calculated with the following equation:

$$(\sum \textit{surface at each slice position}) * (\textit{slice thickness} + \textit{interslice gap})$$

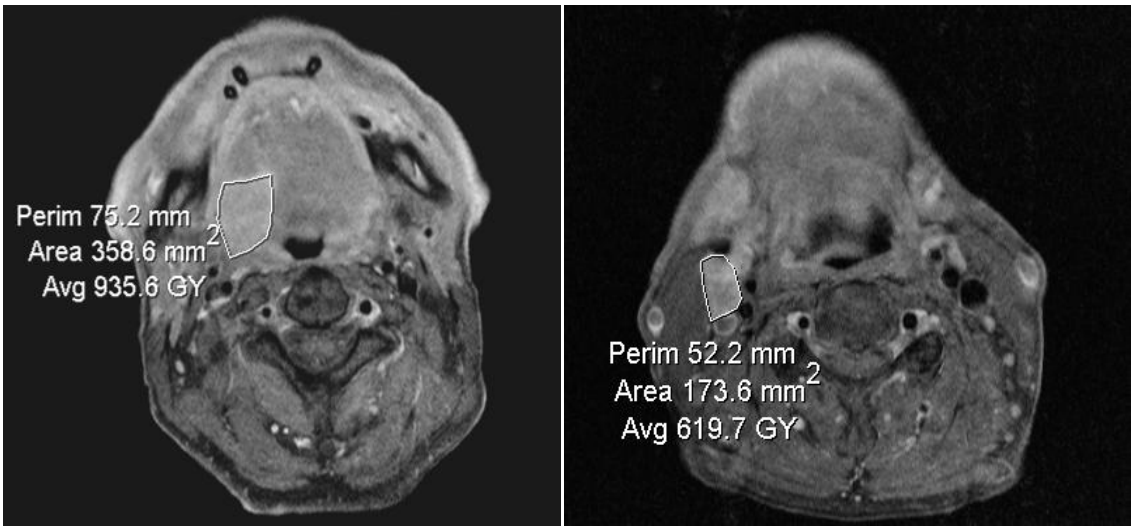

Figure 5: Region of interest delineation in volumetric assessment of primary tumour in the right base of tongue.

In the studies involving early post-treatment assessment, primary tumour site and nodal analysis was based on scoring systems accepted by literature. For primary lesions, anatomical imaging variables included tissue asymmetry or mass (grade 0: no detectable focal abnormality, grade 1: anatomic asymmetry or discrete mass < 10 mm, grade 2a: mass > 10 mm, or 2b, <50% reduction of largest dimension), T2-weighted SI and contrast enhancement. CT imaging variables consisted of tissue asymmetry or mass and contrast enhancement (4).

Lymph nodes were evaluated based on diameter (1 cm short axis respectively 1.5 cm long axis threshold), presence of intranodal focal defects, focal contrast enhancement or calcifications (5,6).

3.2.4 FDG-PET/CT

In the current setting of the thesis, the clinical FDG-PET/(CT) was only used in the studies involving lesion characterization. PET images were qualitatively evaluated. Standard uptake value (SUV) is not routinely used at our institution and was not applied for determination of PET results. Focal areas of increased FDG-uptake were correlated to the co-registered CT and increased uptake of FDG, not related to physiological uptake or treatment effects, was interpreted as positive for tumour.

3.3 Reference standard

3.3.1 Historadiological correlation and histopathological analysis

After surgery, the resection specimens of primary lesions were oriented and tagged in the craniocaudal and were subsequently sectioned in macroslides oriented along the plane of the transverse MRI images. Histopathological analysis of the primary lesions was done by haematoxylin and eosin (HE) staining.

In the neck dissections, the borders of each nodal neck level in the fresh neck dissection specimens were carefully delineated and tagged by the surgeon according to the AAO-HNS criteria (7) (Figure 6).

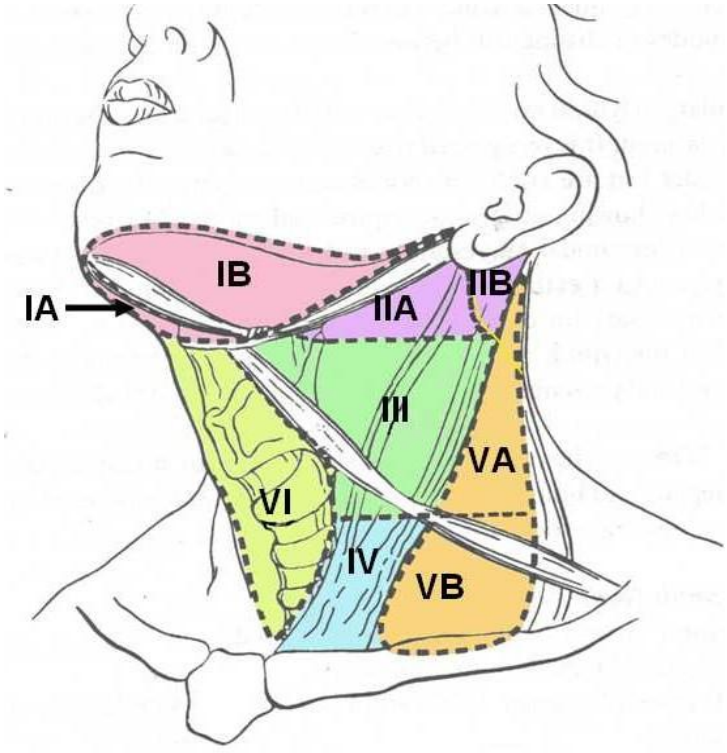

Figure 6: Separation of nodal stations in different levels according to Standardized neck dissection terminology. According to the official report of the Academy's Committee for Head and Neck Surgery and Oncology.

This additional orientation of the neck dissection aimed to facilitate the identification of separate lymph nodes by means of the borders of each separate neck level. To allow identification of small lymph nodes by palpation, the neck dissection specimens were subsequently fixated in 5% formaldehyde for 24 hours, which enables palpation of small lymph nodes as a firmly consistent structure while surrounding fatty tissue can easily be

compressed. Subsequently, the fixated neck dissection specimen was attached to a hardboard in order to approach its anatomical configuration. First, the different lymph nodes were localized in correlation to adjacent anatomical structures, being the submandibular gland, the sternocleidomastoid muscle and the jugular vein. Then, the specimens were axially transected in 4 mm transverse sections corresponding to the plane of the T1-weighted images. Per slice, the lymph nodes were palpated and progressively dissected from the resection specimen while being matched to their corresponding position on the T1-weighted images. Subsequently, each lymph node was put in a separate small plastic container, to allow for precise historadiological correlation with the co-registered conventional MRI and DWI sequences per lymph node. The remaining specimens were then scrutinized by the pathologist for remaining lymph nodes not clearly identified on the imaging studies. All lymph nodes were sectioned with 5 μm slice thickness every 3 mm.

Next to HE staining, prekeratine immunohistochemical staining was applied to improve the detection of micrometastases, defined as nodal tumour deposits smaller than 3 mm (8).

3.3.2 Follow-up and correlation to long-term treatment outcome

In case no histopathological specimen could be obtained, imaging results were correlated to long-term follow-up. As the majority of locoregional tumour recurrences occur within the first 2 years after the end of treatment, the 2-year clinical LRC was chosen as primary endpoint.

Clinical follow-up of the patients was done by radiation oncologists and head and neck surgeons in a joint clinic. The first year after irradiation, the patients were seen clinically every 2 months; the second to third year every 3 to 4 months; from the third year on, once a year. A baseline CT study was performed at 4 months post-CRT. Thereafter, in the absence of signs of persistent or recurrent tumour, a CT study was done yearly or at the discretion of the treating clinician. As such, 2-year LRC as endpoint was defined by the routinely implemented CT study and simultaneous clinical evaluation. Patients did not receive routine neck dissections after treatment, although surgery was considered in patients suspect of residual nodal disease or primary tumour recurrence.

In case of negative biopsy in persistent lesions, clinical and imaging follow-up was continued to evaluate lesion evolution and determine further patient management. Complete remission (CR) was defined as a persistent clinical complete regression of the primary lesion and adenopathies for 2 years follow-up.

Tumour recurrence was defined as a persisting or recurrent primary lesion or adenopathy within the first two years after the end of CRT, consisting of 1) a diameter increase of more than 30% or volume increase of ≥ 65% (9) on serial imaging and 2) histopathological proof of HNSCC on biopsy and/or surgical specimen.

3.4 Estimation of study population size and number of patients included

Study 1: lymph node staging – total included: 33 patients

Sample size estimation was based on preliminary data (10). The sample size estimations were based on a significance level of 0.05 and a power of 0.8, and on the mean differences and standard deviations found in the pilot studies. For an average ADC value of 1.20 x 10^{-3} mm^2/s for benign nodes and 0.80 x 10^{-3} mm^2/s for malignant nodes, with a standard deviation of 0.40 x 10^{-3} mm^2/s, a sample size of 16 patients per group (malignant versus non-malignant) was required, or 32 patients in total.

Study 2: Post-chemoradiotherapy tissue differentiation – total included: 26 patients

For the unpaired Student's t-test, sample size estimation was based on a published small data set of our group regarding DWI for the evaluation of the larynx for tumour recurrence after radiotherapy (11). The reported ADC values averaged to 0.90±0.09 x 10^{-3} mm^2/s for recurrences and 1.64±0.25 x 10^{-3} mm^2/s for benign tissue alterations. Using α of 0.05, a power of 0.8, and a standard deviation of 0.50 x 10^{-3} mm^2/s, to avoid sample size underestimation from the low standard deviation of the small test dataset, at least 8 patients should be included in each group (tumour recurrence versus inflammation/necrosis), or 16 patients in total.

For the DCE-MRI parameters, no data were available prior to study inclusion. Therefore, a difference of 30% between recurrence and benign tissue alterations with a standard deviation of 20% was estimated for the DCE-MRI parameters (c-peak, AS, washout). With a significance level of 0.05 and power of 0.8 this leads to an sample size estimation of 8 patients per group (tumour recurrence versus inflammation/necrosis), or 16 in total.

Study 3: Imaging during treatment – total included: 30 patients

Study 4: early post-treatment imaging – total included: 29 patients

For the Mann-Whitney test between lesions with CR and those with later recurrence, sample size estimation was performed using an average ADC increase of 50% (50% decrease on DCE-MRI) for CR lesions, and 0% change of functional parameters for lesions with later recurrence, always compared to their baseline values. For $\alpha = 0.05$, power = 0.8, and a standard deviation of 40% (of baseline value) a sample size of 11 patients per group (CR versus later recurrence) was required, or 22 patients in total.

3.5 References

1. Razek A, Soliman N, Elkhamary S, Alsharaway M, Tawfik A. Role of diffusion-weighted MR imaging in cervical adenopathy. *Eur Radiol* 2006;16:1468-1477
2. Wang J, Takashima S, Takayama F, et al. Head and Neck lesions: Characterization with Diffusion-weighted Echo-planar MR Imaging. *Radiology* 2001;220:621-630
3. Castelijns JA, van den Brekel MW. Imaging of lymphadenopathy in the neck. *Eur Radiol* 2002;12:727-738
4. Ljumanovic R, Langendijk JA, Hoekstra OS, Knol DL, Leemans CR, Castelijns JA. Pre- and post-radiotherapy MRI results as a predictive model for response in laryngeal carcinoma. *Eur Radiol* 2008;18:2231-2240
5. Liauw SL, Mancuso AA, Amdur RJ, et al. Postradiotherapy neck dissection for lymph node-positive head and neck cancer: the use of computed tomography to manage the neck. *J Clin Oncol* 2006;24:1421-1427
6. Castelijns JA, van den Brekel MW. Imaging of lymphadenopathy in the neck. *Eur Radiol* 2002;12:727-738
7. Robbins KT, Medina JE, Wolfe GT, et al. Standardizing neck dissection terminology. Official report of the Academy's Committee for Head and Neck Surgery and Oncology. *Arch Otolaryngol Head Neck Surg* 1991;117:601-605
8. van den Brekel MW, van der Waal I, Meijer CJ, Freeman JL, Castelijns JA, Snow GB. The incidence of micrometastases in neck dissection specimens obtained from elective neck dissections. *Laryngoscope* 1996;106:987-991
9. Padhani AR, Ollivier L. The RECIST (Response Evaluation Criteria in Solid Tumors) criteria: implications for diagnostic radiologists. *Br J Radiol* 2001;74:983-986
10. Vandecaveye V, De Keyzer F, Vander Poorten V, Nuyts S, Hermans R. Diffusion-weighted magnetic resonance imaging for discrimination of malignant and benign lymph nodes in primary head and neck squamous cell carcinoma: preliminary results. Radiological Society of North America, RSNA 2005, Chicago, USA; abstract
11. Vandecaveye V, De Keyzer F, Vander Poorten V, et al. Evaluation of the larynx for tumour recurrence by diffusion-weighted MRI after radiotherapy: initial experience in four cases. *Br J Radiol* 2006;79:681-687

Chapter 4:
DWI for differentiation of benign and metastatic lymph nodes in HNSCC

4.1 Introduction

Nodal metastases are an adverse prognostic factor in patients with HNSCC requiring accurate detection for optimization of treatment (1). The ability to allow tissue differentiation based on changes in T2 or T1 relaxation has been explored for its potential additional value to anatomical criteria for lymph node differentiation (3). However, differences in T1 and T2 relaxation do not allow for reliable differentiation of benign and metastatic lymph nodes. This is most likely due to the lack of a straightforward relationship between tissue cellularity and T1 or T2 relaxation and technical factors that increase T2- or T1-SI like arbitrary scaling and dependence of coil position (4). Therefore, similarly as CT, MRI needs to rely on size-related and morphological criteria for nodal differentiation and the technique has generally shown similar or slightly inferior results compared to CT (5).

Efforts are ongoing to increase the accuracy of MRI, by using USPIO or by exploiting tumour-induced metabolic, vascular or microstructural changes (6,7,8). A number of prior studies have reported on DWI to detect nodal metastases in HNSCC but have mainly focused on enlarged lymph nodes while the therapeutic impact lays in the additional detection of subcentimetric adenopathy. Moreover, the results of these studies are conflicting regarding ADC-values attributed to benign respectively metastatic lymph nodes (9,10,11).

The aim of this study is to evaluate the value of DWI for the detection of nodal metastases in HNSCC. Additionally, DWI will be compared to conventional MRI and FDG-PET in order to evaluate the additional value of DWI, especially for the differentiation of subcentimetric lymph nodes.

4.2 Materials and Methods

4.2.1 Patient selection and study design

The study was approved by the local ethics committee and all patients gave written informed consent prior to inclusion. From July 2004 to May 2006, 36 patients (age ranging from 48 to 81 years) scheduled for surgical treatment of biopsy-proven HNSCC were prospectively and consecutively included. Patients were included irrespective of clinical T-stage, N-stage, or tumour localization (Table 1). The criteria for T-staging of HNSCC depend on the anatomical subsite from where the primary tumour originates; it is mainly determined by the size of the tumour, depth of invasion and involvement of critical structures, such as the carotid artery. The N-staging of HNSCC is determined by the size, number and localisation of the adenopathies (12). Two patients had to be excluded due to conversion to non-surgical treatment and one patient because of diagnostic excision of a neck node prior to surgical treatment. None of the patients had previously been diagnosed with or treated for head and neck cancer. Thirty-three patients underwent conventional MRI and DWI. Additionally, 11 patients of this group underwent FDG-PET-CT. In none of the patients did major artifacts occur in the DWI-sequence requiring exclusion.

Conventional or TSE-MRI was read blinded from the DWI-images at the time of patient inclusion. The time delay between the reading of conventional imaging, topographic correlation of the neck dissection specimens and the later blinded reading of the DWI images was 18 ± 6 months on average. Similarly to conventional MRI, the FDG-PET-CT examinations were read blinded from the other examinations at the time of patient inclusion. Histological analysis was performed blinded from patient identity 3 months prior to the blinded reading of the DWI images. Historadiological correlation was done after all image analysis had been completed. Histopathology, with prekeratine-immunohistochemical staining was used as a standard reference. A detailed timeline shows the different methodological steps (Figure 1).

Patient	Primary tumour	Histopathology	TSE-MRI	DWI	PET-CT
Patient 1	Nasal cavity/T2	N2b	N2a	N2b	N2a
Patient 2	Supraglottis/T3	N2b	N2b	N2b	N2a
Patient 3	Floor of mouth/T4a	N0	N1	N0	
Patient 4	lateral oropharyngeal wall/T3	N2c	N2b	N2c	N2b
Patient 5	Glottis/T3	N1	N0	N1	
Patient 6	Glottis/T3	N0	N2b	N2b	
Patient 7	Supraglottis/T4a	N2c	N2b	N2c	
Patient 8	Oral tongue/T2	N2b	N0	N2b	
Patient 9	Glottis/T3	N0	N0	N0	
Patient 10	Glottis/T4	N0	N0	N1	N0
Patient 11	Base of tongue/T3	N2c	N2b	N2c	N2b
Patient 12	Glottis/T3	N0	N0	N0	
Patient 13	Oral tongue/T3	N0	N0	N1	
Patient 14	Floor of mouth/T2	N0	N0	N0	
Patient 15	Floor of mouth/T2	N1	N1	N1	
Patient 16	Base of tongue/T2	N2b	N2b	N2b	N2b
Patient 17	Glottis/T3	N0	N0	N0	
Patient 18	Glottis/T4	N1	N0	N1	
Patient 19	Floor of mouth/T3	N2c	N2b	N2c	
Patient 20	Oral tongue/T3	N2b	N2b	N2b	N2b
Patient 21	Oral tongue/T2	N0	N1	N1	
Patient 22	Glottis/T4a	N1	N0	N0	
Patient 23	Hypopharynx/T4	N0	N2b	N0	N0
Patient 24	Supraglottis/T3	N1	N0	N1	
Patient 25	Oral tongue/T2	N0	N0	N0	
Patient 26	unknown/TX	N2b	N2b	N2b	N2b
Patient 27	Floor of mouth/T2	N0	N0	N0	
Patient 28	Oral tongue/T4	N2b	N2b	N2b	N2b
Patient 29	Oral tongue/T2	N2b	N0	N2b	
Patient 30	Oral tongue/T4	N2b	N2b	N2b	N2b
Patient 31	Lateral oropharyngeal wall/T3	N2b	N1	N2c	
Patient 32	Floor of mouth/T2	N2b	N0	N1	
Patient 33	Floor of mouth/T4a	N2c	N2c	N2c	

Table 1: Localization, clinical T-classification and N-staging respectively based on histopathology, turbo-spin echo (TSE)-MRI, diffusion-weighted MRI (DWI), and in the patient subgroup for PET-CT of included patients, according to the guidelines of the International Union Against Cancer.

Histopathology, with prekeratine-immunohistochemical staining was used as a standard reference. A detailed timeline shows the different methodological steps (Figure 1).

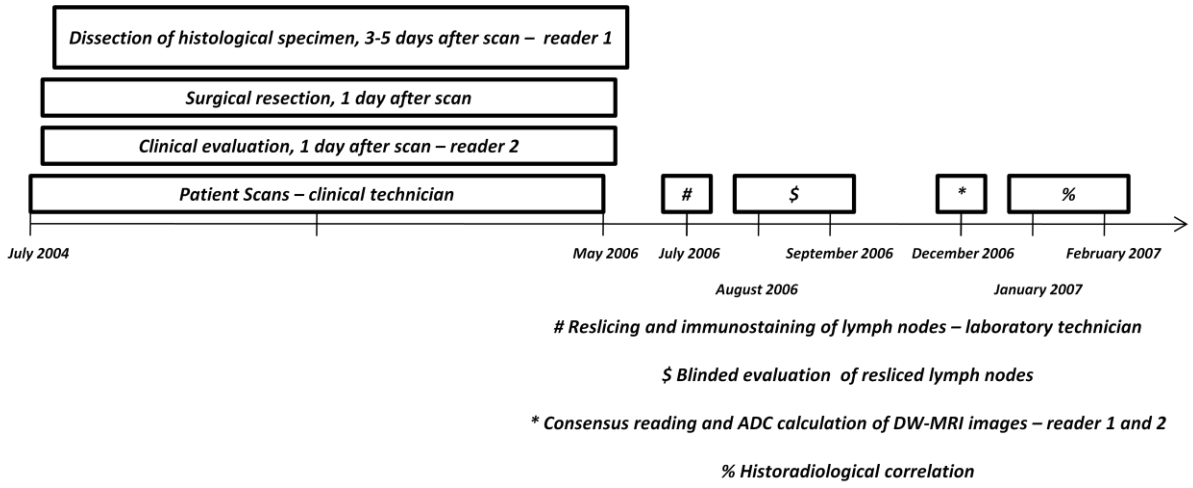

Figure 1: Timeline detailing the exact set-up of study inclusion and data processing used in this study.

4.2.2 Imaging technique

All patients underwent the standardized anatomical and DWI-sequences as described in chapter 3. MRI imaging covered the entire head and neck ranging from the base of skull to the thoracic outlet, and included all regional nodal stations (retropharyngeal space and neck levels).

The 12 patients undergoing FDG-PET-CT were scanned with the standard clinical protocol, described in chapter 3. The imaging protocol consisted of a whole body protocol.

4.2.3 Image analysis

The images of the TSE-MRI, DWI and FDG-PET-CT were interpreted in a blinded fashion. The TSE-MRI was interpreted by a head and neck radiologist with 15 years of experience, prior to surgery as described in chapter 3.3.3. Lymph nodes were differentiated based on the standardized criteria for pretherapeutic nodal characterization as described in chapter 3.3.3. The cut-off point for nodal diameter between benign and malignant lymph nodes was set to 10 mm, according to literature (13,14). Definite diagnosis was made based on the combined findings of plain T1-weighted, T2-weighted and contrast-enhanced T1-weighted images.

The DWI images were quantitatively interpreted by two radiologists in consensus (both 4 years of experience in head and neck DWI) as described in chapter 3.3.1. Nodal status was differentiated solely based on the ADC.
FDG-PET-CT images were qualitatively interpreted by an experienced nuclear medicine staff physician as described in chapter 3.3.4.

4.2.4 Topographic correlation and histopathological analysis

Topographic correlation and histopathological analysis was performed according to the standardized methodology as described in chapter 3.4.1.

4.2.5 Historadiological correlation and comparison of different imaging modalities

Historadiological correlation was done after all image interpretation had been concluded. Historadiological correlation of DW- and conventional MRI was done per lymph node. The optimal threshold for $ADC_{b0\text{-}1000}$ between benign and malignant lymph nodes was obtained with receiver-operating-characteristics (ROC). The imaging appearance of benign and metastatic lymph nodes on conventional MRI was documented in correlation to nodal size, internal contrast enhancement and nodal contour. Subsequently, sensitivity, specificity and accuracy of conventional MRI and DWI were calculated. For historadiological correlation, the PET-CT images were correlated per level seen the lower spatial resolution and the suboptimal settings of full-body CT for detailed evaluation of the head and neck. Levels with pathologic lymph nodes were documented and sensitivity, specificity and accuracy were calculated. Accuracy per lymph node for DWI and conventional MRI was compared for all lymph nodes and for supra- and subcentimetric lymph nodes separately. Accuracy of both techniques was compared per level for lymph nodes. Finally, the N-stage obtained with DWI and the N-stage obtained by TSE-MRI were compared with the histopathological N-stage.
In a subpopulation of 11 patients where FDG-PET-CT was performed, FDG-PET-CT, conventional MRI and DWI were compared per level and per hemi-neck. The N-stage obtained with the three techniques was also compared with the histopathological N-stage.

4.2.6 Statistical analysis

Statistical analysis was done with Microsoft Excel 9.0 (Microsoft Corporation, Washington, US) and SPSS 11.0 for Windows (SPSS Inc., Chicago, Illinois, US). Numerical data are reported as means ± standard deviation (SD). An unbalanced two-way analysis of variance (ANOVA) was used to compare the ADC-values of metastatic with benign lymph nodes, with ADC-values as the dependent variable, benign/metastatic as independent variable, and the patient identifier as blocking factor. The different imaging modalities were compared using paired observations and McNemar's test.

4.3 Results

4.3.1 Histopathology

The localization and clinical T-stage of the primary tumours as well as the histopathological N-stage per patient is shown in Table 1. There were 13 unilateral neck dissections and 20 bilateral neck dissections. In total 650 lymph nodes were dissected. Of these 650, 301 lymph nodes were identified by DWI, all larger or equal to 4 mm in size. The total number of metastatic lymph nodes was 76 (74 larger or equal to 4 mm and 2 smaller). Ten lymph nodes, all smaller than 8 mm, contained micrometastases. The distribution of metastases per nodal size is shown in Table 2.

4.3.2 Historadiological correlation

4.3.2.1 Conventional MRI

The imaging appearance of metastatic and benign lymph nodes in correlation to nodal size is shown in Figure 2. The majority of nodal metastases detected by TSE-MRI were larger than 1 cm. Three subcentimetric nodal metastases were detected based on aberrant contrast enhancement. An irregular nodal contour was only apparent in enlarged metastatic lymph nodes, as well as in a limited number of enlarged benign lymph nodes. The majority of subcentimetric metastatic lymph nodes showed no distinct morphological abnormalities indicative of malignancy. TSE-MRI showed 34 true positives (TP), 10 false positives (FP), 217 true negatives (TN) and 40 false negatives (FN), yielding a sensitivity of 46%, a specificity of 96% and an accuracy of 83% per lymph node.

4.3.2.2 DWI

The $ADC_{b0\text{-}1000}$ was significantly lower for metastatic than for benign lymph nodes. The $ADC_{b0\text{-}1000}$ for benign lymph nodes was 1.19±0.22 x 10^{-3} versus 0.85±0.27 x 10^{-3} mm^2/sec for malignant ($p<0.0001$) (Figure 3.a). The optimal threshold of 0.94 x 10^{-3} mm^2/sec based on ROC-analysis (Figure 3.b), resulted in 62 TP, 14 FP, 213 TN and 12 FN, yielding a sensitivity of 84%, a specificity of 94% and an accuracy of 91%.

Nodal diameter	Number of LN	number of metastatic LN	Prevalence*
> 10 mm	42	32	76%
4-9 mm	259	42	16%
< 4mm or undetected on MRI	349	2	0.6%

* Prevalence calculated as the ratio of metastatic lymph nodes versus total number of lymph nodes in the same size category

Table 2: Pathological distribution of metastases according to nodal size.

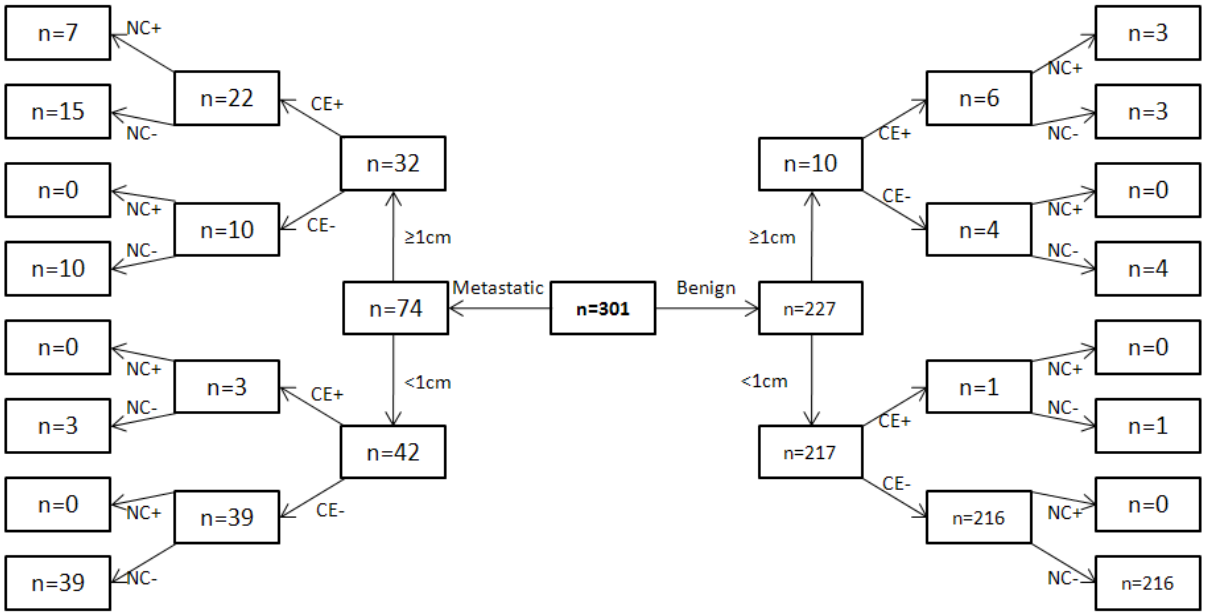

Figure 2: Correlation of histologically proven metastatic and benign lymph nodes to their imaging appearance on turbo-spin echo (TSE)-MRI. The criteria are: nodal size larger than or equal to 1cm, heterogeneous contrast enhancement (CE+) and irregular nodal contour (NC+). Note that the majority of subcentimetric nodal metastases does not show any morphological changes indicative of malignancy. The benign enlarged lymph nodes show a variable internal contrast enhancement and nodal contour.

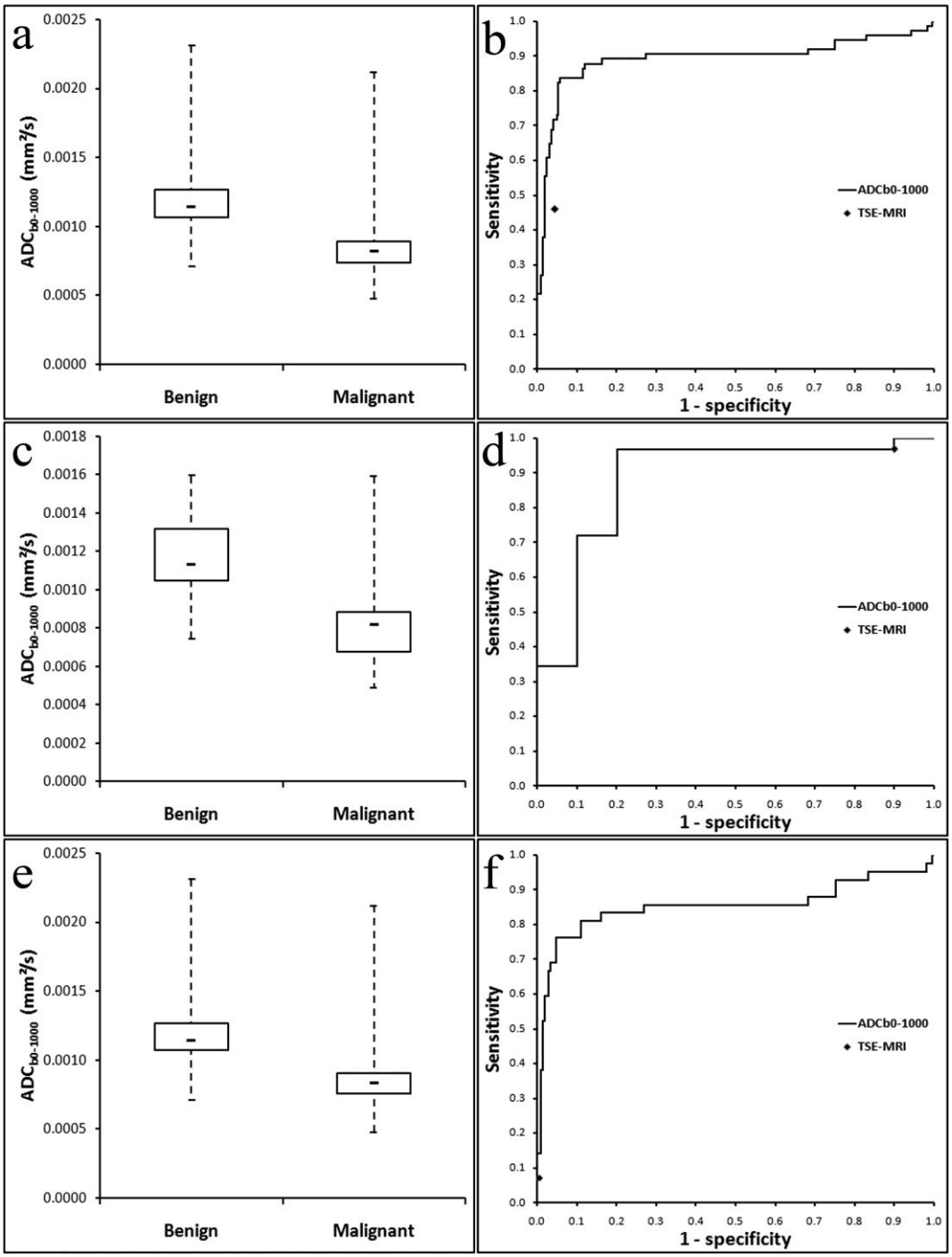

Figure 3: Box-whisker plots of apparent diffusion coefficient ($ADC_{b0-b1000}$) (a) for all lymph nodes, (c) lymph nodes larger or equal to 10 mm and (e) lymph nodes ranging from 4 to 9 mm between metastatic and benign lymph nodes. ADC-values were significantly lower for metastatic than for benign lymph nodes. Box-whisker plots are presented with median (-), interquartile range (box) and minima/maxima. Receiver operator curves are shown for $ADC_{b0-1000}$ (b) for all lymph nodes, (d) lymph nodes larger or equal to 10 mm and (f) lymph nodes ranging from 4 to 9 mm. Results of turbo-spin echo (TSE)-MRI using a combination of nodal size, morphology and contrast enhancement are indicated with a point. Note the markedly higher specificity of DWI for enlarged lymph nodes, while the sensitivity is substantially higher for lymph nodes ranging from 4 to 9 mm.

4.3.2.3 FDG-PET

In the subgroup of 12 patients, sixteen levels showed an FDG-avid lymph node corresponding to a histologically proven metastasis. Twelve of sixteen lymph nodes were supracentimetric, while 4 were subcentimetric, without any internal morphological alterations. Eight levels containing histologically proven lymph nodes could not show any FDG-avid lesions. All these lymph nodes were subcentimetric. One level showed an FDG-avid lymph nodes, which was negative on histopathology. Per level, FDG-PET-CT showed a sensitivity of 67%, specificity of 98%, accuracy of 86%, positive predictive value (PPV) of 94% and NPV of 83%. Additionally, PET-CT indicated 4 lesions suspect for tumour in four separate patients, respectively 1 in a mediastinal lymph node, 1 in the lung 2 and 2 in the large intestine. Neither of the lesions could be confirmed as a progressive tumoral location after additional examinations or during imaging follow-up (colonoscopy, chest CT).

4.3.3 Comparison of DWI and conventional MRI

4.3.3.1 DWI and TSE-MRI per lymph node and per level

Overall sensitivity, specificity, accuracy, PPV and NPV per node and per level for both techniques are shown in Table 3. Sensitivity per lymph node and per level is significantly higher for DWI than for conventional MRI ($p<0.0001$), while no significant difference in specificity is found per lymph node ($p=0.66$) and per level ($p=1$).

Per node	$ADC_{b0\text{-}1000}$	MRI	Per level	$ADC_{b0\text{-}1000}$	MRI
True positive	62	34	True positive	44	27
False positive	14	10	False positive	6	10
True negative	213	217	True negative	212	208
False negative	12	40	False negative	3	20
Sensitivity	84%	46%	Sensitivity	94%	57%
Specificity	94%	96%	Specificity	97%	95%
Accuracy	91%	83%	Accuracy	97%	89%
PPV*	82%	77%	PPV	88%	73%
NPV#	95%	84%	NPV	99%	91%

* Positive predictive value; # Negative predictive value

Table 3: Comparison of apparent diffusion coefficient ($ADC_{b0\text{-}1000}$) with conventional MRI per node and level for all lymph nodes with historadiological correlation (size >= 4mm)

The differences in N-stage are shown in Table 1. Compared to TSE-MRI, DWI led to a correct change in nodal staging in 13/33 patients (39%). Two patients were downstaged from N1 to N0. In 4 patients a contralateral metastasis was diagnosed, initially undetected on pre-operative imaging (Figure 4).

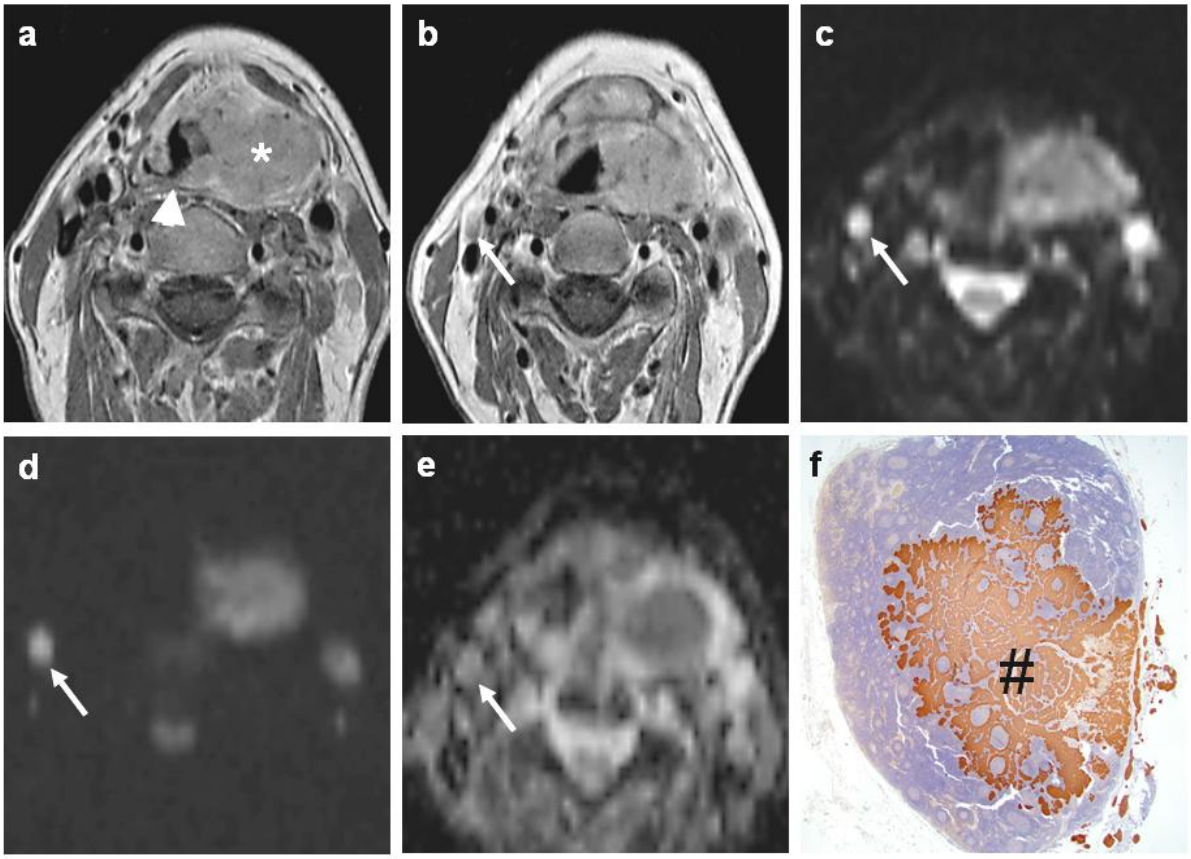

Figure 4: (a) Gadolinium-enhanced T1-weighted turbo-spin echo (TSE) images show large left-sided tumoral mass (*), centred on the piriform sinus involving the supraglottis and crossing the midline on the posterior pharyngeal wall (arrowhead). (b) A small oval-shaped lymph node is seen in level two on the right side, having a shortest transverse diameter of 0.6 cm (arrow); this lymph node was considered negative on TSE-MRI. (c) The lymph node is hyperintense on the b0 diffusion-weighted image (arrow) and (d) shows only limited loss of signal on the b1000 image (arrow), (e) corresponding to an apparent diffusion coefficient (ADC) of 0.71 x 10^{-3} mm^2/sec (arrow); these findings are suspect for metastatic adenopathy. (f) Histopathological slice with prekeratine staining (magnification factor=150) shows intranodal metastatic deposit (#).

Six patients with a pre-operative N0-neck were upstaged: three patients with laryngeal cancer to N1 or N2b, two patients with tongue cancer to N2b and one patient with a floor of mouth cancer to have an ipsilateral metastasis. In one patient with floor of mouth cancer, a contralateral lymph node in level 2 suspect on TSE-MRI was correctly diagnosed as benign on DWI, limiting the extent of the contralateral neck dissection (Figure 5). DWI led to a wrong nodal staging in 4/33 patients (12%). Two patients were falsely upstaged from N0 to N1. DWI failed to downstage one patient correctly from N1 to N0. One patient was falsely upstaged as having a contralateral metastasis.

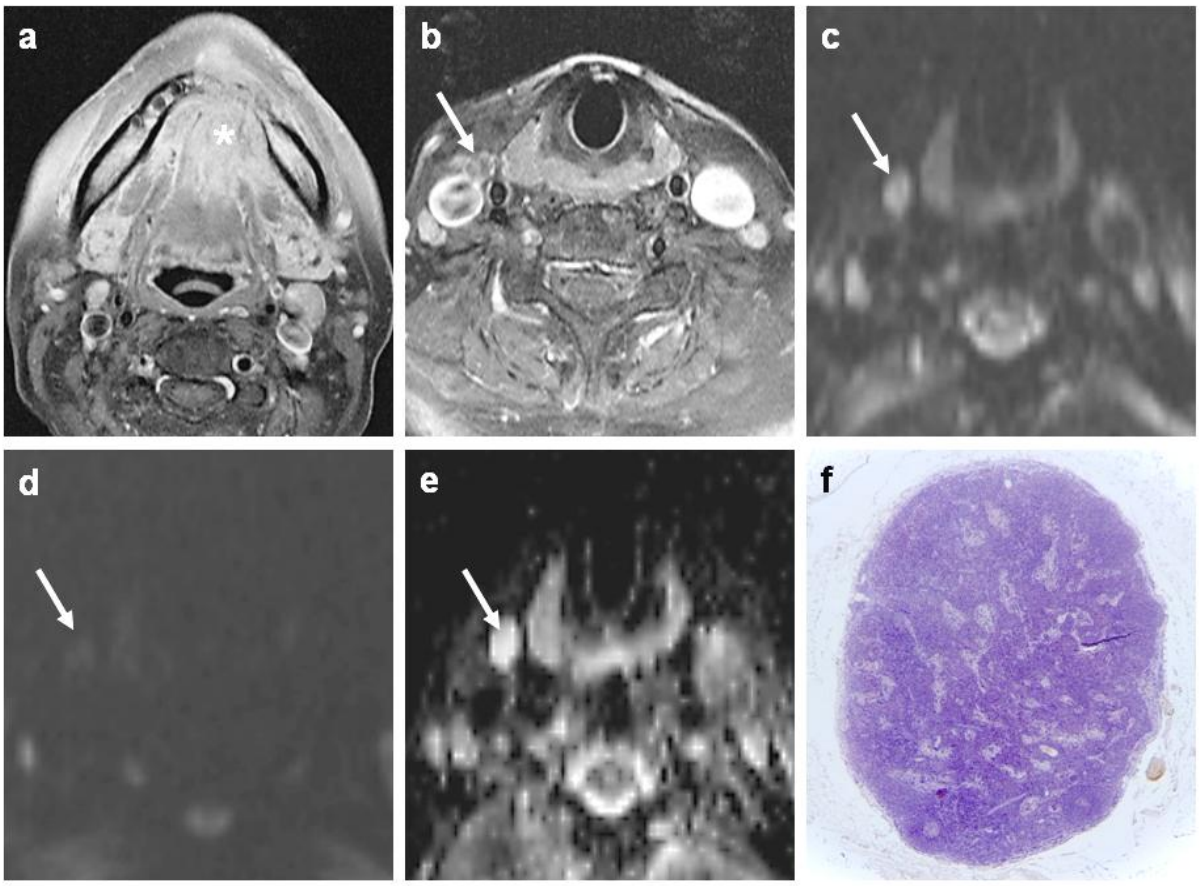

Figure 5: (a-b) Gadolinium-enhanced T1-weighted turbo-spin echo (TSE)-images depict large anterior floor of the mouth tumour involving the mandibular symphysis (*). (b) A small, round lymph node (shortest transverse diameter of 0.9 cm) with heterogeneous contrast enhancement is noted in level three on the right, suspect for small metastatic lymph node (arrow). (c) This lymph node is hyperintense on the b0 diffusion-weighted image and shows substantial loss of signal (d) on the b1000 image, (e) corresponding to an apparent diffusion coefficient (ADC) of 1.4 x 10^{-3}mm^2/sec. These findings indicate a non-tumoral lymph node. Histopathological slice with prekeratine staining (magnification factor=120) shows normal nodal architecture and absence of metastatic deposits.

4.3.3.2 $ADC_{b0\text{-}1000}$ and TSE-MRI in correlation to nodal diameter

The $ADC_{b0\text{-}1000}$ showed similar sensitivity (p=0.5 per lymph node, p=1 per level) for detection of enlarged adenopathies as TSE-MRI but enabled better differentiation of benign enlarged lymph nodes, resulting in a higher specificity (p=0.0078 per lymph node, p=0.5 per level) (Table 4, Figure 3.d). For subcentimetric lymph nodes, DWI showed a significantly higher sensitivity than conventional MRI p<0.0001 per lymph node and per level), at the cost of a diminished specificity (p=0.0063 per lymph node, p=0.125 per level) (Table 4, Figure 3.f). In lymph nodes smaller than 4 mm, none of the 2 metastatic nodes were detected, neither by conventional nor by DWI. An example of a subcentimetric nodal metastasis, detected by DWI is shown in Figure 6.

	ADC >= 10mm	TSE-MRI >= 10mm	ADC 4-9mm	TSE-MRI 4-9mm
True positive	30	31	32	3
False positive	2	9	12	1
True negative	8	1	205	216
False negative	2	1	10	39
sensitivity	94%	97%	76%	7%
specificity	80%	10%	94%	99.5%
accuracy	90%	76%	92%	85%
PPV	94%	78%	73%	75%
NPV	80%	50%	95%	85%

Table 4. Comparison of ADC and TSE-MRI per lymph node size (size >= 4mm).

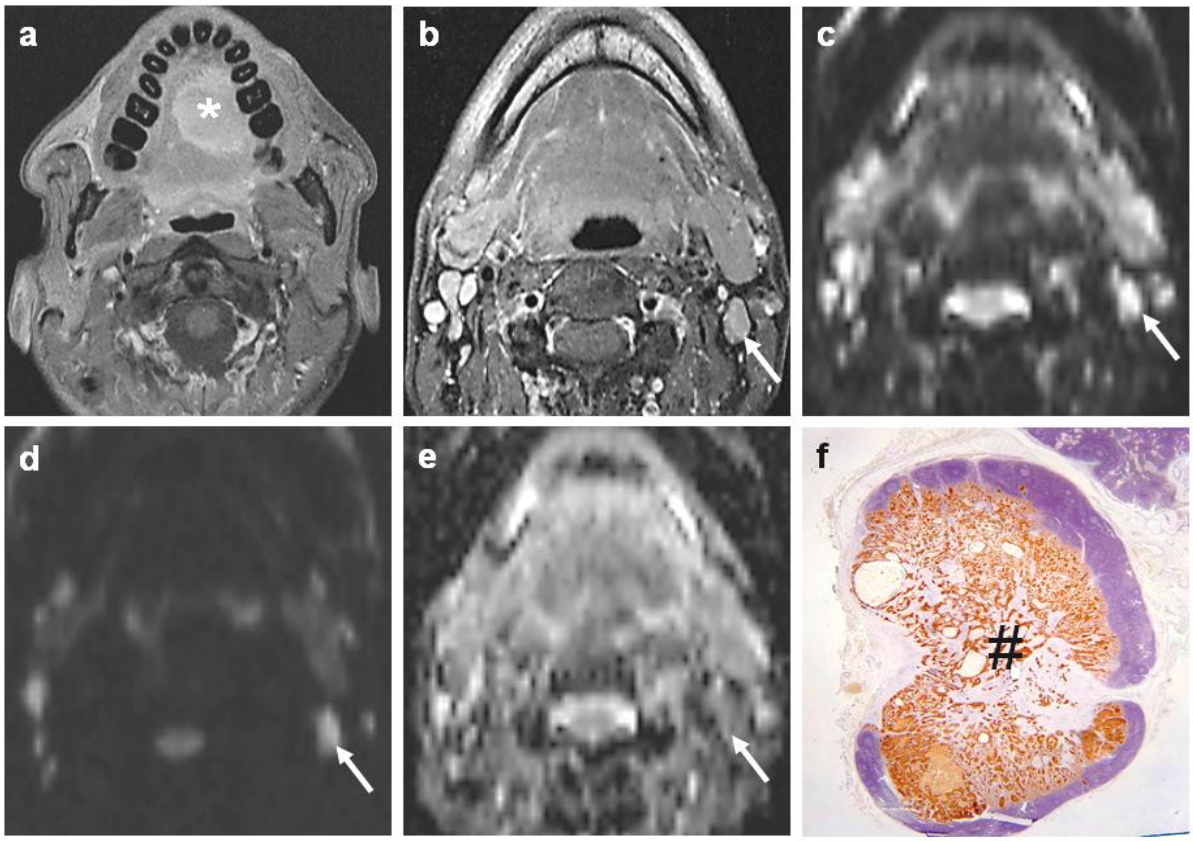

Figure 6: (a) Gadolinium-enhanced T1-weighted turbo-spin echo (TSE)-images show large tumour (*) in the left side of the oral tongue, extending over the midline. (b) A normal shaped lymph node with regular contours, shortest transverse diameter of 0.8 cm and homogeneous contrast enhancement in ipsilateral level 2 on the left (arrow) is considered normal by TSE-MRI. (c) This lymph node is hyperintense on b0 and (d) b1000 diffusion-weighted image (arrows), corresponding to (e) an apparent diffusion coefficient (ADC) of 0.73 x 10^{-3} mm^2/sec, suspect for metastatic adenopathy. (f) Histopathological slice with prekeratine immunostaining (magnification factor=100) shows large solid metastatic deposit diffusely infiltrating in the centre of the lymph node (#).

4.3.4 Comparison of DWI, conventional MRI and FDG-PET in patient subgroup

Sensitivity, specificity, accuracy, PPV and NPV per level and per hemineck are shown for the three different imaging techniques in Table 5.

Per level	$ADC_{b0\text{-}1000}$	MRI	PET-CT	Per Hemineck	$ADC_{b0\text{-}1000}$	MRI	PET-CT
True positive	23	18	16		12	10	10
False positive	1	0	1		1	1	0
True negative	54	55	54		5	5	6
False negative	1	6	8		0	2	2
Sensitivity	96%	75%	67%		100%	83%	83%
Specificity	98%	100%	98%		84%	84%	100%
Accuracy	97%	90%	86%		94%	83%	89%
PPV*	96%	100%	94%		92%	91%	100%
NPV#	97%	87%	83%		100%	83%	83%

* Positive predictive value; # Negative predictive value

Table 5: Comparison of apparent diffusion coefficient ($ADC_{b0\text{-}1000}$) with conventional MRI and FDG-PET-CT per level and hemineck in the subgroup of 11 patients.

Per level, DWI showed higher sensitivity than conventional MRI (p=0.062) and FDG-PET-CT (p=0.0078). Specificity showed no significant differences among the different techniques. DWI correctly upstaged two patients to N2c, staged as N2b by conventional MRI. Furthermore, DWI correctly staged 3 patients as N2b of which 2 were staged as N1 by MRI and 3 staged as N1 by PET-CT (Figure 7).

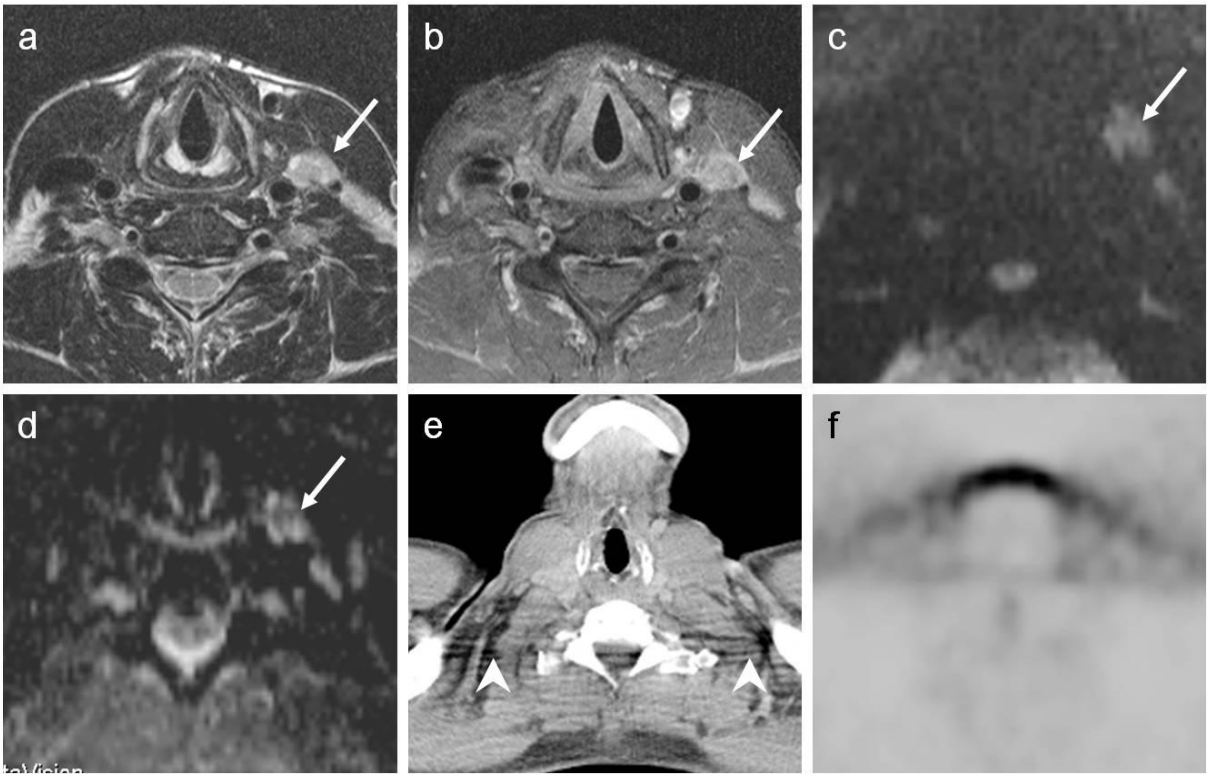

Figure 7: (a) T2-weighted turbo-spin echo (TSE) image shows heterogeneous adenopathy in level 3 left, which shows heterogeneous contrast uptake on the (b) Gadolinium-enhanced T1- TSE image. (c) The lymph node is hyperintense on the b1000 diffusion-weighted image and corresponds to an (d) an apparent diffusion coefficient (ADC) of 0.84 x 10^{-3} mm^2/sec, suspect for metastatic adenopathy. (e,f) the lymph node is not visible nor shows any FDG-uptake on the inline PET-CT (arrowhead shows streaking artifacts on the CT-image). Histological examination showed the lymph node to be obliterated by a partially necrotic metastasis (not shown)

4.4 Discussion

To date, the assessment of neck nodal metastases in HNSCC remains a difficult issue.

Due to the lack of reliable morphological criteria, anatomical imaging modalities like CT and MRI mainly rely on nodal size for detection of metastatic neck disease (15). It should be noted that several size criteria for detecting neck nodal disease have been reported, with each cut-off value constituting a compromise between sensitivity and specificity. The criterion of 10 mm for the short axis diameter, as proposed by van den Brekel et al, has now gained widespread acceptance and was therefore used in this study (14).

Morphologically malignant features, such as necrosis or indistinct margins indicating extranodal spread, are rather infrequent findings, especially in small (< 10 mm) metastatic lymph nodes (4). In our patient group, intranodal heterogeneity and indistinct nodal margins were of minimal or no use in the identification of subcentimetric nodal metastases, as these were mostly present in enlarged lymph nodes. Consequently, the high number of small lymph nodes most likely accounts for the low sensitivity of TSE-MRI in this study compared to literature (16).

Only a limited number of reports have studied DWI to characterize head and neck lesions and discriminate malignant and benign lymph nodes (10,11,17,18). DWI has been shown to differentiate malignant from benign lymph nodes with reported sensitivities ranging from 52 to 98% and specificities ranging from 88% to 97%, be it with different ADC-thresholds (10,11). Remarkably and contrary to findings of other studies, Sumi et al found higher ADC-values for metastatic than for benign lymph nodes (10). These differences can not solely be explained by different b-value settings used for ADC-calculation. Probably, a contributing factor for the discrepancy was the high number of necrotic metastatic lymph nodes included in Sumi's study. On the other hand, so far, DWI has only been used for characterization of enlarged lymph nodes, while the clinical impact relies mainly in the identification of metastases in subcentimetric lymph nodes. In this study, DWI using the $ADC_{b0\text{-}1000}$ showed higher accuracy for detection of metastatic lymph nodes than TSE-MRI, mainly by improving the detection of subcentimetric nodal metastases. The technique also improved the identification of benign enlarged lymph nodes. In the subcentimetric size group, DWI showed a sensitivity of 76% for lymph nodes ranging from 4 to 9 mm, while the sensitivity of TSE-MRI dropped to 7%.

Several factors allow for detection of small nodal metastases by DWI. Improved EPI technology, use of dedicated coils and dedicated sequence optimization enables a maximal reduction of EPI-related artifacts at relatively high spatial resolution (19). The reduction of these artifacts, in combination with high gradient strength available on current MRI-systems, substantially increases the SNR, propagating sufficient signal generation in small lymph nodes and reducing the influence of noise in the ADC-calculation. The application of a higher number of b-values is likely to reduce the influence of noise propagation on the ADC-calculation and reduce the risk of motion-related artifacting.

Moreover, as background tissue is usually suppressed on the native DWI images, the conspicuity of small lymph nodes is markedly improved compared to conventional sequences, which enables their depiction and subsequent ROI-delineation (20). Finally, the low prevalence of necrosis in small nodal metastases makes the inverse correlation with intranodal cellularity in a more straightforward way, potentially diminishing the variability of ADC-values in metastatic lymph nodes. This is likely to decrease the overlap of ADC-values of metastatic with benign lymph nodes and improve ADC-based nodal differentiation.

In our study, metastatic lymph nodes showed a significantly lower ADC than benign lymph nodes, corroborating the results of prior investigators (11,17). The decreased ADC most likely correlates to the tumoral microstructure, demonstrating a high number of cells, cellular polymorphism and increased mitosis. These features probably diminish the EES and decrease the ADC (21). However, the equally low ADC seen in partially invaded lymph nodes suggests the presence of additional mechanisms. For instance, keratinisation and peritumoral nodal reactivity, may have contributed to the diffusion-restriction (22,23). Although these tumour-related changes were seen in a number of histological specimens we did not further analyze or quantify them in this study setting. From literature, it is known that keratin impairs water movement and therefore this feature – specific for metastases of SCC - may intensify the ADC decrease in metastatic lymph nodes (22). Peritumoral reactive changes, as an immune response to the tumoral tissue, lead to an increase of peritumoral lymphocytes, additionally reducing the EES and further decreasing the ADC (11,17). However, as the extent or presence of peritumoral reactivity was highly variable on histopathology, it is very likely that this is subordinate to the effect of the tumoral microstructure itself. (23).

Nevertheless, as previously described by Wang et al, in benign lymph nodes, falsely decreased ADC may correlate with the presence of nodal reactive changes showing multiple germinal centres and fibrotic stroma, which act as microstructural barriers (17). In this study, this was most apparent in subcentimetric lymph nodes in the proximity of metastatic adenopathies, probably as part of a tumour-induced immunological response. Therefore, the overall influence on diagnostic accuracy and treatment impact was only minor when the neck was staged per level. Nevertheless, falsely decreased ADC due to nodal reactive changes may lead to an overestimation of the metastatic burden. This was, in our study, reflected by the lower specificity of DWI compared to TSE-MRI in the subcentimetric nodal range. Combining DWI with anatomical features indicative of benign nature may help decrease the false positive rate (24). Other false positive readings may be due to diffusion restriction in recent haemorrhage or hematoma (25,26). Therefore, DWI should probably not be performed directly after biopsy.

In our study, false negative findings in the majority of enlarged lymph nodes were associated with diffuse intranodal necrosis, evidently characterized by lack of microstructural barriers as reported in prior literature, (9,27). However, the impact on diagnostic accuracy was low as native DWI sequences were able to identify small solid metastatic from necrotic depositions in most patients (11,28). Although we did not assess the impact on diagnostic accuracy of combining DWI with TSE-MRI, the combined use of both imaging techniques should be able to avoid the majority of necrosis induced false negative findings, in view of the high sensitivity of conventional sequences to depict necrosis (29). Another cause of false negative ADC, mainly in small lymph nodes, was an insufficient intranodal metastatic volume. Dispersed small deposits in the otherwise normal nodal architecture are less likely to build up sufficient tissue boundaries to restrict water diffusion and probably explain the lower detection rate of intranodal micrometastatic deposits.

It might be premature to speculate on the relevant clinical impact of nodal staging with DWI in HNSCC as the technique needs to be further refined before it can be used in routine clinical practice. The interpretation of DWI in the head and neck is not always straightforward and requires training and expertise. Both benign and malignant lymph nodes are hyperintense on high b-value images necessitating the use of ADC for nodal characterization (30). As ADC-maps are difficult to interpret, a quantitative – and possibly more complicated - assessment with ROI-analysis is necessary. Therefore, the further development of DWI into clinical routine will likely depend on an improved standardization of imaging technique and image interpretation (31).

Nevertheless, the findings indicate that the degree in which DWI changed the accuracy of nodal differentiation by detecting subcentimetric nodal metastases, compared to conventional MRI and in the smaller group compared to PET-CT, the technique shows additional value in nodal staging and may impact clinical management in specific indications. In tumours growing close to the midline or with extensive ipsilateral nodal metastatic involvement, the detection or exclusion of metastatic spread to the contralateral neck is pivotal for treatment (13,32). The high sensitivity of DWI for contralateral metastases, combined with the high NPV allowed for reliable detection or exclusion of contralateral neck disease in mainly small lymph nodes. As such, the technique harbours potential value as an ancillary tool to determine the required extent of neck dissection in advanced disease stage, but also for radiotherapy planning. The increasing ability of functional imaging techniques such as DWI to detect small volume disease, raises the question whether remaining tumoral deposits too small for characterization may not be effectively treated with de-escalated doses. In this setting, the high NPV of DWI appears promising and warrants further research. An improved differentiation of nodal metastases may lead to closer conformity between the radiation target volume and the regional tumour extent, potentially decreasing the treatment-induced side-effects. As such, the technique may show future use in the selection and treatment planning for unilateral or parotid sparing 3 dimensional conformal RT or IMRT (33,34,35).

The detection of subclinical skip metastases in nodal level IV by DWI in two patients with tongue cancer supports the general reluctance of surgeons in the application of supraomohyoid neck dissection in patients with oral cancer, even with clinically N0-neck (36). However, given the high sensitivity and high NPV per lymph node and per level seen in this study, DWI may help in the selection of patients eligible for limited neck dissection, evidently in correlation to the appropriate clinical risk factors and tumoral T-stage (37).

Whether the technique will enable surgeons to avoid neck dissection in all patients with clinically N0-neck is unclear. Although the high NPV may help to decrease the risk of nodal metastases to an acceptable level, DWI currently lacks sufficient sensitivity - similar to anatomical or metabolic imaging modalities - to avoid elective neck dissections (38). Further studies on larger patient groups with N0-neck are therefore warranted.

The main – and clinically most relevant - advantage of DWI in this study was the improved detection of subcentimetric metastatic lymph nodes compared with conventional MRI and – in the smaller subgroup of patients – with PET-CT. The large majority of false negative findings on PET-CT consisted of small lymph nodes ranging between 4 and 8 mm for which no clear morphological alterations were visible on the inline PET-CT images. As conventional MRI showed slightly higher sensitivity than PET-CT, it is likely that part of the lower detection rate of smaller lymph nodes could be attributed to the suboptimal CT parameter settings of the CT-component of the combined PET-CT studies, hampering the adequate detection of subtle morphological alterations suggesting metastatic nodal involvement. The sensitivity of PET-CT for small nodal metastases may be improved by using a dedicated PET protocol, with a coverage limited to the head and neck region, which may show additional value in cases where standard PET is inconclusive (39). However, the accuracy of this approach may be diminished by a non-uniform radionuclide uptake in lesions and background, potentially diminishing lesion conspicuity, patient movement, which decreases lesion detection and causes misregistration with the CT-acquisition. Also, the increased sensitivity of dedicated PET-CT may be gained at the cost of a decreased specificity compared to standard PET-CT due to the better visualization of FDG-uptake in inflammatory lymph nodes (39).

The findings of the study indicate that DWI could be of complementary value to FDG-PET for the detection of small nodal metastases. The high lesion-to-background contrast, ultrafast imaging properties which make the technique relatively insensitive to movement are likely to facilitate the detection and characterization of small lesions. DWI may help compensate the lower sensitivity to small volume disease of FDG-PET. Therefore, the technique may be used in conjunction with FDG-PET offering a microstructural correlate to the metabolic findings. Evidently comparison of both imaging techniques in larger patient groups will be necessary to further compare and elucidate a potential synergistic role of microstructural and metabolic imaging in this setting.

Nevertheless, the application of advanced imaging techniques in the head and neck should be judiciously outweighed against clinical indication and relevance. Despite the previously reported higher sensitivity of FDG-PET/CT - not confirmed in this limited study population - for detection of non-palpable nodal metastases compared to anatomical imaging modalities, its added clinical value has not unambiguously been proved in the pre-operative assessment of HNSCC and the same may account for DWI (40,41,42). This is in part reflected by the similar accuracy of DWI, PET-CT and conventional MRI for nodal staging per hemineck; although it

should be outlined that DWI correctly identified subcentimetric contralateral metastatic lymph nodes. These findings underscore the need of developing advanced imaging techniques, either molecular or microstructural, in respect to proper clinical indications and in close cooperation with clinicians involved in the treatment of HNSCC.

There are some limitations to this study. Not all patients received a bilateral neck dissection. As such a number of micrometastases in the contralateral neck may have remained undetected and eradicated by post-operative radiotherapy. However, in none of the patients receiving a unilateral neck dissection did the tumour come near the midline, or was there any indication of extensive nodal involvement, nor signs of extranodal spread, which minimized the likelihood of contralateral metastases (32). Additionally, potential bias in the image interpretation cannot be entirely excluded as 1 radiologist reviewed both conventional MR- and DWI images and 1 radiologist performed histological imaging correlation and evaluation of the DWI. However, as indicated above and illustrated on the included timeline, careful precautions were undertaken to minimize the effects of double reading. Moreover, the results of the study suggest that DWI analysis was not biased by the results of conventional MRI as DWI detected the majority of metastases in anatomically apparently normal lymph nodes and showed a lower false positive ratio in enlarged lymph nodes than TSE-MRI.

4.5 Conclusion

The higher accuracy of DWI based on ADC-calculation for detection of nodal metastases compared to conventional MRI -and in a smaller subpopulation- compared to PET-CT, was most beneficial for the detection of subcentimetric metastatic lymph nodes.

This suggests that DWI can be of complementary use to conventional MRI; as size-related and morphological criteria lack sufficient reliability for differentiation of small nodal metastases in patients with HNSCC, and to PET-CT, for which the lower spatial resolution potentially hampers the detection of small nodal metastases. Further studies reproducing the promising results on a wider scale and focusing on standardization of imaging technique and image interpretation are required before DWI can be used in the routine clinical setting.

4.6 References

1. Johnson JT. A surgeon looks at cervical lymph nodes. *Radiology* 1990;75:607-610
2. van den Brekel MW, Castelijns J. What the clinician wants to know: surgical perspective and ultrasound for lymph node imaging of the neck. *Cancer Imaging* 2005;5:S41-S49
3. Yousem DM. Dashed hopes for MR imaging of the head and neck: The power of the needle. *Radiology* 1992;184:25-26
4. Dooms GC, Hricak H, Moseley ME, Bottles K, Fisher MR, Higgins CB. Characterization of lymphadenopathy by magnetic resonance relaxation times: preliminary results. *Radiology* 1985;155:691-697
5. Curtin HD, Ishwaran H, Mancuso A, Dalley RW, Caudry DJ, McNeil BJ. Comparison of CT and MRI imaging in staging of neck metastases. *Radiology* 1998;207:123-130
6. Sigal R, Vogl T, Casselman J, et al. Lymph node metastases from head and neck squamous carcinoma: MR imaging with ultrasmall superparamagnetic iron oxide particles (Sinerem MR) – results of a phase-III multicenter clinical trial. *Eur Radiol* 2002;12:1104-1113
7. Mack MG, Balzer JO, Straub R, Vogl TJ. Superparamagnetic iron oxide-enhanced MR imaging of head and neck lymph nodes. *Radiology* 2002;222:239-244
8. Shah GV, Fischbein NJ, Patel R, Mukherji SK. Newer MR techniques for head and neck. *Magn Reson Imaging Clin N Am* 2003;11:449-469
9. Herneth AM, Guccione S, Bednarski M. Apparent diffusion coefficient: a quantitative parameter for in vivo tumor characterization. *Eur J Radiol* 2003;45:208-213
10. Sumi M, van Sakihama N, Sumi T, et al. Discrimination of metastatic cervical lymph nodes with diffusion-weighted MR imaging in patients with head and neck cancer. *Am J Neuroradiol* 2003;24:1627-1634
11. Razek A, Soliman N, Elkhamary S, Alsharaway M, Tawfik A. Role of diffusion-weighted MR imaging in cervical adenopathy. *Eur Radiol* 2006;16:1468-1477
12. International Union Against Cancer (UICC). Head and Neck Tumours. In: *Sobin LH, Wittekind C (eds.),* TNM Classification of Malignant Tumours. 6th ed. New York, Wiley, 2002;19-42
13. Castelijns JA, van den Brekel MW. Imaging of lymphadenopathy in the neck. *Eur Radiol* 2002;12:727-738

14. van den Brekel MW, Stel HV, Castelijns JA, et al. Cervical lymph node metastasis: assessment of radiologic criteria. *Radiology* 1990;380:379-384
15. van den Brekel MW. Lymph node metastases: CT and MRI. *Eur J Radiol* 2000;33:230-238
16. de Bondt RB, Nelemans PJ, Hofman PA, et al. Detection of lymph node metastases in head and neck cancer: a meta-analysis comparing US, USgFNAC, CT and MR imaging. *Eur J Radiol* 2007;64:266-272
17. Wang J, Takashima S, Takayama F, et al. Head and Neck lesions: Characterization with Diffusion-weighted Echo-planar MR Imaging. *Radiology* 2001;220:621-630
18. King AD, Ahuja AT, Yeung DK, et al. Malignant cervical lymphadenopathy: diagnostic accuracy of diffusion-weighted MR imaging. *Radiology* 2007;245:806-813
19. Vandecaveye V, De Keyzer F, Nuyts S, et al. Detection of head and neck squamous cell carcinoma with diffusion weighted MRI after (chemo)radiotherapy: correlation between radiologic and histopathologic findings. *Int J Radiat Oncol Biol Phys* 2007;67:960-971
20. Takahara T, Imai Y, Yamashita T, Yasuda S, Nasu S, Van Cauteren M. Diffusion weighted whole body imaging with background body signal suppression (DWIBS): Technical improvement using free breathing, STIR and high resolution 3D display. *Radiation Medicine* 2004;22:275-282
21. Koh DM, Collins DJ. Diffusion-weighted MRI in the body: applications and challenges in oncology. *Am J Roentgenol* 2007;188:1622-1635
22. White ML, Zhang J, Robinson RA. Evaluating tumors and tumorlike lesions of he nasal cavity, the paranasal sinuses, and the adjacent skull base with diffusion-weighted MRI. *J Comp Assist Tomogr* 2006;30:490-495
23. Kubota R, Yamada S, Kubota K, Ishiwata K, Tamahashi N, Ido T. Intratumoral distribution of Fluorine-18-Fluorodeoxyglucose in vivo: High accumulation in macrophages and granulation tissues studied by microautoradiography. *J Nucl Med* 1992;33:1972-1980
24. Sumi M, Van Cauteren M, Nakamura T. MR microimaginig of benign and malignant nodes in the neck. *Am J Roentgenol* 2006;186:749-757
25. Choi KD, Jo JW, Park KP, et al. Diffusion-weighted imaging of intramural hematoma in vertebral artery dissection. *J Neurol Sci* 2007;253:81-84
26. Silvera S, Oppenheim C, Touzé E, et al. Spontaneous intracerebral hematoma on diffusion-weighted images: influence of T2-shine-through and T2-blackout effects. *Am J Neuroradiol* 2005;26:236-241

27. Thoeny HC, De Keyzer F, Chen F, et al. Diffusion-weighted MR imaging in monitoring the effect of a vascular targeting agent on rhabdomyosarcoma in rats. *Radiology* 2005;234:756-764
28. Lang P, Wendland MF, Saeed M, et al. Osteogenic sarcoma: noninvasive in vivo assessment of tumor necrosis with diffusion-weighted MR imaging. *Radiology* 1998;206:227-235
29. King AD, Tse GM, Ahuja AT, et al. Necrosis in metastatic neck nodes: Diagnostic accuracy of CT, MR imaging and US. *Radiology* 2004;230:720-726
30. Low RN, Gurney J. Diffusion-weighted MRI (DWI) in the oncology patient: Value of breathhold DWI compared to unenhanced and gadolinium-enhanced MRI. *J Magn Reson Imaging* 2007;25:848-858
31. Hermans R, Vandecaveye V. Diffusion-weighted MRI in head and neck cancer. *Cancer Imaging* 2007;7:126-127
32. Suoglo Y, Erdamar B, Katircioglu OS, Karatay MC, Sunay T. Extracapsular spread in ipsilateral and contralateral neck metastases in laryngeal cancer. *Ann Otol Rhinol laryngol* 2002;111:447-454
33. Kagei K, Shirato H, Nishioka T, et al. Ipsilateral irradiation for carcinomas of tonsillar region and soft palate based on computed tomographic simulation. *Radiother Oncol* 2000;54:117-121
34. Bussels B, Maes A, Hermans R, Nuyts S, Weltens C, Van den Bogaert W. Recurrences after conformal parotid-sparing radiotherapy for head and neck cancer. *Radiother Oncol* 2004;72:119-127
35. Lee N, Xia P, Fischbein NJ, Akazawa P, Akazawa C, Quivey JM. Intensity-modulated radiation therapy for head-and-neck cancer: the UCSF experience focusing on target volume delineation. *Int J Radiat ONcol Biol Phys* 2003;57:49-60
36. Capote A, Escorial V, Munoz-Guerra MF, Rodriguez-Campo FJ, Gamallo C, Vanal L. Elective neck dissection in early stage oral squamous cell carcinoma – does it influence recurrence and survival? *Head Neck* 2007;29:3-11
37. Clark JR, Naranjo N, Franklin JH, de Almeida J, Gullane PJ. Established prognostic variables in N0 oral carcinoma. *Otolaryngol Head Neck Surg* 2006;135:748-753
38. Nahmias C, Carlson ER, Duncan LD, et al. Positron emission tomography/computerized tomography (PET/CT) scanning for preoperative staging of patients with oral/head and neck cancer. *J Oral Maxillofac Surg* 2007;65:2524-2535

39. Yamamoto Y, Wong TZ, Turkington TG, Hawk TC, Coleman RE. Head and neck Cancer: Dedicated FDG PET/CT protocol for detection – Phantom and Initial Clinical Studies. *Radiology* 2007;244:263-272
40. Rohren EM, Turkington TG, Coleman E. Clinical application of PET in oncology. *Radiology* 2004;231:305-332
41. Wong RJ. Current status of FDG-PET for head and neck cancer. *J Surg Oncol* 2008;97:649-652
42. Ng SH, Yen TC, Chang JT, et al. Prospective study of [18]fluorodeoxyglucose positron emission tomography and computed tomography and magnetic resonance imaging in oral cavity squamous cell carcinoma with palpably negative neck. *J Clin Oncol* 2006;24:4371-4376

Chapter 5:
DW- and DCE-MRI for differentiation of recurrent head and neck squamous cell carcinoma after chemoradiotherapy: a correlative study to histopathology

5.1 Introduction

At the time of diagnosis, HNSCC usually presents as locoregional disease, for which both surgery and CRT are primary treatment options (1,2,3).

Treatment failure in the head and neck after CRT is mainly related to locoregional tumour recurrence, while distant metastases less frequently occur as an isolated event (4). At the time of follow-up, however, clinical or imaging findings are sometimes not straightforward due to the difficult differentiation of tumour recurrence and complications like necrosis or severe inflammatory alterations.

The obvious microstructural differential properties between CRT-induced non-tumoral tissue changes such as oedema, inflammation, fibrosis, and necrosis and tumour recurrence can be expected to produce different imaging properties on DWI and DCE-MRI based on differences in tissue cellularity and vascularisation (5,6,7). The purpose of this study was to evaluate DWI and DCE-MRI for differentiation of recurrent or persistent tumour from post-radiotherapeutic alterations and necrosis, in comparison to routine imaging methods and histopathology of the resected specimens.

5.2 Materials and Methods

5.2.1 Patient selection

Twenty-eight patients (ranging from 49 to 83 years old) with a suspected tumour recurrence after CRT for HNSCC (median time of suspected recurrence: 8 months after end of treatment, interquartile range (IQR): 6-21) were prospectively included. CRT had been applied according to a standardized treatment protocol. Chemotherapy consisted of Cisplatinum, 100 mg/ml at week 1 and 4 . Radiotherapy was delivered to a total dose of 72 Gray (Gy) according to a hybrid fractionation schedule in 28 patients: 20 daily fractions of 2 Gy,

followed by 20 fractions of 1,6 Gy twice daily (32 Gy), to a total dose of 72 Gy. Two patients were excluded from the study due to lack of histopathological correlation. These two patients suffered concurrent metastatic disease and were therefore treated non-surgically. The initial tumour localization, staging and treatment are summarized in Table 1.

	primary tumour prior to therapy	Initial treatment
Patient 1	T4N2bM0 - piriform sinus	CRT (70Gray)
Patient 2	T2N0M0 - left vocal cord	RT (70Gray)
Patient 3	T2N1M0 - supraglottis	CRT (72Gray)
Patient 4	T2N0M0 - supraglottis	RT (70Gray)
Patient 5	T1bN0M0 - glottis	RT (55Gray)
Patient 6	T2N2bM0 - left posterior hypopharynx	RT (72Gray)
Patient 7	T2N0M0 - right glottis	RT (70Gray)
Patient 8	T1N1M0 - left nasal cavity	RT (70Gray)
Patient 9	T2N1M0 - tonsil right	RT (72Gray)
Patient 10	T1N2bM0 - right piriform sinus	CRT (70Gray)
Patient 11	T2N2cM0 - right lateral oropharynx	surgery - RT (60Gray)
Patient 12	T2N2cM0 - right lateral oropharynx	RT (60Gray)
Patient 13	T4N2M0 - right piriform sinus	surgery - RT (50Gray)
Patient 14	T3N1M0 - supraglottis	CRT (70Gray)
Patient 15	T3N1M0 - left base of tongue	CRT (70Gray)
Patient 16	T1N2aM0 - right tonsil	neck dissection - RT (50Gray)
Patient 17	T1N0M0 - right glottis	RT (55Gray)
Patient 18	T1N0M0 - right glottis	RT (55Gray)
Patient 19	T2N0M0 - right tonsil	RT (72Gray)
Patient 20	T3N0M0 - right tonsil	RT (72Gray)
Patient 21	T2N2bM0 - right base of tongue	CRT (70Gray)
Patient 22	T2N0M0 - left glottis	RT (70Gray)
Patient 23	T1N2M0 - right base of tongue	neck dissection - CRT (66Gray)
Patient 24	T2N0M0 - right soft palate	RT (72Gray)
Patient 25	T3N2bM0 - right hypopharynx	RT (72Gray)
Patient 26	T3N2bM0 - left supraglottis	CRT (70Gray)

CRT: Chemoradiotherapy
RT: Radiotherapy

Table 1: Initial tumour localization, TNM-staging and treatment in all 26 patients

The remaining 26 patients were selected for salvage surgery based on clinical and radiological findings. Routine diagnostic examinations included contrast-enhanced CT in all patients; in 1 patient, contrast agent injection was not possible because of diabetic nefropathy. FDG-PET was performed in 17 patients, and pre-operative panendoscopy with biopsy in 7 patients. A

conventional MRI examination with additional DCE-MRI and DWI was added the day before surgery in these 26 patients.

Eighteen patients were primarily investigated for a suspect lesion in the primary tumour bed, and 8 for a persistent or recurrent neck adenopathy. One of these 8 patients also underwent an endoscopic examination for a clinically suspect supraglottic lesion in the primary tumour bed.

The result of the histopathological examination of the surgical specimens in 23 patients (including one patient with an additional biopsy of the supraglottic lesion during the scheduled neck dissection procedure), and bioptic material obtained in three patients constituted the reference standard. None of the patients received postoperative re-irradiation nor chemotherapy. All patients were followed for at least one year after salvage surgery by clinical examination and CT to exclude sampling error or to exclude occult tumour localizations in the non-resected areas. After correlation with the histopathological results, the sensitivity, specificity and accuracy of DCE- and DW-MRI was calculated. The additional value of DWI and DCE-MRI was compared with CT and FDG-PET.

This study was approved by the local ethics committee, and all patients gave informed consent prior to inclusion.

5.2.2 Imaging technique

All patients underwent the standardized anatomical (CT and TSE-MRI), DWI- and DCE-MRI sequences as described in chapter 3. MRI imaging covered the entire head and neck ranging from the base of skull to the thoracic outlet, and included all regional nodal stations (retropharyngeal space and neck levels).

The 17 patients undergoing FDG-PET were scanned with a standard clinical protocol, described in chapter 3. The imaging protocol consisted of a whole body protocol without co-registered CT-images.

5.2.3 Image analysis

The images of the TSE-MRI, CT studies, DWI, DCE-MRI and FDG-PET were interpreted in a blinded fashion. The TSE-MRI and CT studies were interpreted by a head and neck radiologist with 15 years of experience, prior to surgery as described in chapter 3.3.3. Primary lesions and lymph nodes were differentiated based on clinically accepted criteria for characterization with morphologic imaging modalities. The cut-off point for nodal diameter between benign and malignant lymph nodes was set to 10 mm, according to literature (8,9).

Definite diagnosis was made based on the combined findings of plain T1-weighted, T2-weighted and contrast-enhanced T1-weighted images.

The DWI images were quantitatively interpreted by two radiologists in consensus (both 4 years of experience in head and neck DWI) as described in chapter 3.3.1. Primary lesions and lymph nodes were differentiated solely based on the ADC.

DCE-MRI images were interpreted by two radiologists in consensus (both 4 years of experience in head and neck DWI) with the semi-quantitative parameters as described in chapter 3.3.2. FDG-PET images were qualitatively interpreted by an experienced nuclear medicine staff physician as described in chapter 3.3.4.

5.2.4 Topographic correlation and histopathological analysis

Topographic correlation and histopathological analysis was performed according to the standardized methodology as described in chapter 3.4.1.

5.2.5 Historadiological correlation and comparison of different imaging modalities

Historadiological correlation was done by one radiologist and pathologist in consensus. For DWI, the ADC-values were correlated to the presence of viable tumour, tumour necrosis without remaining viable tumour cells, or radiotherapy-induced tissue changes for the separate delineated tissue subsites. The same was done for DCE-MRI where the values of AS, washout and c-peak were compared to histopathology.

First an optimal threshold for DWI and DCE-MRI parameters was determined to differentiate between HNSCC, tissue necrosis, and post-radiotherapeutic tissue changes, based on ROC-analysis. Based on these thresholds, sensitivity, specificity, accuracy, PPV and NPV of DWI and DCE-MRI using the most accurate parameter for detection of tumoral recurrence at the separate delineated tissue subsites were compared.

Finally, DWI and DCE-MRI were compared with CT and conventional MRI for the entire group and with FDG-PET in 17 patients, in order to determine potential additional value.

For comparison with the anatomical and metabolic imaging results, the DWI- and DCE images were averaged per lesion.

5.2.6 Statistical analysis

Statistical analysis was done with Microsoft Excel 9.0 (Microsoft Corporation, Washington, US) and SPSS 11.0 for Windows (SPSS Inc., Chicago, Illinois, US). Numerical data are reported as means ± SD. To compare DWI and DCE-MRI parameters between all tumoral ROIs and all non-tumoral ROIs, an unpaired two-tailed Student's t-test was used. The same was done to compare the results between lymph nodes and primary site. As ADC-values cannot be considered as independent, a Bonferroni correction for multiple testing was applied. P-values <0.05 were considered as significant.

5.3 Results

5.3.1 Histopathology

Histopathological material consisted of 10 laryngectomies (with 2 pharyngolaryngectomies), 2 pharyngectomies, 4 hemiglossectomies, 16 unilateral neck dissections and 6 bilateral neck dissections. For one floor of mouth lesion and 2 supraglottic lesions, only histological material obtained during endoscopic examination was available.

Fifteen of 19 suspect primary lesions proved to be positive for cancer; 4 lesions contained only post-radiotherapeutic non-tumoral or necrotic tissue. The surrounding tissues showed radiotherapy-induced tissue changes or necrosis in all resection specimens without tumour. Of all performed neck dissections, eight were performed for a persisting or recurrent lymph node. The other neck dissections (11 unilateral and 6 bilateral) were elective dissections performed during the resection of a recurrent lesion at the primary site. In total, 16 metastatic lymph nodes were found on histopathology in nine different patients.

At the primary site, the maximal tumour diameter ranged between 5 mm to 30 mm. The nodal diameter ranged from 6 mm to 18mm; six metastatic lymph nodes were smaller than 10 mm.

5.3.2 Historadiological correlation

5.3.2.1 DWI

No DWI examinations failed due to artifacting and all examinations were included in the analysis. In total 165 ROIs were delineated over tissue subsites, including all target lesions at the primary site and nodal stations.

ADC-values were significantly lower for HNSCC than for non-tumoral post-radiotherapeutic tissue (0.00111±0.00029 mm²/s versus 0.00185±0.00035mm²/s; $p<0.0001$) (Figure 1).

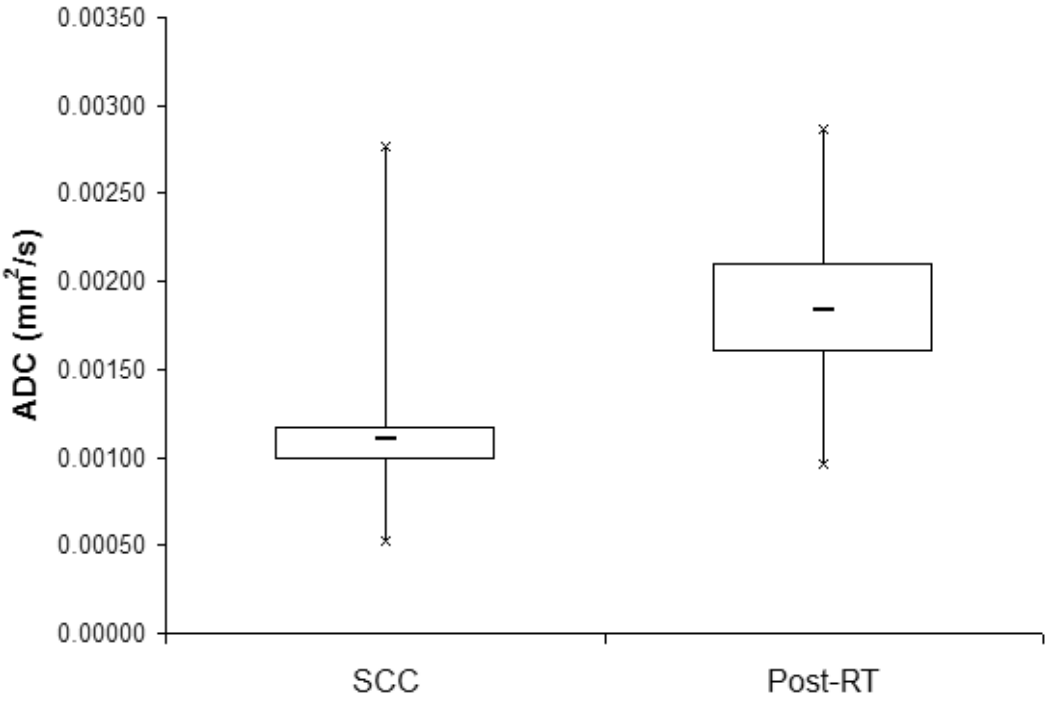

Figure 1: Comparison of ADC-values between recurrent or persistent HNSCC and post-radiotherapeutic benign alterations (post-RT); ADC-value in SCC was significantly lower than in post-CRT normal tissue. ADC-value shows minimal overlap between SCC and post-RT. Box-whisker plots are presented with median (-), interquartile range (box) and minima/maxima (x).

No significant difference was found for the ADC-values and threshold between lymph nodes and the primary sites when comparing similar tissue types ($HNSCC_{primary\ site}$ versus $HNSCC_{lymph\ node}$; Post-RT $changes_{primary\ site}$ versus Post-RT $changes_{lymph\ node}$). The calculated optimal threshold for the ADC-value and resulting sensitivities, specificities, accuracies, PPV and NPV for all delineated tissue subsites at the primary site and lymph nodes separately are reported in Table 2.

DWI	ADC primary	ADC lymph nodes
True positive at tissue subsite	41	22
False positive at tissue subsite	3	4
True negative at tissue subsite	60	32
False negative at tissue subsite	1	2
Sensitivity	96%	92%
Specificity	97%	85%
Accuracy	97%	88%
PPV	94%	85%
NPV	98%	92%
Threshold	0.0013	0.0013

Table 2: Comparison of diagnostic performance for ADC based DWI for all delineated tissue subsites and for subsites at lymph nodes and primary sites separately.

5.3.2.2 DCE-MRI

In 3 patients, DCE-MRI examinations were non-diagnostic due to movement artifacting and were subsequently excluded from further analysis.

In total 145 ROIs were delineated over tissue subsites, including all target lesions at the primary site and lymph nodes. The AS was significantly higher for HNSCC than for non-tumoral post-radiotherapeutic tissue at the primary site and in lymph nodes (19.45±18.81 versus 14.41±10.2; p=0.04), as well as the c-peak (5.07±4.8 versus 2.89±4.9; p=0.008), washout (0.57±2.02 versus -0.024±1.19; p= 0.03). A significant difference was found between the thresholds of all DCE-MRI parameters between lymph nodes and the primary sites when comparing similar tissue types ($HNSCC_{primary\ site}$ versus $HNSCC_{lymph\ node}$; Post-RT $changes_{primary\ site}$ versus Post-RT $changes_{lymph\ node}$) ($p< 0.0001$ all DCE-MRI parameters).

The calculated optimal thresholds for the separate DCE-MRI values and resulting sensitivities, specificities, accuracies, PPV and NPV for all delineated tissue subsites at the primary site and lymph nodes separately are reported in Table 3.

DCE-MRI	Primary site		
	c-peak	arterial slope	washout
True positive at tissue subsite	29	34	24
False positive at tissue subsite	11	9	26
True negative at tissue subsite	40	42	25
False negative at tissue subsite	11	6	16
Sensitivity	73%	83%	60%
Specificity	78%	82%	49%
Accuracy	76%	82%	54%
PPV	73%	79%	48%
NPV	78%	86%	61%
Threshold	3.15	14.79	-0.44
DCE-MRI	**Lymph nodes**		
	c-peak	arterial slope	washout
True positive at tissue subsite	14	16	12
False positive at tissue subsite	9	15	14
True negative at tissue subsite	25	19	22
False negative at tissue subsite	6	4	8
Sensitivity	70%	80%	60%
Specificity	74%	56%	59%
Accuracy	72%	65%	59%
PPV	61%	52%	46%
NPV	81%	83%	71%
Threshold	2	7.5	-0.01

Table 3: Comparison of diagnostic performance for the separate DCE-MRI parameters for the delineated subsites at lymph nodes and primary sites separately.

5.3.3 Comparison of DWI with CT/conventional MRI and FDG-PET

When compared with CT and TSE-MRI in all patients (Table 4), DWI correctly characterized two persistent enlarged lymph nodes in two different patients and one enlarged lymph node (13 mm) in one patient with a tumour recurrence at the primary site as non-tumoral. Consequently, these patients were downstaged to N0 (Figure 2).

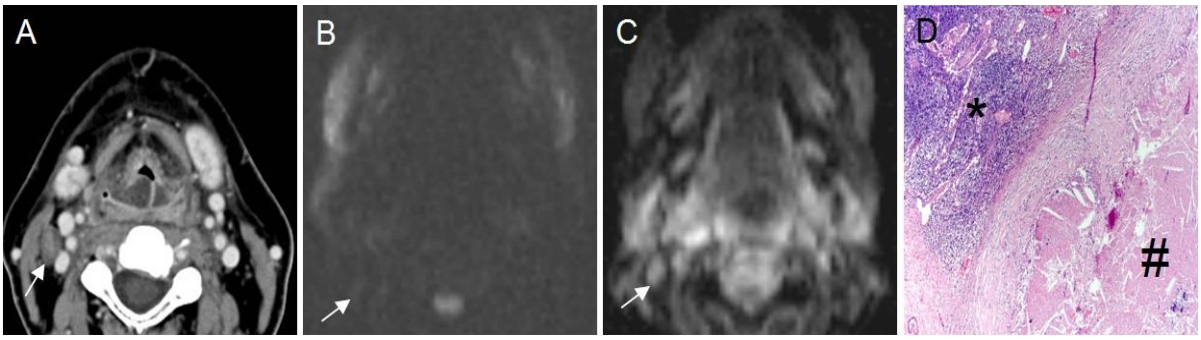

Figure 2: (a) CT scan shows lymph node short axis diameter of 1.2 cm in level II in the right neck; (b) on DW-MRI this node shows no substantial signal on the b1000-image, (c) while on ADC-map this node is hyperintense (ADC = 0.00180 mm²/sec) suggesting absence of tumour tissue; (d) histology showed presence of lymphoid tissue (*) and partially necrotic and sclerotic stroma (#) and excluded tumour.

DWI detected an additional contralateral subcentimetric nodal metastasis (6, 8 and 8 mm diameter, respectively on CT/conventional MRI) in 3 different patients (Figure 3), and two additional nodal metastases (7 and 9 mm diameter, respectively on CT/conventional MRI) at the ipsilateral site in one other patient.

A persistent contrast-enhancing ulcer in the base of tongue, visualized on CT/conventional MRI, was correctly identified as non-tumoral by DWI (Figure 4).

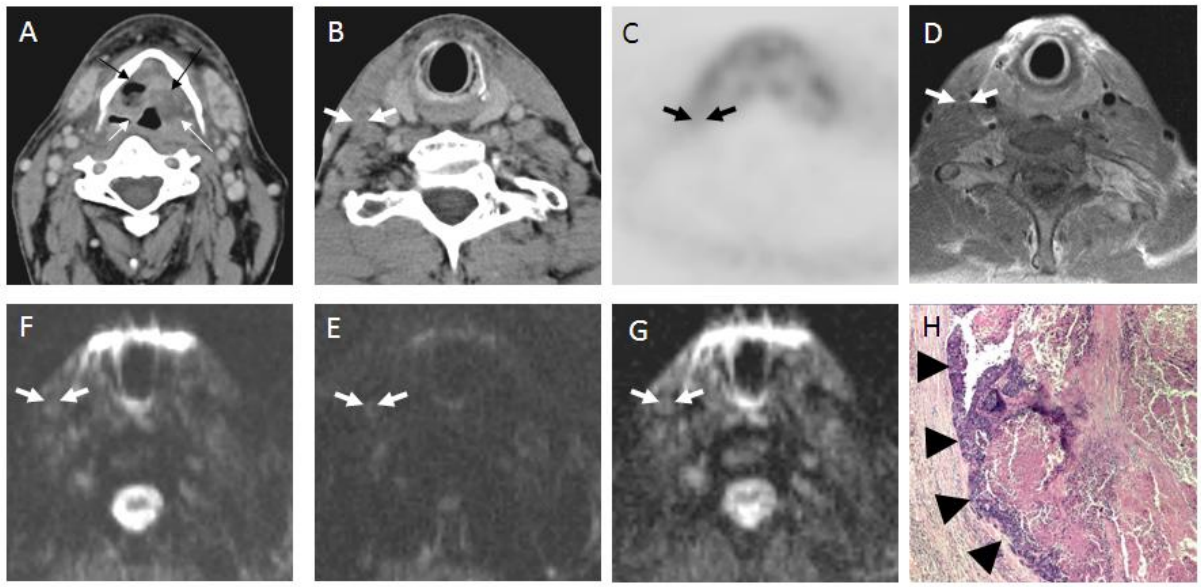

Figure 3: (a) CT scan shows supraglottic tumour recurrence after (chemo)radiotherapy (small arrows); (b) no enlarged lymph nodes were visible, however a lymph node (arrowheads) with a diameter of 6 mm is visible in level III on the right, possibly showing subtle rim enhancement; (c) this node shows no tracer uptake on FDG-PET; (d) Contrast-enhanced MRI confirms the presence of the small lymph node; (e) on DW-MRI the node is hyper-intense on the b0-image and shows nearly no signal loss on the b1000-image; (f) low signal is seen on the ADC-map; (g) corresponding to an ADC of 0.00089 mm^2/sec, indicating diffusion restriction, suggestive for lymphatic metastasis; (h) histology confirmed the presence of metastatic SCC in this subcentimetric lymph node (arrowheads).

In one case of laryngeal necrosis, depicted as an enhancing ulcerated mass on conventional MRI, DWI correctly predicted absence of tumour.

When compared with FDG-PET (Table 4) (17 patients), DWI correctly excluded tumour in 2 hypermetabolic lymph nodes in two different patients. In one patient, DWI correctly excluded tumour in a hypermetabolic lymph node and a concurrent hypermetabolic spot in the ipsilateral piriform sinus. DW-MRI correctly identified a subcentimetric contralateral nodal metastasis which showed no FDG-uptake, in 2 different patients (Figure 3).

Also, tumour was excluded in two isolated hypermetabolic lesions at the primary site, in the base of tongue (Figure 4) and larynx respectively, in 2 different patients.

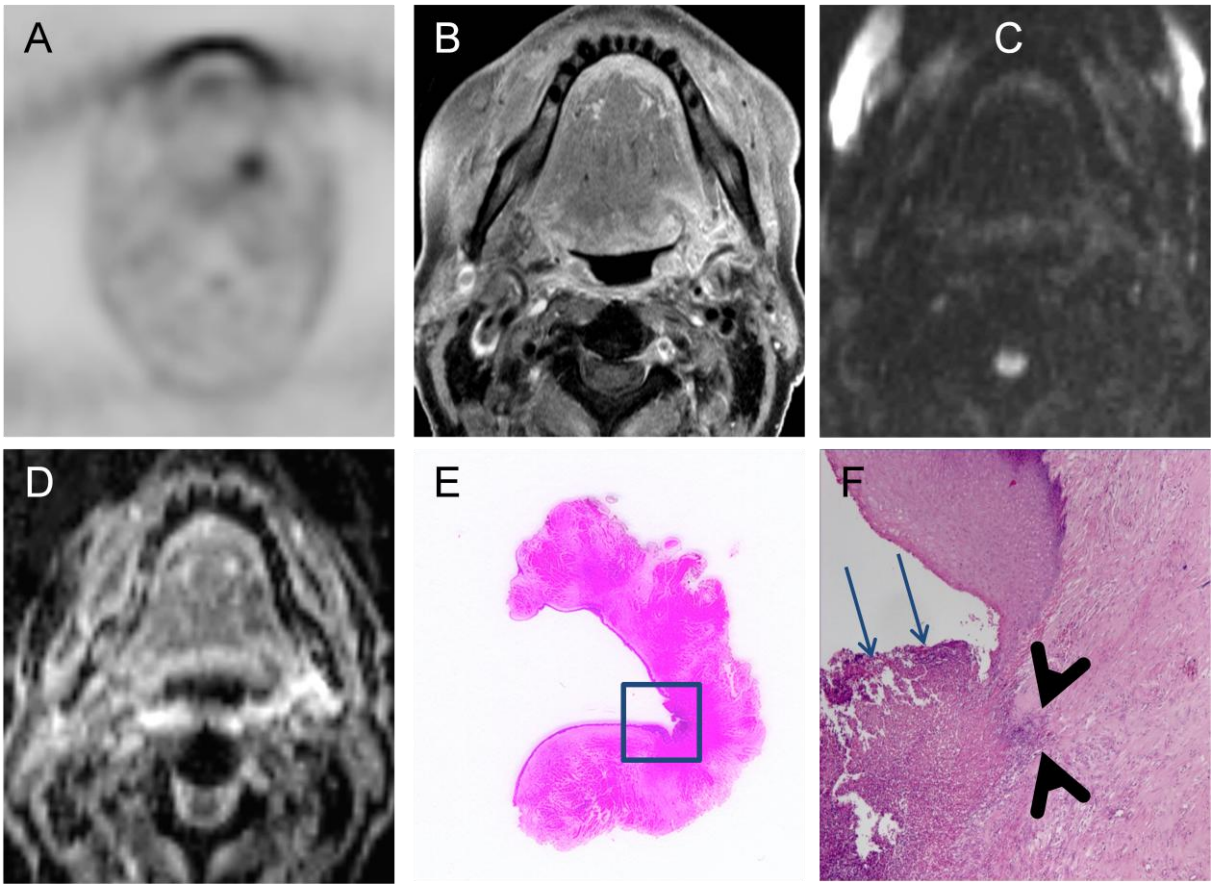

Figure 4: (a) Increased FDG-uptake in the base of tongue on the left side, corresponding to persisting left glossotonsillar ulcer on (b) post-contrast T1-weighted TSE-image suspect for persisting tumour 6 weeks after end of CRT; on DW-MRI, no substantial signal is visible on the (c) b1000-image, while the (d) ADC-map shows a hyperintense appearance of the ulcer (ADC = 0.00167 mm^2/sec) excluding the presence of restrictive tissue such as HNSCC. (e) Histology confirmed the absence of HNSCC on the histological macroslide. (f) Magnification view shows limited necrosis (arrows) in the ulcer with adjacent inflammatory cells (arrowheads).

DWI showed false positive findings in 4 subcentimetric nodes adjacent to a metastatic node in two separate patients, and in one subcentimetric lymph node in another patient. CT, TSE MR-images, and FDG-PET were negative for these lymph nodes. Histologically, these lymph nodes showed reactive changes, with loss of normal follicular structure and presence of giant cells. DW-MRI showed no false positive findings at the primary sites.

DWI failed to identify 2 lymph nodes containing micrometastases (< 3 mm); none of these adenopathies were identified by the other imaging modalities.

5.3.4 Comparison of DCE-MRI to CT/conventional MRI and FDG-PET

When compared with CT and TSE-MR (Table 4) (23 of 26 patients) DCE-MRI correctly characterized 2 persistent enlarged lymph nodes in 2 separate patients as non-tumoral. A persistent contrast-enhancing ulcer in the base of tongue, visualized on CT/conventional MRI, was correctly identified as non-tumoral by DCE-MRI. In one case of laryngeal necrosis, depicted as an enhancing ulcerated mass on conventional MRI, DCE-MRI correctly predicted absence of tumour. In one patient with a recurrence at the primary site DCE-MRI correctly detected an ipsilateral nodal metastasis (Figure 5).

Compared to FDG-PET (Table 4), (15 patients), DCE-MRI correctly excluded tumour in 2 hypermetabolic lymph nodes in two different patients and correctly downstaged one patient with a primary tumour recurrence FDG-avid ipsilateral adenopathy to N0. Also, tumour was excluded in two isolated hypermetabolic lesions at the primary site, in the base of tongue and larynx respectively, in 2 different patients (Figure 6).

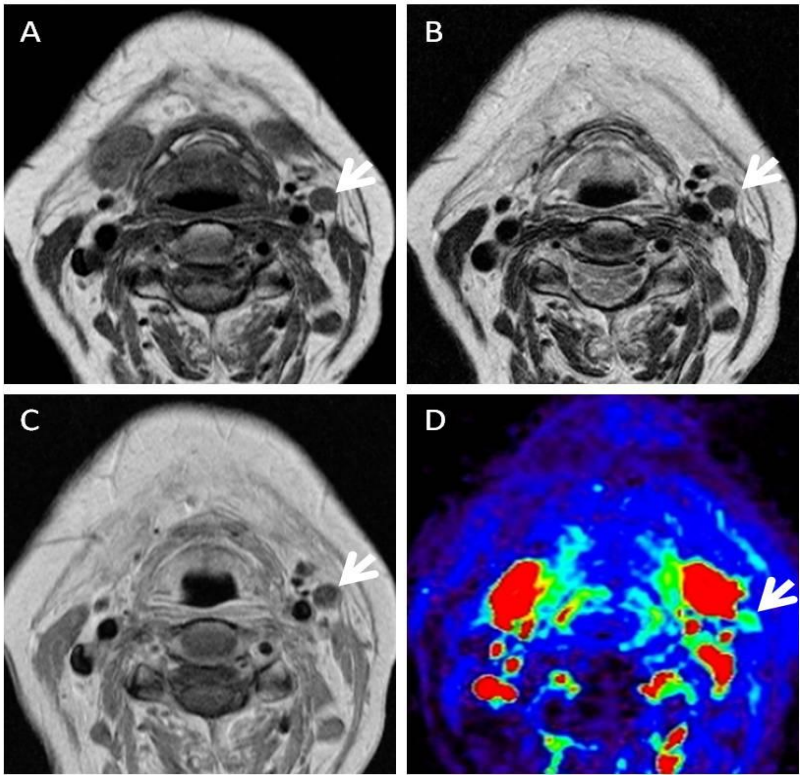

Figure 5: (a) T1-weighted TSE-image, (b) T2-weighted TSE-image and (c) Gadolinium-enhanced T1-weighted TSE-image shows non-enhancing 8 mm lymph node within level II left (arrows). (d) Perfusion map depicting the arterial slope show increased arterial enhancement, suspect for metastasis. Metastatic involvement of the lymph node was histologically confirmed.

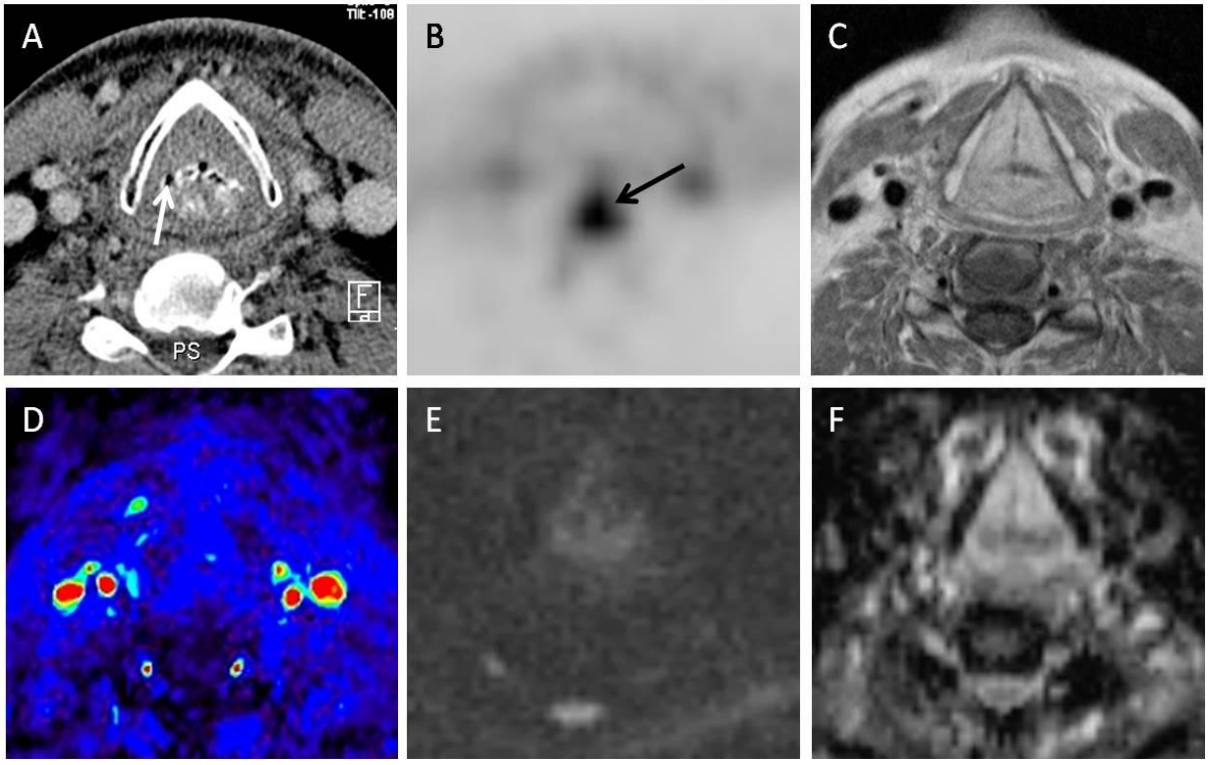

Figure 6: (a) Transverse CT image shows diffuse thickening and contrast enhancement of the false vocal cords, without focal nodular mass. Small air bubble adjacent to the right arytenoid can be appreciated (arrow). (b) Transverse FDG-PET image shows tracer uptake at the laryngeal level (arrow). (c) Contrast-enhanced T_1 weighted MR image show diffuse thickening and contrast enhancement of the false vocal cords, without focal nodular mass. (d) Perfusion map depicting the arterial slope shows no focal areas of accelerated arterial contrast uptake. (e) No asymmetric hyperintensity is revealed by b1000 and (f) the ADC map shows diffuse hyperintensity of the soft tissues at the same level. Histological examination showed granulation tissue and inflammatory infiltrate (image not shown).

Contrary, DCE-MRI was false negative for three necrotic recurrent tumour at the primary site. Furthermore, DCE-MRI failed to detect subcentimetric nodal metastases in 4 separate patients, including metastatic disease at the contralateral neck. DCE-MRI falsely upstaged the ipsilateral neck in two separate patients with a recurrence at the primary site.

Patient	CT/MRI	FDG-PET	DWI	DCE-MRI	Histology	Lesion size
Patient 1	*4 months*					
primary	NA	NA	NA	NA	NA	NA
lymph nodes	1(+)	1(+)	1(+)	1(+)	SCC	> 1.5 cm
Patient 2	*6 months*					
primary	+	+	+	-	SCC	0.4x0.5 cm
lymph nodes right	-	-	-	-	post-RT	< 1.5 cm
lymph nodes left	-	-	-	1	post-RT	< 1.5 cm
Patient 3	*6 months*					
primary	NA	NA	NA	NA	NA	NA
lymph nodes	1(+)	1(+)	-	-	post-RT	>1.5 cm
Patient 4	*12 years*					
primary	+	+	+	+	SCC	3x4 cm
lymph nodes	NA	NA	NA	NA	NA	NA
Patient 5	*13 years*					
primary	+	+	+	+	SCC	2.1x1 cm
lymph nodes right	-	-	-	-	post-RT	<1.5 cm
lymph nodes left	-	-	-	-	post-RT	<1.5 cm
Patient 6	*7 months*					
primary	NA	NA	NA	NA	NA	NA
lymph nodes	1(+)	NA	2(+)	1(+)	SCC (4)	>1.5 cm
Patient 7	*4 months*					
primary	-	+	-	-	post-RT	1.5x1.5 cm
lymph nodes	NA	NA	NA	NA	NA	NA
Patient 8	*8 months*					
primary	NA	NA	NA	NA	NA	NA
lymph nodes	1(+)	1(+)	3(+)	2(+)	SCC (1)	>1.5 cm
Patient 9	*7 years*					
primary	NA	NA	NA	NA	NA	NA
lymph nodes	1(+)	NA	1(+)	-	SCC (1)	1-1.5 cm
Patient 10	*10 months*					
primary	-	+	-	NA	post-RT	0.9x0.9 cm
lymph nodes	1(+)	1(+)	-	NA	post-RT	>1.5 cm
Patient 11	*3 months*					
primary	+	+	+	+	SCC	0.9x1 cm
lymph nodes	NA	NA	NA	NA	NA	NA
Patient 12	*6 months*					
primary	NA	NA	NA	NA	NA	NA
lymph nodes	1(+)	1(+)	1(+)	-	SCC (1)	1-1.5 cm
Patient 13	*7 years*					
primary	+	+	+	+	SCC	3.2 x 1.8 cm
lymph nodes	-	-	-	-	post-RT	<1.5 cm
Patient 14	*12 months*					
primary	+	+	+	-	SCC	2.7x1.6 cm
lymph nodes right	-	-	1(+)	-	SCC (1)	<1 cm
lymph nodes left	2(+)	2(+)	2(+)	2(+)	SCC (2)	> 1.5 cm

Patient 15	*7 months*					
primary	+	+	-	-	post-RT	1.4x1.2 cm
lymph nodes	-	-	-	-	post-RT	< 1cm
Patient 16	*4 years*					
primary	+	+	+	+	SCC	0.9x0.9 cm
lymph nodes	NA	NA	NA	NA	NA	NA
Patient 17	*3 months*					
primary	+	NA	+	+	SCC	1.5x2 cm
lymph nodes	-	NA	-	1(+)	post-RT	< 1 cm
Patient 18	*7 months*					
primary	+	NA	+	+	SCC	1.7x0.9 cm
lymph nodes	-	NA	1(+)	4(+)	post-RT	< 1 cm
Patient 19	*11 months*					
primary	+	+	+	+	SCC	2.3x2.4 cm
lymph nodes	-	-	-	-	post-RT	< 1 cm
Patient 20	*6 weeks*					
primary	+	NA	+	+	SCC	1.1x1 cm
lymph nodes	-	NA	-	-	post-RT	< 1cm
Patient 21	*9 months*					
primary	+	+	+	-	SCC	4.1x3.2 cm
lymph nodes	-	-	-	-	post-RT	< 1 cm
Patient 22	*10 months*					
primary	+	NA	-	NA	post-RT	2x1.5 cm
lymph nodes right	-	NA	-	NA	post-RT	<1cm
lymph nodes left	-	NA	-	NA	post-RT	<1cm
Patient 23	*4 years*					
primary	+	+	+	+	SCC	2.5x2.8 cm
nodes	-	1	-	-	post-RT	< 1cm
Patient 24	*10 months*					
primary	NA	NA	NA	NA	NA	NA
nodes	1(+)	1(+)	1(+)	1(+)	SCC	<1.5 cm
Patient 25	*8 months*					
primary	+	+	+	NA	SCC	1.3x1.8 cm
lymph nodes right	1(+)	1(+)	1(+)	NA	SCC (1)	< 1.5 cm
lymph nodes left	-	1(+)	1(+)	NA	SCC (2)	< 1 cm
Patient 26	*6 months*					
primary	+	+	+	+	SCC (1)	2.1 x 2.1 cm
nodes right	-	-	3(+)	-	SCC (1)	< 1 cm
nodes left	-	-	-	-	post-RT	< 1 cm

SCC: tumour recurrence; Post-RT: post-radiotherapy benign changes

+: scored as tumour recurrence by imaging modality

-: scored as benign by imaging modality

NA: not applicable

Table 4: Comparison of CT/TSE-MRI, FDG-PET and DW-MRI and DCE-MRI in correlation to histopathology.

5.4 Discussion

In this study, recurrent HNSCC at the primary site and in lymph nodes showed a significantly lower ADC and significantly higher AS, c-peak and washout than post-CRT non-tumoral tissue.

Similarly as for other tumour types, the significant difference in ADC between recurrent HNSCC and non-tumoral post-CRT tissue is most likely attributable to differences in tissue cellular density and volume of the interstitial space. This is confirmed by the histopathological findings in our study. In the resection specimens, HNSCC consisted of large cells, ordered in girdle-like hypercellular microstructures. Similar to previous animal and clinical studies, the presence of HNSCC correlated significantly with low ADC-values (10,11). This low ADC is thought to be caused by the restriction of proton movement in the EES secondary to tumour hypercellularity (12).

Contrary, the non-tumoral post-CRT areas showed higher ADC which correlated histologically to necrosis, fibrosis and inflammation which correlated to an increased interstitial space and low cell density on histological slices (13). These changes diminish the number of microstructural barriers and, thus, facilitate the tissue free water movement, leading to an increased ADC when compared with tumoral tissue.

DCE-MRI aims to distinguish malignant from benign or normal tissue by exploiting differences in contrast agent behaviour in their respective microcirculations. Of all used semi-quantitative parameters, the AS showed highest accuracy for differentiation of lesions at the primary site and lymph nodes. The AS or rate of upslope is predominantly influenced by blood volume and first pass extraction of contrast agent (14). The higher accuracy of the AS appears to be in agreement with a prior study that showed early arterial phase enhancement in HNSCC (7).

Nevertheless, the underlying microstructural substrate for differences in dynamic enhancement patterns are not entirely clear. A variable correlation of T1-kinetic parameters with MVD has been found in several tumour types (15,16). For HNSCC, only limited data are available. In a study performed by Guckel et al, a correlation was found between dynamic enhancement patterns of nodal metastatic HNSCC, with a higher micro vessel density (MVD) for nodal metastatic HNSCC compared to non metastatic lymphoid tissue (17). Vessel permeability and vascular endothelial growth factor (VEGF) may have an additional role in determining the MRI signal enhancement as a correlation has been shown between VEGF-expression and vascular permeability estimated by the k_{ep} (18). Other factors that have been

correlated with enhancement patterns include the degree of stromal cellularity, fibrosis and tissue oxygenation (7,19). Ultimately, the significant difference in enhancement between tumoral and non-tumoral sites in this study may reflect differences in tissue cellularity. As such, the absence of tumoral tissue in non-tumoral post-CRT tissue will lead to vascular compromise due to insufficient neo-angiogeneic acitivity.

When compared, DWI showed higher accuracy than DCE-MRI for differentiation of tumour recurrence from post-CRT non-tumoral tissue. Several factors may attribute to the observed differences in diagnostic accuracy. One of the major limitations of DCE-MRI is that it does not enable direct visualisation of viable and necrotic tumoral tissue portions (20). Although the tissue perfusion correlates to a certain degree with the presence of malignancy, the overlap with perfusion rates in non-tumoral tissue changes, such as inflammation, may cause loss of specificity of the technique. Especially in the early post-CRT phase, inflammation and nodal reactivity may be responsible for an accelerated arterial perfusion, making the differentiation with post-treatment recurrence particularly difficult (7). Similarly as in this study, this may generate false positive findings in persistent lesions after the end of CRT, but may also lead to failed detection of small tumoral remnants, masked by the early and strong enhancement in the surrounding inflammatory tissue. Contrary, in highly necrotic lesions, vascularity may be compromised related to insufficient tumoral load, leading to erroneously low perfusion values. In this study, this led to false negative findings in 3 large recurrent primary tumours. On the other hand, the evaluation of partially necrotic or small lesions by DCE-MRI may be difficult due to the lower lesion-to background contrast and the inability to adequately differentiate small solid from necrotic intratumoral areas. This may lead to inaccurate ROI-delineation with the potential inclusion of surrounding normal tissue or necrotic areas in the ROI, which may adversely affect imaging results (21).

Contrary, for DWI, as inflammation is expected to increase expansion of the interstitial space due to tissue congestion, the contrast with diffusion restrictive or tumoral areas is likely to be more pronounced and intensify differences in ADC between tumoral and non-tumoral tissue areas. This may in part explain the higher accuracy of DWI in this study and the higher mean ADC-values for non-tumoral lesions, when compared with previous DWI studies in the head and neck, which were performed on non-irradiated patients (11,12,22).

Furthermore, the ability of DWI to asses spatial tissue heterogeneity and separate intratumoral viable and necrotic tumoral areas as small as 4 mm, combined with the signal suppression of the surrounding non-tumoral tissue normal, may also have contributed to the higher accuracy of DWI (23). The subsequent improved conspicuity of small solid tumoral lesions, as seen in prior studies, may have improved lesion detection and ROI-delineation compared to DCE-MRI and probably explains the lower false negative ratio for partially necrotic tumoral lesions and small nodal metastases.

Finally, another issue that may explain the lower sensitivity for small nodal metastases by DCE-MRI is the variability in blood flow and size of extravascular extracellular space between normal lymphoid tissue and metastatic HNSCC, which may result in considerable overlap between semi-quantitative perfusion parameters of benign and metastatic lymph nodes (24,25). It remains important to note however, that despite the high accuracy of DWI for differentiation of post-CRT nodal HNSCC, nodal reactivity was the main cause of false positive findings of DWI and correlation with anatomical nodal features may be necessary to improve proper differentiation. Similarly as in the prior study of this thesis, these lymph nodes occurred mainly adjacent to metastatic lymph nodes, which limited the impact on diagnostic accuracy.

When compared to CT/TSE-MRI and/or FDG-PET, both DWI and DCE-MRI decreased the false positive ratio rate for persistent lesions at the primary site and persistent nodal disease in the post-RT period. DWI and to lesser extent DCE-MRI provided additional information to more correctly characterize non-tumoral persistent ulcers, persistent enlarged lymph nodes or hypermetabolic lesions caused by inflammation. On FDG-PET examinations, inflammatory cells contribute substantially to the uptake of FDG, making them a major cause of false positive findings in the early post-RT phase (26). The presence of inflammatory cells, as histopathologically identified, did not correlate with decreased ADC-values. Most probably their small cell size, compared to HNSCC, cannot compensate for the increased water mobility in inflammatory tissue or oedema.

Additionally, unlike DCE-MRI, DWI improved the detection of subcentimetric nodal metastases compared to CT/TSE-MRI and FDG-PET. At our institution, in case of a local recurrence, an ipsilateral neck dissection is routinely performed, to eradicate potential micrometastases (27). Nevertheless, DWI may be of clinical interest by limiting the extent of neck dissection in such patients, or by selecting patients more adequately for contralateral neck dissection. Further studies in a larger population are needed to address this specific issue.

Persistent lesions at the primary site, the difficult differentiation of laryngeal necrosis from recurrence or the presence of a persistent adenopathy after radiotherapy may cause a diagnostic and therapeutic dilemma. While invasive procedures – potentially leading to iatrogenic complications - and unnecessary surgery should be avoided, delay of treatment holds the risk of disease progression, eventually depriving the patient from salvage treatment. DW-MRI, showing a high accuracy for tissue differentiation in the post-RT phase independently from inflammatory or necrosis-induced tissue distortions, can provide complementary diagnostic information in the non-invasive assessment of the post-RT head and neck. As such DWI may help in the timely selection of patients towards surgery or conservative treatment. Although DCE-MRI may show additional value in the correct differentiation of persistent non-tumoral lesions at the primary site and persistently enlarged non-tumoral lymph nodes, the false negative findings in partially necrotic tumours and the inability to detect subcentimetric nodal metastases probably limits the value of the technique as a single modality in the post-CRT setting.

5.5 Conclusion

In this patient group, DWI showed additional value for detecting or excluding persistent or recurrent HNSSC after CRT and for detection of subcentimetric nodal metastases. Although DCE-MRI helped in the correct differentiation of persistently enlarged non-tumoral lesions, the lower accuracy for differentiation of partially necrotic tumours and subcentimetric nodal metastases limits the additional value and excludes its role as a standalone diagnostic tool in the post-CRT evaluation of the head and neck.

The ability to investigate the tissue micro-structure non-invasively, based on proton movement, opens a potential novel approach in the evaluation of the post-radiotherapeutic neck, complementary to currently used imaging modalities. The applied DWI technique allows a comprehensive evaluation of the entire head and neck region. Further studies are required to evaluate this technique for treatment monitoring during and after radiotherapy and its potential to influence patient management.

5.6 References

1. Ang KK, Harris J, Garden AS, et al. Concomitant boost radiation plus concurrent cisplatinum for advanced head and neck carcinomas: Radiation Therapy Oncology Group phase II trial 99-14. *J Clin Oncol* 2005; 23:3008-3015
2. Kaanders JH, Pop LA, Marres HA, et al. ARCON: experience in 215 patients with advanced head-and-neck cancer. *Int J Radiat Oncol Biol Phys* 2002; 52:769-778
3. El-Deiry M, Funk GF, Nalwa S, et al. Long-term quality of life for surgical and nonsurgical treatment of head and neck cancer. *Arch Otolaryngol Head Neck Surg* 2005; 131:879-885
4. Agra IM, Carvalho AL, Ulbrich FS, et al. Prognostic factors in salvage surgery for recurrent oral and oropharyngeal cancer. *Head Neck* 2006;28:107-113
5. Nomayr A, Lell M, Sweeney R, et al. MRI appearance of radiation-induced changes of normal cervical tissues. *Eur Radiol* 2001;11:1807-1817
6. Le Bihan D, Breton E, Lallemand D, Aubin ML, et al. Separation of diffusion and perfusion in intravoxel incoherent motion MR imaging. *Radiology* 1988;168:497-505
7. Baba Y, Furusawa M, Murakami R, et al. Role of dynamic MRI in the evaluation of head and neck cancers treated with radiation therapy. *Int J Radiat Oncol Biol Phys* 1997;37:783-787
8. Castelijns JA, van den Brekel MW. Imaging of lymphadenopathy in the neck. *Eur Radiol* 2002;12:727-738
9. van den Brekel MW, Stel HV, Castelijns JA, et al. Cervical lymph node metastasis: assessment of Radiologic criteria. *Radiology* 1990;380:379-384
10. Herneth AM, Guccione S, Bednarski M. Apparent diffusion coefficient: a quantitative parameter for in vivo tumor characterization. *Eur J Radiol* 2003;45:208-213
11. Wang J, Takashima S, Takayama F, et al. Head and neck lesions: Characterization with diffusion-weighted echo-planar MR imaging. *Radiology 2001*; 220:621-630
12. Lyng H, Haraldseth O, Rofstad EK. Measurement of cell density and necrotic fraction in human melanoma xenografts by diffusion weighted magnetic resonance imaging. *Magn Reson Med* 2000;43:828-836
13. Mukherji SK, Mancuso AA, Kotzur IM, et al. Radiologic appearance of the irradiated larynx. Part I. Expected changes. *Radiology* 1994;193:141-148

14. Padhani AR. MRI for assessing antivascular cancer treatments. *Br J Radiol* 200376:S60-S80
15. Hawighorst H, Knapstein PG, Weikel W, et al. Angiogenesis of uterine cervical carcinoma: characterization by pharmacokinetic magnetic resonance parameters and histological microvessel density with correlation to lymphatic involvement. *Cancer Res* 1997;57:4777-4786
16. Su MY, Cheung YC, Fruehauf JP, et al. Correlation of dynamic contrast enhancement MRI parameters with microvessel density and VEGF for assessment of angiogenesis in breast cancer. *J Magn Reson Imaging* 2003;18:467-477
17. Guckel C, Schnabel K, Deimling M, Steinbrich W. Dynamic snap-shot gradient-echo imaging of head and neck malignancies: time dependency and quality if contrast-to-noise ratio. *MAGMA* 1996;4:61-69
18. Knopp MV, Weiss E, Sinn HP, et al. Pathophysiological basis of contrast enhancement in breast tumours. *J Magn Reson Imaging* 1999;10:260-266
19. Newbold K, Castellano I, Charles-Edwards E, et al. An exploratory study into the role of dynamic contrast-enhanced magnetic resonance imaging or perfusion computed tomography for detection of intratumoral hypoxia in head-and-neck cancer. *Int J Radiat Oncol Biol Phys* 2009;74(1):29-37
20. Thoeny HC, De Keyzer F, Vandecaveye V, et al. Effect of vascular targeting agent in rat tumor model: dynamic contrast-enhanced versus diffusion-weighted MR imaging. *Radiology* 2005;237:492-499
21. Fischbein J, Noworolski SM, Henry RG, Kaplan MJ, Dillon WP, Nelson SJ. Assessment of metastatic cervical adenopathy using dynamic contrast-enhanced MR imaging. *Am J Neuroradiol* 2003;24:301-311
22. Razek A, Soliman N, Elkhamary S, Alsharaway M, Tawfik A. Role of diffusion-weighted MR imaging in cervical adenopathy. *Eur Radiol* 2006;16:1468-1477
23. Razek AA, Megahed AS, Denewer A, Motamed A, Tawfik A, Nada N. Role of diffusion weighted MRI in differentiation between the viable and necrotic parts of head and neck tumors. *Acta Radiol* 2008;49:364-370
24. Vaupel P. Tumor blood flow. In: Molls M, Vaupel P, eds *Blood Perfusion and Micorenvironment of Human Tumors.* Berlin: Springer-Verlag; 1998:43
25. Evelhoch JL. Key factors in the acquisition of contrast kinetic data for oncology. *J Magn Reson Imaging* 1999;10:254-259

26. Min Y, Russel B, Graham M, et al. The role of FDG-PET in management of neck metastases from head-and-neck cancer after definitive radiation treatment. *Int J Radiation Oncology Biol Phys* 2005;63:991-999
27. van den Brekel MW, van der Waal I, Meijer CJ, et al. The incidence of micrometastases in neck dissection specimens obtained from elective neck dissections. *Laryngoscope* 1996;106:987-991

Chapter 6:
Value of DW- and DCE-MRI as imaging biomarkers during chemoradiotherapy of head and neck squamous cell carcinoma

6.1 Introduction

Currently, bio-adaptive treatment strategies such as IMRT, the addition of radio-sensitizers or targeted agents are increasingly researched and introduced in clinical applications (1,2,3). Cure rates and patient survival may be further improved by adapting the non-surgical treatment scheme to the individual patients treatment response. Therefore, early diagnostic biomarkers are warranted (4).

Studies in abdominal, breast and brain tumours have shown a correlation of pre-treatment ADC, DCE-parameters and ADC- and DCE-changes early after non-surgical treatment with final treatment response (5,6). In a study in an orthotopic HNSCC mouse model, DWI allowed early evaluation of treatment response during chemoradiation (7). The aim of this prospective study in locally advanced HNSCC was to evaluate DWI and DCE-MRI during CRT for early response assessment and prediction of LRC at two years after end of treatment, in comparison with volumetric tumour measurements.

6.2 Materials and Methods

6.2.1 Study design

Thirty-one patients (29 men, 2 women, mean age: 53 years, range: 38 to 66 years) with histologically proven HNSCC, were consecutively included in this prospective study. One patient was excluded due to detection of metastatic disease. The primary tumour localization and clinical stage of the remaining 30 patients are summarized in Table 1.

Patient	primary tumour localization	Staging
Patient 1	tonsil	T2N3
Patient 2	tonsil	T2N2a
Patient 3	piriform sinus	T4a2b
Patient 4	supraglottic	T3N1
Patient 5	piriform sinus	T4aN2b
Patient 6	supraglottic	T4aN2c
Patient 7	glottic	T1N0
Patient 8	base of tongue	T3N1
Patient 9	lateral oropharynx	T4aN2c
Patient 10	supraglottic	T3N2b
Patient 11	posterior hypopharynx	T4aN2c
Patient 12	supraglottic	T3N2b
Patient 13	base of tongue	T3N2b
Patient 14	lateral oropharynx	T4N1
Patient 15	piriform sinus	T2N1
Patient 16	supraglottic	T4aN2c
Patient 17	glottic	T3N0
Patient 18	supraglottic	T4aN2c
Patient 19	lateral oropharynx	T2N1
Patient 20	lateral oropharynx	T3N2c
Patient 21	piriform sinus	T1N2b
Patient 22	lateral oropharynx	T4aN2c
Patient 23	tonsil	T3N0
Patient 24	piriform sinus	T4aN1
Patient 25	base of tongue	T3N2c
Patient 26	lateral oropharynx	T4
	piriform sinus	T3N1
Patient 27	supraglottic	T3N2b
Patient 28	piriform sinus	T3N2c
Patient 39	tonsil	T2N2b
Patient 30	tonsil	T4aN1

Table 1: Initial tumour localization, and TNM-staging in the included patient group

Treatment consisted of concomitant CRT in 27 patients and radiotherapy 3 patients, for which diagnosis, staging and treatment planning was done according to current international standards. Radiotherapy was delivered to a total dose of 72 Gray (Gy) according to a hybrid fractionation schedule in 28 patients: 20 daily fractions of 2 Gy, followed by 20 fractions of 1.6 Gy twice daily (32 Gy), to a total dose of 72 Gy. In the patient with a T1 glottic cancer, a total dose of 55Gy was delivered. All patients completed the planned treatment scheme.
Chemotherapy consisted of Cisplatinum, 100 mg/ml at week 1 and 4.

A timeline shows the different methodological steps in the study (Figure 1). Routine pre-treatment examinations included diagnostic contrast-enhanced CT, FDG-PET-CT in 14 patients, and panendoscopy with biopsy in all patients. MRI with anatomical, DCE- and DWI-sequences was added just prior to and at 2 and 4 weeks after the start of CRT. All MRI-studies were of sufficient technical quality to allow analysis. The study was approved by the local ethics committee and all patients gave written informed consent prior to inclusion.

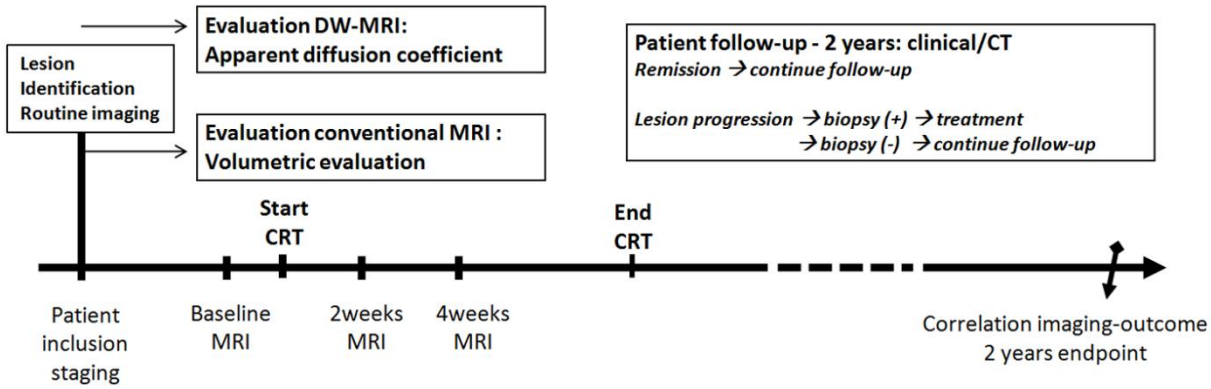

Figure 1: Timeline detailing the exact set-up of study inclusion and data processing used in this study.

6.2.2 Imaging technique

All patients underwent the standardized anatomical TSE-MRI, and functional DWI- and DCE-MRI sequences as described in chapter 3. MRI imaging covered the entire head and neck ranging from the base of skull to the thoracic outlet, and included all regional nodal stations (retropharyngeal space and all neck levels).

6.2.3 Image analysis

6.2.3.1 Lesion identification and correlation

The primary tumours and nodal metastases were identified on the baseline TSE-MRI and DWI in correlation to the clinical information and the pre-therapeutic routine imaging results. Primary tumours were topographically annotated by their slice position and anatomical position in the upper aerodigestive tract. Adenopathies were topographically annotated by their position in correlation to anatomical structures in the neck - the submandibular gland, the sternocleidomastoid muscle and the jugular vein and level position according to the AAO-HNS classification (8). The primary tumours and metastatic adenopathies were identified on the 2 and 4 weeks follow-up TSE-MRI and DWI

examinations by visual correlation and correlation of slice positions with the baseline examination.

6.2.3.2 Image analysis

The images of the TSE-MRI, DWI and DCE-MRI were quantitatively interpreted in a blinded fashion as described in chapter 3.2.

For both DWI, DCE-MRI and TSE-MRI lesion ADC, respectively lesion perfusion and lesion volume at 2 and 4 weeks after the start of CRT were correlated to the baseline values for treatment assessment and correlation to treatment outcome.

The ADC changes (ΔADC_N) in % for each lesion between the baseline and the 2 and 4 weeks time point were calculated using the formula:

$$\Delta ADC_N=[(ADC_N - ADC_B)/ADC_B]*100$$

Where ADC_B represents pre-treatment ADC-value and ADC_N represents the ADC on the N^{th} time point after the start of CRT.

The changes of the perfusion parameter ($\Delta PERF_N$) in % in for each lesion between the baseline and the 2 and 4 weeks time point was calculated using the formula:

$$\Delta PERF_N=[(PERF_N - PERF_B)/PERF_B]*100$$

Where $PERF_B$ represents pre-treatment ADC-value and $PERF_N$ represents the PERF on the N^{th} time point after the start of CRT.

The volume changes (ΔV_N) in % for each lesion between the baseline and the 2 and 4 weeks time point were calculated using the formula

$$\Delta V_N=[(V_N - V_B)/V_B]*100$$

Where V_B represents pre-treatment lesion volume and V_N represents the volume on the N^{th} time point after the start CRT.

6.2.4 Correlation to treatment outcome

As in our institution neither routine biopsies nor routine elective neck dissections are performed after CRT, the imaging findings were primarily correlated to post-treatment patient follow up as described in chapter 3.4.2.

6.2.5 Statistical analysis

The software package Statistica 8® (StatSoft Inc, Tulsa, OK, USA) was used for the statistical analysis. A p-value < 0.05 was considered statistically significant.

The ΔADC_N, $\Delta PERF_N$ and the ΔV_N of primary lesions and adenopathies showing CR versus those with later tumour recurrence were compared with a Mann-Whitney test. ROC analysis with the area under the curve (AUC) was employed to investigate the discriminatory capability of the ΔV_N, $\Delta PERF_N$ and ΔADC_N. For calculation of the sensitivity, specificity, accuracy, PPV and NPV for of the ΔV_N, $\Delta PERF_N$ and ΔADC_N, the optimal threshold was determined as the point giving equal weighting to sensitivity and specificity on the ROC curve.

Cumulative LRC was estimated with the Kaplan-Meier product-limited (actuarial) method and the statistical significance of differences between curves were compared with the log-rank test. In the univariate analysis the following clinical variables were entered: tumour localization (laryngeal versus pharyngeal), age, T-stage (T1-2 vs. T3-4), N-stage (N1-2a vs. N2b-3), initial primary tumour volume and initial nodal volume. All clinical variables with a p-value < 0.1 were included in a multivariate analysis comparing the predictive value of the separate imaging variables; the ΔV_N, $\Delta PERF_N$ and ΔADC_N.

6.3 Results

6.3.1 Treatment outcome

Complete LRC at 2 years after the end of treatment was achieved in 15 of 30 patients (50%). Six of 30 patients (20%) developed an isolated local recurrence (at a median of 129 days post-CRT, range: 27 to 189 days) for which salvage surgery could be performed in 5 patients. Seven of 30 patients (23%) developed a regional recurrence without primary tumour recurrence (at a median of 224 days post-CRT, range: 91 to 364 days), of whom 4 were eligible for neck dissection at time of diagnosis. Two of 30 patients (7%) developed a

simultaneous locoregional tumour recurrence (at 126 and 161days after CRT, respectively); one patient received salvage surgery with bilateral neck dissection, the other was inoperable because of the extent of disease. Nine of 30 patients (30%) deceased during the 2 years follow-up: 7 patients because of a tumour recurrence. The death of two patients was unrelated to the HNSCC.

6.3.2 Clinical variables and volumetric tumourassessment: lesion based assessment and correlation with locoregional control

The univariate analysis of clinical pre-treatment variables showed a substantial correlation between nodal volume and N-stage and 2-year LCR (p=0.06 respectively 0.08), no correlation was found for the other variables (p>0.2) (Table 2). In the multivariate analysis, the N-stage and nodal volume no longer showed any correlation with LCR (p>0.5).

The ΔV_{2weeks} was significantly lower for primary tumours with post-CRT recurrence than with CR (in %, -2.8.1±34.5 versus 31.3±32.1, p=0.03) but no significant difference was found for adenopathies (-15.4±58.9 versus 19.9±39.7, p=0.1). The ΔV_{4weeks} showed no significant difference for either lesions (in %, primary tumour: 46.4±27.0 vs. 56.3±30.8; adenopathies: 15.1±67.4 vs. 49.3±41.3, both p>0.1). The ΔV_{2weeks} and ΔV_{4weeks} showed no significant correlation with the LRC (p>0.05) in the multivariate analysis.

Pre-treatment parameter	Locoregional control
Volume primary tumour (≥ 12.31 cc vs. < 12.31 cc)	p=0.23987
Volume adenopathy (≥ 18.612 cc vs. < 18.612 cc)	p=0.06463
T-stage (T1-2 vs. T3-4)	p=0.21938
N-stage (N0-1-2a vs. N 2b-2c-3)	p=0.08019
age (≥ 53 jr vs. < 53 jr)	p=0.92106
Tumour localization (Laryngeal versus pharyngeal)	p=0.66

Table 2: The univariate analysis of tumour-specific properties prior to treatment. N-stage and volume of adenopathies showed a p-value smaller than 0.1 and were included in the subsequent multivariate analysis.

6.3.3 Tumour diffusion: correlation with locoregional control

The ΔADC_{2weeks} was significantly lower for primary tumours and adenopathies with post-CRT recurrence than CR (in %, primary tumour: -1.6±9.7 vs. 40.5±25.6, p<0.0001; adenopathies: 10.9±26 vs. 52.4±36.1, p<0.0001). The ΔADC_{4weeks} was significantly lower for primary tumours and adenopathies with post-CRT recurrence than with CR (in %; primary tumour: -1.0±24.6 vs. 65.1±36, p<0.0001; adenopathies: 15.8±25.6 vs. 67.6±41.4, p<0.0001). In the multivariate analysis, the ΔADC_{2weeks} and ΔADC_{4weeks} correlated significantly to 2-year LRC; (ΔADC_{2weeks} ; p=0.003, ΔADC_{4weeks} ;p<0.0001) (Figure 2).

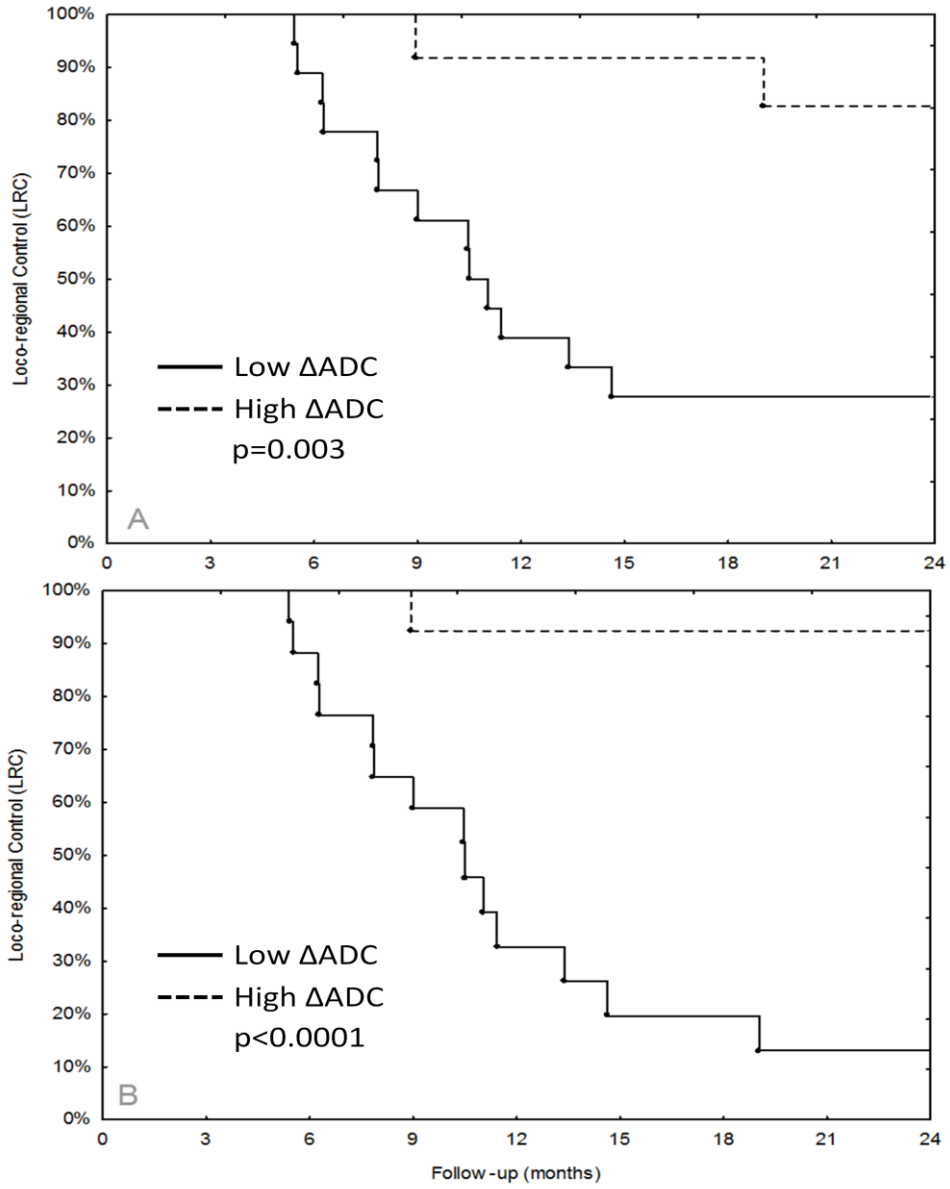

Figure 2: Multivariate analysis shows significant correlation of ΔADC with locoregional control (Y-axis) at (A) 2 and (B) 4 weeks.

6.3.4 Tumour perfusion assessment and correlation with locoregional control

Changes in the AS showed highest AUC and accuracy compared to the c-peak and washout at all time points and was chosen for further assessment and comparison. Changes in the AS will be further referred to as ΔPERF.

The $\Delta PERF_{2weeks}$ showed no significant difference between primary tumours or adenopathies with post-CRT recurrence than with CR (in %, primary tumour: 73.5±86.6 vs. 9.9±52.4,p=0.08; adenopathies: 29.8±66.85 vs. -1.1±50.5,p=0.11). For primary tumours, non-responding lesions showed tendency to have higher ΔPERF than responding lesions.

The $\Delta PERF_{4weeks}$ showed no significant difference between primary tumours or adenopathies with post-CRT recurrence than with CR (in %, primary tumour: 46.8±46.8 vs. 41.1±113.6,p=0.8; adenopathies: 36.8±84.2 vs. 37.5±121.9,p=0.9).

After multivariate analysis, the $\Delta PERF_{2weeks}$ and $\Delta PERF_{4weeks}$ showed no significant correlation with the LRC ($p>0.1$).

6.3.5 Comparison of different tumour imaging methods

The sensitivity, specificity accuracy, PPV and NPV of DWI, DCE-MRI and TSE-MRI are shown in Table 3.

At 2 and 4 weeks during CRT, the ΔADC showed highest AUC and accuracy for prediction of treatment outcome compared to the ΔV and ΔPERF. Except for primary tumours at 4 weeks during CRT, where the ΔPERF showed slightly higher accuracy than the ΔV, the ΔPERF had lowest accuracy at 2 and 4 weeks during CRT.

Examples of early response assessment at 2 weeks for primary lesions and 4 weeks during CRT for lymph node metastases are shown in Figure 3 – 6.

Threshold (%)	14	20	60	Threshold (%)	14	33	18
Primary lesion	ΔADC	ΔV	ΔPERF	**Nodal metastases**	ΔADC	ΔV	ΔPERF
True positive	7	7	5	**True positive**	8	9	6
False positive	2	10	1	**False positive**	5	23	20
True negative	21	13	22	**True negative**	39	21	24
False negative	1	1	3	**False negative**	2	1	4
Sensitivity	88%	88%	63%	**Sensitivity**	80%	90%	60%
Specificity	92%	57%	96%	**Specificity**	89%	48%	55%
Accuracy	94%	65%	87%	**Accuracy**	87%	56%	56%
PPV	78%	41%	83%	**PPV**	62%	28%	23%
NPV	96%	93%	88%	**NPV**	95%	96%	85%

Threshold (%)	25	65	45	Threshold (%)	19	50	25
Primary lesion	ΔADC	ΔV	ΔPERF	**Nodal metastases**	ΔADC	ΔV	ΔPERF
True positive	7	6	6	**True positive**	8	7	5
False positive	2	10	7	**False positive**	2	17	17
True negative	21	13	17	**True negative**	42	27	27
False negative	1	2	2	**False negative**	2	3	5
Sensitivity	88%	75%	75%	**Sensitivity**	80%	70%	50%
Specificity	92%	57%	71%	**Specificity**	95%	61%	61%
Accuracy	94%	61%	72%	**Accuracy**	93%	63%	59%
PPV	78%	38%	46%	**PPV**	80%	29%	23%
NPV	96%	87%	89%	**NPV**	95%	90%	84%

PPV: positive predictive value

NPV: negative predictive value

Table 3: Comparison of accuracy of ΔADC versus ΔV versus ΔPERF at (upper table) 2 weeks and (bottom table) 4 weeks.

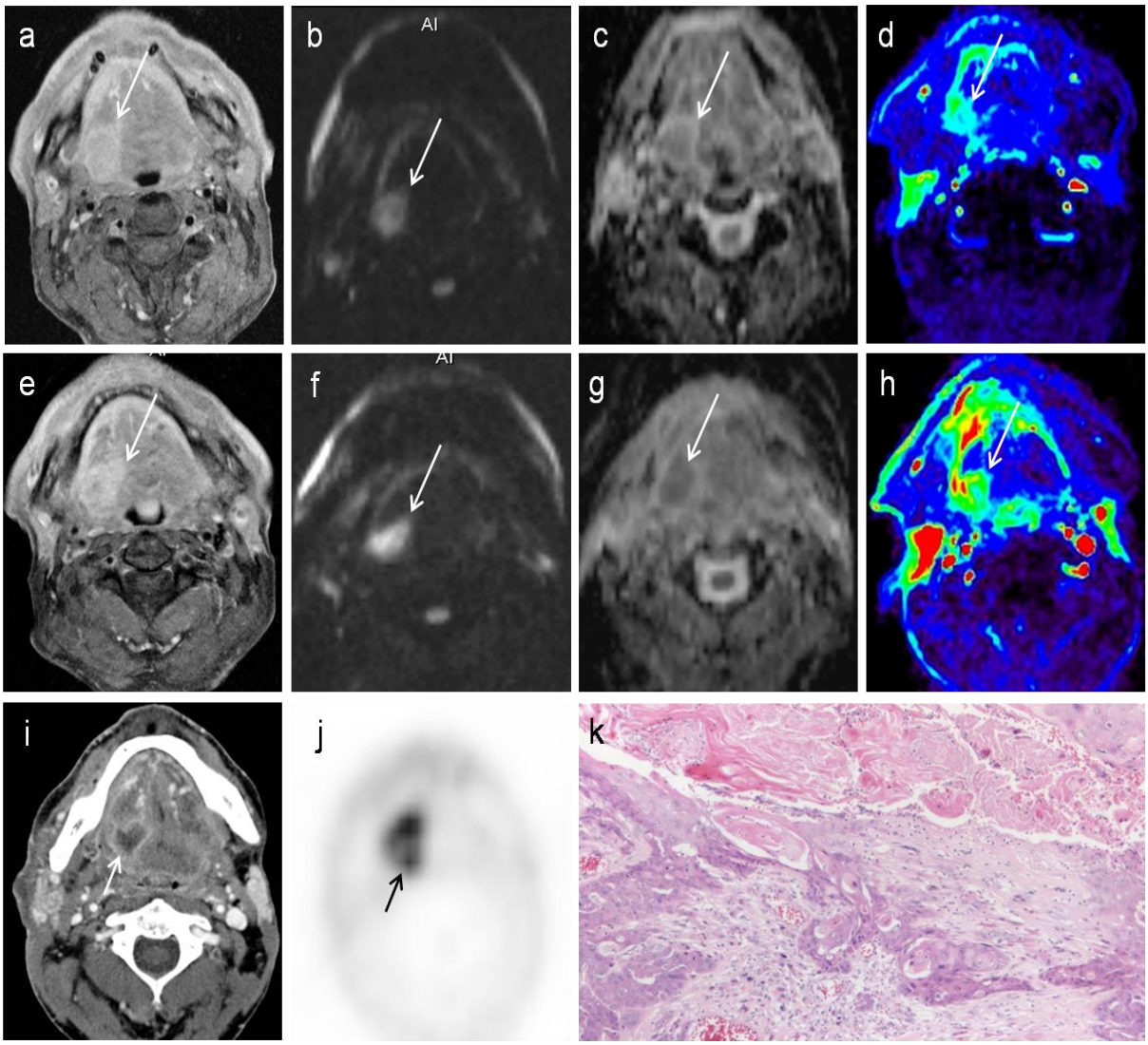

Figure 3: Upper row shows tumoral mass in the right base of tongue on (a) contrast-enhanced T1-weighted turbo-spin echo (TSE) MRI, (b) b1000 diffusion-weighted image, (c) ADC-map and (d) arterial slope perfusion map. Middle row: tumour at 2 weeks during chemoradiotherapy (e) is unchanged in tumour dimensions, (f) shows unchanged signal intensity on the b1000 diffusion-weighted image, (g) ΔADC (in %) < 15 and ΔPERF (in %) < 18, indicative of treatment failure. Bottom row shows tumour recurrence on (i) CT study and (j) FDG-PET at 4 months after completion of chemoradiotherapy. Recurrent SCC was confirmed by (k) histopathology after surgical excision.

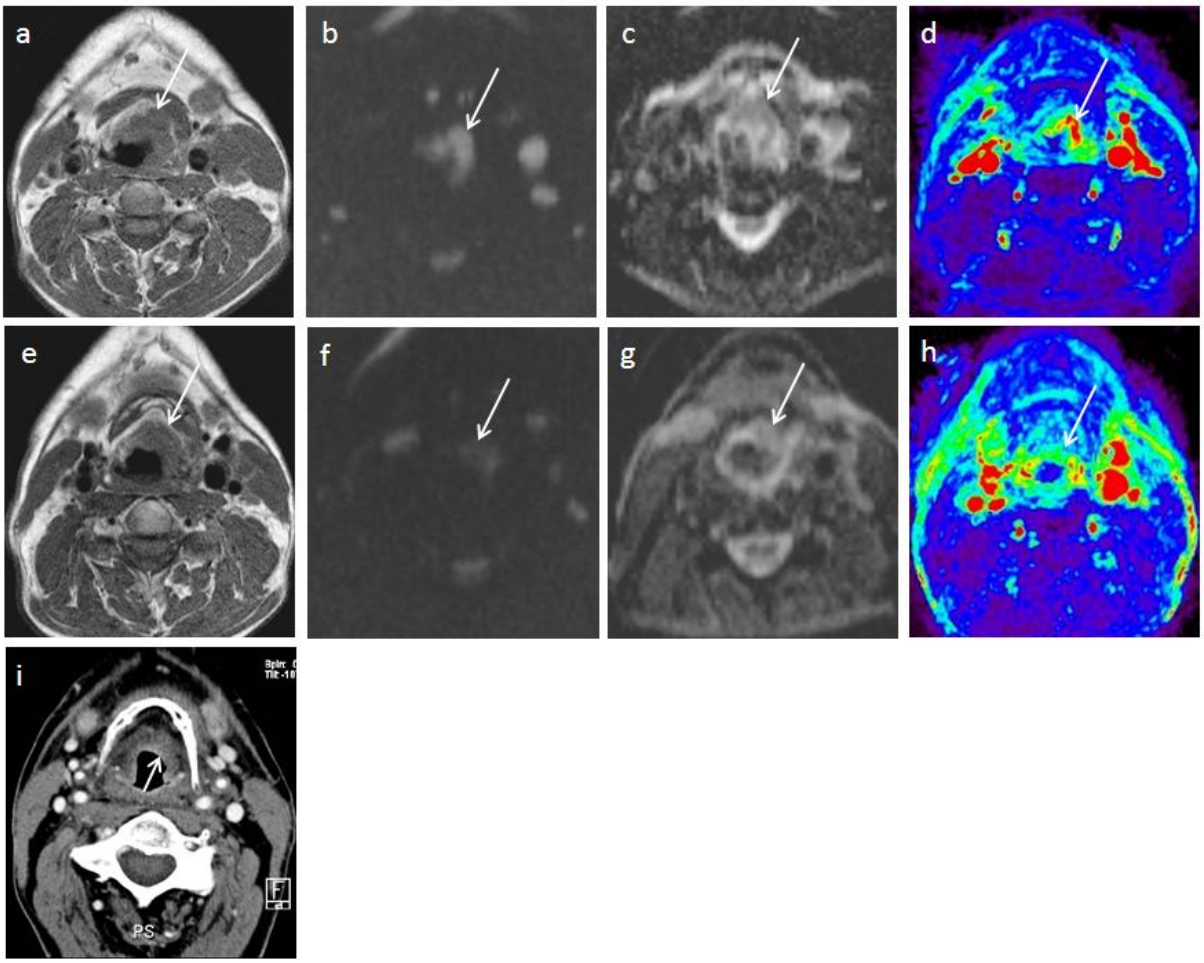

Figure 4: Upper row: Left supraglottic ulcerated tumoral mass on (a) contrast-enhanced T1-weighted turbo-spin echo (TSE) MRI, (b) b1000 diffusion-weighted image, (c) ADC-map and (d) arterial slope perfusion map. Middle row: (e) The supraglottic tumour shows unchanged volume at 2 weeks during chemoradiotherapy. (f) the tumour shows substantial decrease of signal intensity on the b1000 diffusion-weighted image, corresponding to (g) a ΔADC (in %) > 40 and ΔPERF (in %) > 50. These findings are indicative of good treatment response. (i) Follow-up CT scan after 2 years shows complete remission of the primary tumour site.

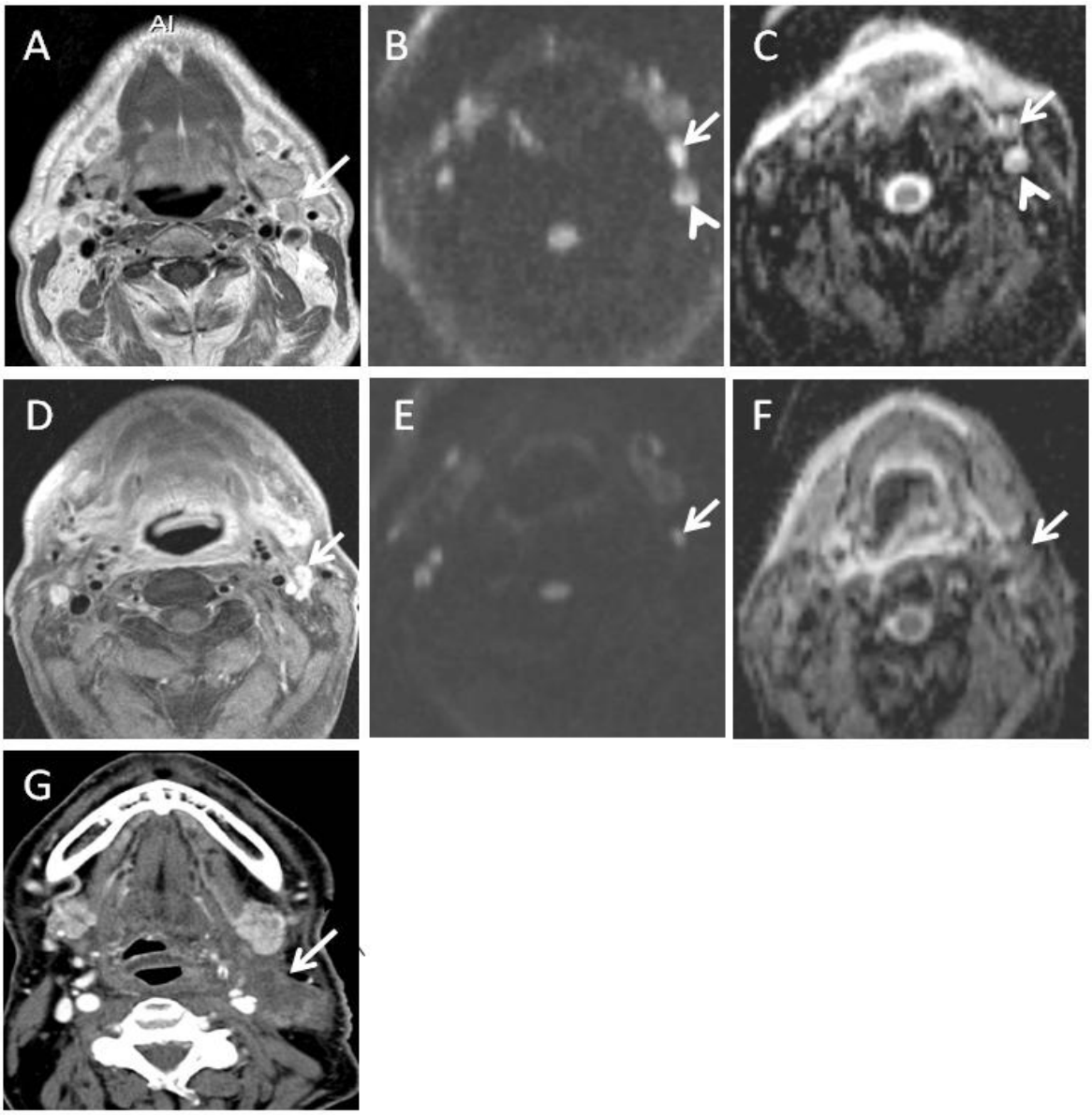

Figure 5: Patient with left tonsillar cancer shows two subcentimetre nodal metastases in left level 2 of the neck prior to treatment on (a) contrast-enhanced T1-weighted turbo-spin echo (TSE) MRI, (b) b1000 diffusion-weighted image and (c) ADC-map (arrow, arrowhead). At 4 weeks during chemoradiotherapy, (d) the posterior adenopathy has completely regressed (arrowhead), while the more anterior lymph node has partially regressed (arrow). (e) Persistent hyperintensity is present in the anterior lymph node correlating to (f) a ΔADC (in %) < 5, indicative of bad treatment response (arrows). (g) Follow-up CT scan shows nodal tumour recurrence at 8 months after completion of chemoradiotherapy (arrow).

6.4 Discussion

In this study group, DWI allowed prediction of 2-year LRC at 2 and 4 weeks during CRT and showed a substantially higher accuracy than serial volumetric assessment for differentiation between responding and non-responding lesions.

During CRT, the ΔV_{2weeks} was only significantly different between responding and non-responding primary tumours. Although no significant correlation with LRC was found, the ΔV_{2weeks} with a threshold of 20% and ΔV_{4weeks} with 65% allowed a high NPV. In a study of Jaulerry et al, tumour volume regression of 25% at 2 weeks during RT was predictive for CR after RT (9). However, in the current study, a high number of primary tumoral and nodal metastatic lesions, including eventually responding lesions, showed no substantial volume regression early during CRT. Therefore, the resulting poor PPV of volumetric measurements hampered the identification of non-responding lesions and is a probable reason why volumetric assessment lacks sufficient reliability to select lesions for treatment intensification, such as dose escalation.

The ability to probe the tissue microstructure and the high sensitivity of DWI for low levels of intratumoral cell destruction may explain the high accuracy of DWI for early response assessment (10,11). Tumoral lesions with CR after CRT showed a significantly higher ΔADC than tumoral lesions that recurred. Historadiological correlation during treatment follow-up in prior studies showed a relation between the ADC increase and necrosis and apoptosis, in response to cytotoxic and radiation treatment (12,13). The loss of tissue cellularity in apoptosis and necrosis will increase the ADC (14,15). Contrary, absent ADC increase in primary tumours or adenopathies during CRT corresponded to lesions with a high likelihood of recurrence post-CRT, which is probably related to diffusion restriction in the dense microstructure of persistent tumour (11,16). These findings are in agreement with the results in a recent study by Kim et al, which also found a significant ADC increase in responding compared to non-responding metastatic adenopathies (17). Moreover, using similar thresholds a near identical accuracy is found in this study for nodal metastases at the 2 weeks' time point, compared to the 1 week time point during CRT in the study of Kim et al (17). These similar findings demonstrate the robustness of DWI as a potential biomarker for early prediction of treatment response.

In addition to the findings of the study of Kim et al (17), our findings indicate that the ΔADC_{2weeks} and ΔADC_{4weeks} correlate significantly to 2-year LRC. Recently, DWI was shown to predict at 2 weeks during CRT the final imaging and clinical response in uterine cervical cancer (18). In patients with primary cerebral neoplasms, the combination of DWI before and at three weeks after the initiation of treatment has been demonstrated to accurately predict later radiographic response, time to progression and overall survival (16,19,20). The underlying causative link between ADC-changes during CRT and later LRC remains unclear due to lack of historadiological correlation in our study. The relation between the observed signal changes on DWI and the underlying pathophysiological processes, such as apoptosis, hypoxia, proliferation index or tumour grade, are to be further investigated (21).

Unlike DWI, DCE-MRI with semi-quantitative perfusion parameters was only of limited value for the early differentiation of responding and non-responding lesions. Compared to the other perfusion variables, the ΔPERF based on the AS showed highest accuracy, but also failed to show significant differences at 2 and 4 weeks during CRT between lesions with later CR and lesions with later tumour recurrence.

So far, the role of DCE-MRI as an imaging biomarker during chemoradiation has mainly been investigated in uterine cervical cancer. In this tumour type, different studies have shown a positive correlation between either pre-treatment enhancement or initial enhancement rate, 2 weeks during chemoradiation, and local tumour control (22,23). A recent pilot study in a limited number of patients investigating DCE-MRI during radiotherapy of HNSCC showed a significant correlation between increased blood volume and local control while no substantial change was found in blood flow or blood volume in adenopathies (24).

In our study, the lack of statistically significant differences of perfusion variables between responding and non-responding lesions may reflect the complexity of intratumoral physiological changes that occur during fractionated CRT. Usually, changes in tissue contrast enhancement relate to changes in vascular supply, capillary permeability and cell density (25). The dynamic contrast enhancement patterns in tumours during CRT may be averaged out by the simultaneous physiological processes known to occur during radiation treatment. Radiation-induced cell loss may lead to a decrease of dynamic tissue enhancement, due to direct radiation-induced vascular damage and decrease of intralesional tumour load with loss of angiogeneic activity. However, simultaneously, the increase of leakage space secondary to cell loss may lead to an increased tissue enhancement. Finally, the variable occurrence of tumour hypoxia prior to and during CRT is usually associated with decreased tumour perfusion as measured by DCE-MRI.

In a previous study in head and neck cancer, an increased tumour perfusion measured by DCE-MRI correlated to favourable tumour response to radiation treatment; it has been suggested that the increased tumour perfusion may indicate an increased tumour oxygenation which could lead to increased tumour cell radio-sensitivity (24). However, this hypothesis is in contradiction with a prior report in patients treated with induction chemotherapy (26) as well as the findings of our study. Moreover, although decreased perfusion has been related to tumour hypoxia (27,28), it is currently unclear to what extent DCE-MRI directly reflects fractions of radiobiologically hypoxic cells (29).

Although not significantly different, non-responding primary tumours showed a tendency to increased tissue perfusion – as measured by the AS – during treatment. This may indicate persistent angiogeneic activity in non-responding compared to responding lesions. However, the large overlap with responding primary tumours in which the tissue AS increased during treatment, limits the diagnostic accuracy of DCE-MRI . This underscores the inability of the technique to directly assess tissue viability, but also raises the question to what extent the technique is hampered by treatment-induced inflammation. Inflammatory induced rapid tissue enhancement, initiated by CRT-induced tumour necrosis, is difficult to differentiate from tumour-related tumour enhancement (30,31).

Part of the poorer results of DCE-MRI in this study may relate to the sole use of semi-quantitative perfusion variables which do not accurately reflect contrast medium concentration in tissues. The K^{trans} and k_{ep} allow for quantitative evaluation of the tumoral vascular response to chemoradiation by depicting changes in tissue permeability as a marker for response. Permeability parameters have the advantage that they provide information that can be linked to underlying biologic processes of the vasculature, such as the permeability surface area and flow (25). However, quantified models are more complex to derive, less robust to noise and more susceptible to artifacting secondary to patient or physiological movement, making application and interpretation of quantitative DCE-MRI in the head and neck currently difficult. Further studies are required to further elucidate the potential role of these parameters in the treatment follow-up of HNSCC solely or in combination with other imaging modalities like DWI or PET with hypoxia markers (32).

As a functional marker for the head and neck, DWI may be advantageous over other functional MR modalities, such as MR-spectroscopy and, as previously mentioned, DCE-MRI. Unlike MR-spectroscopy, DWI is less restricted in its anatomical coverage and is, if appropriately optimized, able to comprehensively evaluate the primary tumour and all nodal stations in an acceptable scanning time. Also, being a quantification of signal loss, the ADC is

a robust imaging parameter as it will be less susceptible to variations induced by the magnetic field or tissue position in the coil (11). Moreover, the ADC-quantification is based on a relatively simple model and represents more directly tissue properties compared to DCE-MRI (17). Preferentially, a standardized ADC-calculation including at least 3 b-values with maximum b-values exceeding b500 sec/mm^2 should be performed (5,11,21). In order to optimize DWI for early treatment follow-up, time-dependable ADC thresholds may need to be defined (5). The ADC may falsely decrease if necrosis resolves. Contrary, the induction of liquefaction necrosis may interfere with DWI-measurements and falsely increase the ADC of small remnant solid tumoral components due to partial volume averaging (21). This may in part explain the lower PPV of the ΔADC_{2weeks} compared to the ΔADC_{4weeks} in adenopathies, often showing cystic necrotic degeneration prior to CRT. Early during CRT, necrosis may have been absorbed in a number of responding adenopathies, and may have led to an initial decrease of ADC, falsely suggesting poor response. As such, adenopathies may be preferably evaluated at a later time point during CRT compared to primary tumours.

Contrary, the incorrect prediction of good treatment response in a primary tumour, respectively at 2 and 4 weeks during CRT, was probably secondary to extensive intratumoral necrosis obscuring small persistent solid tumour depositions. Although lesions were visually assessed on b1000-images for tumour heterogeneity, a more automated evaluation incorporating tumour heterogeneity may be needed to avoid interpretation error. A histogram-based approach classifies different tumour diffusion environments but cannot depict spatial heterogeneity and may therefore fall short to guide topographically guided treatment like CRT (33). A voxel-wise approach incorporating registration of image data sets between treatment interval examinations, which allows to depict the topographical heterogeneity of tumour response to treatment between consecutive examinations may help to further develop DWI as a marker for bio-adaptive treatment (16).

Despite the current limitations involving image interpretation and imaging standardization, the microstructural driven imaging properties of DWI may be advantageous over metabolic imaging modalities like FDG-PET for early response assessment during CRT. Brun et al found that metabolic response measured by FDG-PET early during CRT for HNSCC was associated with treatment outcome (34). In patients with a low metabolic response, 23 of 24 obtained LRC, opposed to only 11 of 20 in patients with a high response. However, potential applications of FDG-PET remains unclear. The progressive inflammation of the normal surrounding tissues during CRT may obscure the tumoral lesion (4). Moreover, the association of FDG-uptake with tumour hypoxia and inflammation may increase the

variability of tracer uptake in tumoral and non-tumoral tissue and decrease the predictive value of the technique during fractionated RT (35). Alternatively, mid-treatment presence of hypoxia as depicted by [(18)^{F}]-Misonidazole PET ((18)F-MISO)-PET has shown variable correlation with patient outcome (36,37).

Contrary, as inflammation expands the extracellular space, it will increase the microstructural contrast with persistent tumoral or hypercellular areas, and is likely to improve the differentiation between responding and non-responding lesions on DWI (11).

The higher microstructural contrast may lead to an improved conspicuity, detection and subsequent ROI-delineation of tumoral lesions on the native high b-value images due to a more pronounced signal suppression of the inflammatory tissues at higher b-values. Moreover, the increased microstructural contrast between inflammatory/necrotic and tumoral tissue, is likely to increase the differences in ADC between viable and non-viable tumoral tissue, facilitating their differentiation with DWI (11).

6.5 Conclusion

DWI with the ΔADC at 2 and 4 weeks during CRT for HNSCC allow early response prediction, correlating significantly with LRC and DFS. DWI is more accurate than DCE-MRI and serial volumetric assessment for prediction of treatment outcome. DCE-MRI with semi-quantitative assessment failed to show significant differences between responding and non responding tumours, and was of no additional value to the volumetric assessment for early prediction of treatment response.

These findings indicate that DWI can be used as an early biomarker of treatment response in CRT of HNSCC. As such, the technique may be of value as a per-treatment response biomarker.

6.6 References

1. Ang KK, Harris J, Garden AS, et al. Concomitant boost radiation plus concurrent cisplatinum for advanced head and neck carcinomas: Radiation Therapy Oncology Group phase II trial 99-14. *J Clin Oncol* 2005;23:3008-3015
2. Nuyts S, Dirix P, Clement P et al. Impact of adding concomitant chemotherapy to hyperfractionated accelerated radiotherapy for advanced head-and-neck squamous cell carcinoma. *Int J Radiat Oncol Biol Phys* 2009;73:1088-1095
3. Pignon JP, Bourhis, Domenge C, Designé L. Chemotherapy added to locoregional treatment for head and neck squamous-cell carcinoma: three meta-analyses of updated individual data. MACH-NC collaborative group. Meta-analysis of chemotherapy on head and neck cancer. *Lancet* 2000;355:949-955
4. Gregoire V, De Neve W, Eisbruch A, Lee N, Van den Weyngaert D, Van Gestel D. Intensity-modulated radiation therapy for head and neck carcinoma. *Oncologist* 2007;12:555-564
5. Koh DM, Collins DJ. Diffusion-weighted MRI in the body: applications and challenges in oncology. *Am J Roentgenol* 2007;188:1622-1635
6. Padhani AR. Dynamic contrast-enhanced MRI in clinical oncology: current status and future directions. *J Magn Reson Imaging* 2002;16:407-422
7. Hamstra DA, Lee KC, Moffat BA, Chenevert TL, Rehemtulla A, Ross BD. Diffusion magnetic resonance imaging: an imaging treatment response biomarker to chemoradiotherapy in a mouse model of squamous cell cancer of the head and neck. *Transl Oncol* 2008;1:187-194
8. Robbins KT, Medina JE, Wolfe GT, et al. Standardizing neck dissection terminology. Official report of the Academy's Committee for Head and Neck Surgery and Oncology. *Arch Otolaryngol Head Neck Surg* 1991;117:601-605
9. Jaulerry C, Dubray B, Brunin F, et al. Prognostic value of tumor regression during radiotherapy for head and neck cancer: a prospective study. *Int J Radiat Oncol Biol Phys* 1995;33:271-279
10. Yankeelov TE, Lepage M, Chakravarthy A, et al. Integration of quantitative DCE-MRI and ADC mapping to monitor treatment response in human breast cancer: initial results. *Magn Reson Imaging* 2007;25:1-13

11. Vandecaveye V, De Keyzer F, Nuyts S, et al. Detection of head and neck squamous cell carcinoma with diffusion weighted MRI after (chemo)radiotherapy: correlation between radiologic and histopathologic findings. *Int J Radiat Oncol Biol Phys* 2007;67: 960-971
12. Moffat BA, Chenevert TL, Meyer CR, et al. The functional diffusion map: an imaging biomarker for the early prediction of cancer treatment outcome. *Neoplasia* 2006;8:259-267
13. Patterson DM, Padhani A, Collins DJ. Technology insight: water diffusion MRI – a potential new biomarker of response to cancer therapy. *Nat Clin Pract Oncol* 2008;5:220-233
14. Kim H, Morgan DE, Zeng H, et al. Breast tumor xenografts: diffusion-weighted MR imaging to assess early therapy with novel apoptosis-inducing anti-DR5 antibody. *Radiology* 2008;248:844-851
15. Seierstad T, Røe K, Olsen DR. Noninvasive monitoring of radiation-induced treatment response using proton magnetic resonance spectroscopy and diffusion-weighted magnetic resonance imaging in a colorectal tumor model. *Radiother Oncol* 2007;85:187-194
16. Moffat BA, Chenevert TL, Lawrence TS, et al. Functional diffusion map: a noninvasive MRI biomarker for early stratification of clinical brain tumor response. *Proc Natl Acad Sci USA* 2005;102:5524-5529
17. Kim S, Loevner L, Quon H, et al. Diffusion-weighted magnetic resonance imaging for predicting and detecting early response to chemoradiation therapy of squamous cell carcinomas of the head and neck. *Clin Cancer Res* 2009;15:986-994
18. Harry VN, Semple SI, Gilbert FJ, Parkin DE. Diffusion-weighted magnetic resonance imaging in the early detection of response to chemoradiation in cervical cancer. *Gynecol Oncol* 2008;111:213-220
19. Mardor Y, Pfeffer R, Spiegelmann R, et al. Early detection of response to radiation therapy in patients with brain malignancies using conventional and high b-value diffusion-weighted magnetic resonance imaging. *J Clin Oncol* 2003;21:1094-1100
20. Hamstra DA; Galbán CJ, Meyer CR, et al. Functional diffusion map as an early imaging biomarker for high-grade glioma: correlation with conventional radiologic response and overall survival. *J Clin Oncol* 2008;26:3387-3394
21. Padhani AR, Liu G, Koh DM, et al. Diffusion-weighted magnetic resonance imaging as a cancer biomarker: consensus and recommendations. *Neoplasia* 2009;11:102-125

22. Loncaster JA, Carrington BM, Sykes JR, et al. Prediction of radiotherapy outcome using dynamic contrast-enhanced MRI of carcinoma of the cervix. *Int J Radiat Oncol Biol Phys* 2002;54:759-767
23. Mayr NA, Yuh WT, Magnotta VA, et al. Tumor perfusion studies using fast magnetic resonance imaging technique in advanced cervical cancer: a new noninvasive predictive assay. *Int J Radiat Oncol Biol Phys* 1996;36:623-633
24. Cao Y, Popovtzer A, Li D, et al. Early prediction of outcome in advanced head and neck cancer based on tumor blood volume alterations during therapy: a prospective study. *Int J Radiat Oncol Biol Phys* 2008;72:1287-1290
25. Padhani AR, Leach MO. Antivascular cancer treatments: functional assessment by dynamic contrast-enhanced magnetic resonance imaging. *Abdom Imaging* 2005;30:324-341
26. Gandhi D, Chepeha DB, Miller T, et al. Correlation between initial and early follow-up CT perfusion parameters with endoscopic tumor response in patient with advanced squamous cell carcinomas of the oropharynx treated with organ-preservation therapy. *Am J Neuroradiol* 2006;27:101-106
27. Hermans R. Estimation of tumour oxygenation levels with dynamic contrast-enhanced magnetic resonance imaging. *Radiother Oncol* 2000;57:1-3
28. Ellingsen C, Egeland TA, Gulliksrud K, Gaustad JV, Mathiesen B, Rofstad EK. Assessment of hypoxia in human cervical carcinoma xenografts by dynamic contrast-enhanced magnetic resonance imaging. *Int J Radiat Oncol Biol Phys* 2009;73:838-845
29. Benjaminsen IC, Melås EA, Mathiesen BS, Rofstad EK. Limitations of dynamic contrast-enhanced MRI in monitoring radiation-induced changes in the fraction of radiobiologically hypoxic cells in human melanoma xenografts. *J Magn Reson Imaging* 2008;28:1209-1218
30. Baba Y, Furusawa M, Murakami R, et al. Role of dynamic MRI in the evaluation of head and neck cancers treated with radiation therapy. *Int J Radiat Oncol Biol Phys* 1997; 37:783-787
31. Demaria S, Formenti SC. Sensors of ionizing radiation effects on the immunological microenvironment of cancer. *Int J Radiat Biol* 2007;83:819-825
32. Cho H, Ackerstaff E, Carlin S, et al. Noninvasive multimodality imaging of the tumor microenvironment: registered dynamic magnetic resonance imaging and positron emission tomography studies of a preclinical tumor model of tumor hypoxia. *Neoplasia* 2009;11:247-259

33. Tozer DJ, Davies GR, Altmann DR, Miller DH, Tofts PS. Principal component and linear discriminant analysis of T1 histograms of white and grey matter in multiple sclerosis. *Magn Reson Imaging* 2006:24:793-800
34. Brun E, Kjellén E, Tennvall J, et al. FDG PET studies during treatment: prediction of therapy outcome in head and neck squamous cell carcinoma. *Head Neck* 2002;24:127-135
35. Madani I, Duthoy W, Derie C, et al. Positron emission tomography-guided, focal-dose escalation using intensity-modulated radiotherapy for head and neck cancer. *Int J Radiat Oncol Biol Phys* 2007;68:126-135
36. Lee N, Nehmeh S, Schöder H, et al. Prospective Trial Incorporating Pre-/Mid-Treatment [(18)F]-Misonidazole Positron Emission Tomography for Head-and-Neck Cancer Patients Undergoing Concurrent Chemoradiotherapy. *Int J Radiat Oncol Biol Phys* 2009; Epub ahead of print.
37. Rischin D, Hicks RJ, Fisher R, et al. Prognostic significance of [18F]-misonidazole positron emission tomography-detected tumor hypoxia in patients with advanced head and neck cancer randomly assigned to chemoradiation with or without tirapazamine: a substudy of Trans-Tasman Radiation Oncology Group Study 98.02. *J Clin Oncol* 2006;24:2098-2104

Chapter7:
DWI and DCE-MRI for assessment of early post-treatment tumour response in head and neck squamous cell carcinoma after (chemo)radiotherapy

7.1 Introduction

Previous studies have shown that DWI allows for differentiation of post-radiotherapeutic changes, necrosis and tumour recurrence at the time of diagnosis or clinical presentation (1,2). However, the imaging diagnosis of persistent or recurrent cancer, established at the time of clinical symptoms, may come too late to allow successful tumour salvage.

For instance, patients with T3 or T4 non-laryngeal cancers may only have a short window of opportunity to initiate successful salvage surgery and at the time that a tumour recurrence becomes clinically apparent, operability may be compromised. It has been shown that the addition of a planned clinical, pathological or imaging restaging (using CT) at 4 to 8 weeks after CRT may improve overall local control and overall survival rates (3).

The aim of this study was to evaluate the potential value of DWI and DCE-MRI to anatomical imaging for prediction of treatment response in the early post-CRT phase.

7.2 Materials and Methods

7.2.1 Study design

Thirty-one patients (mean age 54 years, range 39 to 67 years) with histologically proven HNSCC, were consecutively included in this prospective study. One patient was excluded due to detection of metastatic disease prior to treatment. Another patient refused MRI due to claustrophobia. The tumour localization, stage of the remaining 29 patients are summarized in Table 1.

Patient	primary tumour localization	Staging
Patient 1	tonsil	T2N3
Patient 2	tonsil	T2N2a
Patient 3	piriform sinus	T4a2b
Patient 4	supraglottic	T3N1
Patient 5	piriform sinus	T4aN2b
Patient 6	supraglottic	T4aN2c
Patient 7	glottic	T1N0
Patient 8	base of tongue	T3N1
Patient 9	lateral oropharynx	T4aN2c
Patient 10	supraglottic	T3N2b
Patient 11	lateral oropharynx	T4aN2c
Patient 12	base of tongue	T3N2b
Patient 13	lateral oropharynx	T4N1
Patient 14	piriform sinus	T2N1
Patient 15	supraglottic	T4aN2c
Patient 16	glottic	T3N0
Patient 17	supraglottic	T4aN2c
Patient 18	lateral oropharynx	T2N1
Patient 19	lateral oropharynx	T3N2c
Patient 20	piriform sinus	T1N2b
Patient 21	lateral oropharynx	T4aN2c
Patient 22	tonsil	T3N0
Patient 23	piriform sinus	T4aN1
Patient 24	base of tongue	T3N2c
Patient 25	base of tongue	T4
	piriform sinus	T3N1
Patient 26	supraglottic	T3N2b
Patient 27	piriform sinus	T3N2c
Patient 28	tonsil	T2N2b
Patient 29	tonsil	T4aN1

Table 1: Initial tumour localization, and TNM-staging in the included patient group

Treatment consisted of concomitant CRT in 26 patients and radiotherapy in 3. Radiotherapy was delivered to a total dose of 72 Gray (Gy) according to a hybrid fractionation schedule in 28 patients: 20 daily fractions of 2 Gy, followed by 20 fractions of 1.6 Gy twice daily (32 Gy), to a total dose of 72 Gy. Chemotherapy consisted of Cisplatinum, 100 mg/ml at week 1 and 4. In one patient with a T1 glottic cancer, a total dose of 55 Gy was delivered in 25 fractions of 2.2 Gy. All patients completed the planned CRT-scheme. Pre-treatment diagnostic examinations included contrast-enhanced computed tomography (CT), FDG-PET-CT in 14 patients, and pre-operative panendoscopy with biopsy in all patients. MRI with

anatomical, DCE-MRI and DWI sequences was added prior to and 3 weeks after CRT. Routine follow-up CT was performed at 3±1 months after CRT (CT_{3m}). Clinical outcome after 2 years follow-up and histopathology served as reference standard. DWI was compared to conventional MRI at 3 weeks post-CRT (MRI_{3w}) and the CT_{3m}. A time line shows the different methodological steps in the study (Figure 1).

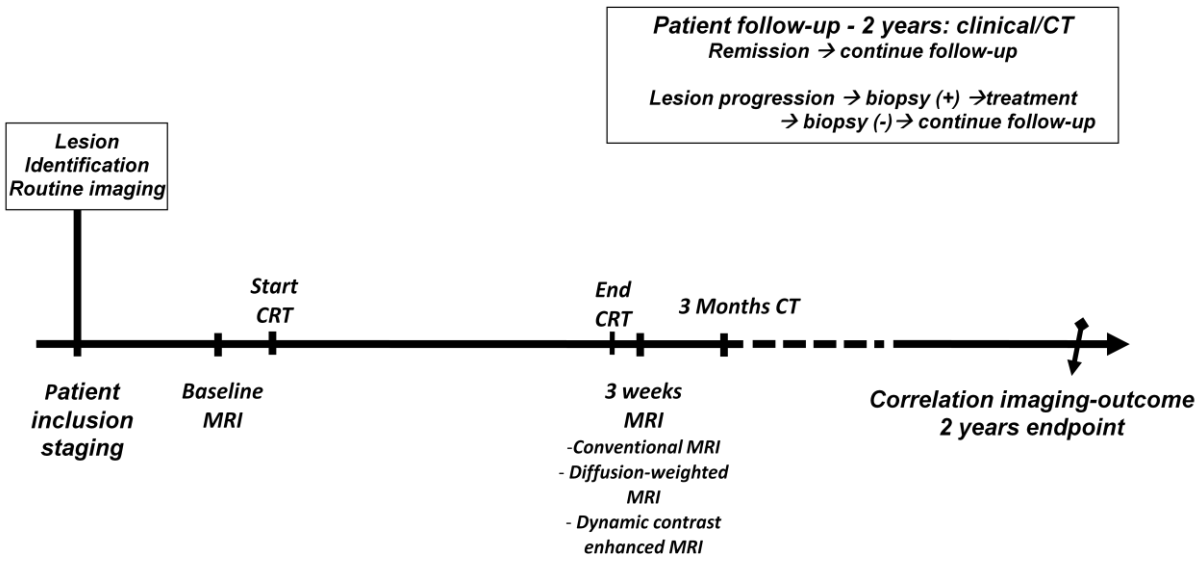

Figure 1: Timeline detailing the exact set-up of study inclusion and data processing used in this study.

The study was approved by the local ethics committee and all patients gave written informed consent prior to inclusion.

7.2.2 Imaging technique

All patients underwent the standardized anatomical TSE-MRI, and functional DWI- and DCE-MRI sequences as well as the CT study as described in chapter 3. Similar as for the CT, MRI imaging covered the entire head and neck ranging from the base of skull to the thoracic outlet, and included all regional nodal stations (retropharyngeal space and all neck levels).

7.2.3 Image analysis

7.2.3.1 Lesion identification and correlation

The primary tumours and nodal metastases were identified on the baseline TSE-MRI and DWI in correlation to the clinical information and the pre-therapeutic routine imaging

results. Primary tumours were topographically annotated by their slice position and anatomical position in the upper aerodigestive tract. Adenopathies were topographically annotated by their position in correlation to anatomical structures in the neck, including the submandibular gland, the sternocleidomastoid muscle and the jugular vein, and level position according to the AAO-HNS classification (4). The primary tumours and metastatic adenopathies were identified on the DWI examinations by visual correlation and correlation of slice positions with the baseline examination.

7.2.3.2 Image analysis

The images of DWI and DCE-MRI were quantitatively interpreted in a blinded fashion as described in chapter 3.2.

For both DWI and DCE-MRI, ADC respectively perfusion parameters of the lesions at 3 weeks after the end of CRT were correlated to the baseline values for treatment assessment and correlation to treatment outcome.

The ADC changes (ΔADC_N) in % for each lesion between the baseline and the 3weeks post-CRT time point were calculated using the formula:

$$\Delta ADC_N = [(ADC_N - ADC_B)/ADC_B] * 100$$

Where ADC_B represents pre-treatment ADC-value and ADC_N represents the ADC on the N^{th} time point after CRT.

The changes of the perfusion parameter ($\Delta PERF_N$) in % in for each lesion between the baseline and the 3weeks time point after CRT was calculated using the formula:

$$\Delta PERF_N = [(PERF_N - PERF_B)/PERF_B] * 100$$

Where $PERF_B$ represents pre-treatment ADC-value and $PERF_N$ represents the PERF on the N^{th} time point after CRT.

7.2.3.3 Comparison with anatomical imaging criteria

The findings of DWI and DCE-MRI were compared with currently accepted anatomical imaging criteria for post-CRT follow-up. The primary site and lymph nodes were evaluated by comparison of the MRI_{3w} (Radiologist; 7 years of experience in head and neck radiology) and the CT_{3m} (radiologist, 16 years of experience in head and neck radiology) with the baseline pre-treatment MRI. Both readers were blinded from all other imaging data.

For evaluation of primary lesions, MRI imaging variables included tissue asymmetry or mass (grade 0: no detectable focal abnormality, grade 1: anatomic asymmetry or discrete mass <

10 mm, grade 2a: mass > 10 mm, or 2b, <50% reduction of largest dimension), T2-SI and contrast enhancement. CT imaging variables consisted of tissue asymmetry or mass and contrast enhancement (5).

Lymph nodes were evaluated based on diameter (1 cm shortest transverse diameter respectively 1.5 cm longest transverse diameter as described in literature), presence of intranodal focal defects, focal contrast enhancement or calcifications (6,7).

7.2.4 Correlation to treatment outcome

As in our institution, routine biopsies nor routine elective neck dissections are performed after CRT, the imaging findings were primarily correlated to post-treatment patient follow up as described in chapter 3.4.2.

7.2.5 Statistical analysis

The software package Statistica 8® (StatSoft Inc, Tulsa, OK, USA) was used for the statistical analysis. A p-value < 0.05 was considered statistically significant.

The ΔADC and ΔPERF of primary lesions and adenopathies showing CR versus tumour recurrence were compared with a Mann-Whitney test. Only the parameters with significantly different values were included for further analysis. ROC-analysis with the AUC was employed to investigate the discriminatory capability of the imaging parameters. For calculation of the sensitivity, specificity, accuracy, PPV and NPV, the optimal threshold was determined as the point giving equal weighting to sensitivity and specificity on the ROC-curve.

For evaluation of the MRI_{3w} and CT_{3m}, the appearance and size of the primary tumour site and lymph nodes were documented in correlation to post-CRT follow-up and histopathology. The sensitivity, specificity, accuracy, PPV and NPV were subsequently calculated.

Finally, the selected DWI- and DCE-MRI parameters were compared per patient with the MRI_{3w} and CT_{3m}.

7.3 Results

7.3.1 Treatment outcome

At 2 years post-CRT, complete LCR was achieved in 15 of 29 patients (50%).

Six of 29 patients (21%) developed an isolated local recurrence (at a median of 129 days post-CRT, range: 27 to 189 days) for which salvage surgery was performed. Six of 30 patients (20%) developed a regional recurrence without primary tumour recurrence (at a median of 224 days post-CRT, range: 91 to 364 days), of whom 3 were eligible for neck dissection at time of diagnosis. Two of 30 patients (10%) developed a simultaneous locoregional tumour recurrence (at 126 and 161days after CRT, respectively); one patient received salvage surgery with bilateral neck dissection, one was inoperable because of the extent of disease. Nine of 30 patients (30%) deceased during the 2 years follow-up: 8 patients because of a tumour recurrence. One patients death was non-tumour related.

7.3.2 Primary tumour

None of the perfusion parameters showed statistical difference between lesions with later post-CRT recurrence compared to lesions with CR (c-peak: recurrence : 0.59±2.1 versus CR : 0.3±1.3 ; AS: recurrence : 0.02±0.59 versus CR : -0.28±0.71 ; washout : recurrence : 0.4±5.87 versus CR : 4.02±27.27 ; $p>0.1$).

The ΔADC_{post} was significantly lower for lesions with post-CRT recurrence than with CR (-2.25±0.3 versus 79.8±41;$p<0.0001$) (Figure 2).

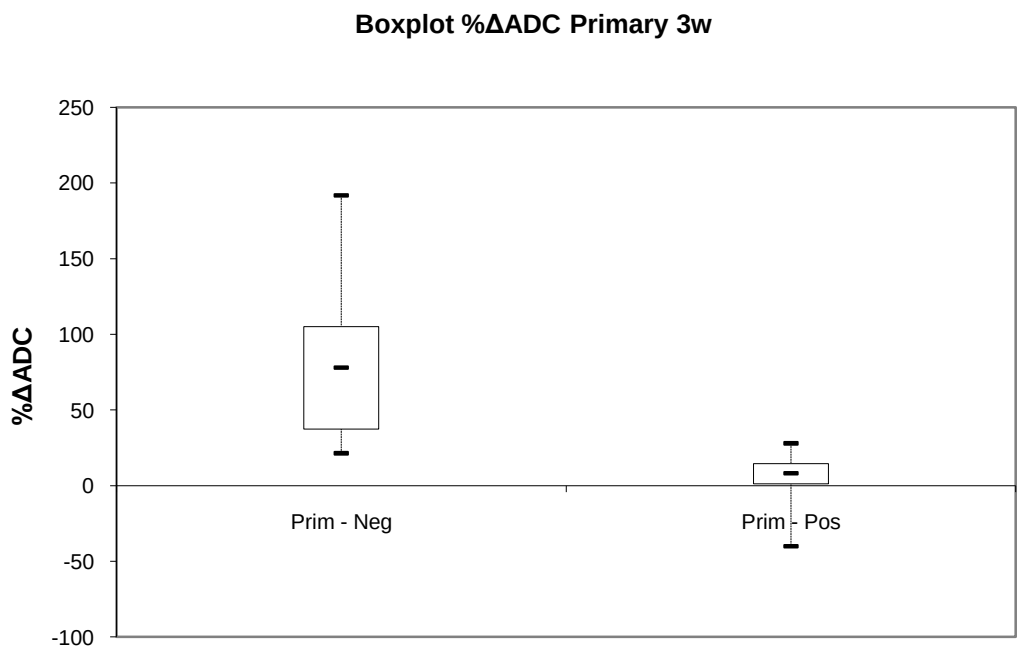

Figure 2: Comparison of ΔADC_{post} between primary tumours showing complete remission 2 years after the end of chemoradiotherapy and primary tumours showing recurrence during follow-up. The ΔADC_{post} was significantly lower in lesions showing later recurrence. Box-whisker plots are presented with median (-), interquartile range (box) and minima/maxima (-).

The imaging appearance of primary lesions at the MRI_{3w} are shown in table 2. Primary site findings compatible with CR mostly showed a grade 0 or 1 and T2 hypo-intensity, while primary site findings compatible with later tumour recurrence mostly showed grade 2a or 2b and increased or mixed T2-SI. Contrast enhancement was of limited discriminatory value.

The imaging appearance of primary lesions at the CT_{3m} are shown in Table 2. Primary site findings compatible with later CR mostly showed grade 0 or 1 and lack of contrast enhancement while primary site findings compatible with later tumour recurrence showed substantial correlation with grade 2a or 2b and contrast enhancement.

Comparative sensitivity, specificity, accuracy, PPV and NPV for the ΔADC_{post} at the optimal threshold of 25% and MRI_{3w} and CT_{3m} are shown in Table 3. Compared to the MRI_{3w}, the ΔADC_{post} showed higher PPV and NPV. Compared to the CT_{3m}, the ΔADC_{post} showed higher PPV. DWI showed higher sensitivity for detection of persistent tumoral lesions that showed complete morphological regression (grade 0) and higher specificity by excluding persistent tumour that showed a persistent mass (grade 2a or b) or showed persistent mixed signal intensity of T2 weighted images.

MRI_{3w} Primary site	True negative	True positive	False positive	False negative
	of 18 lesions	of 6 lesions	of 4 lesions	of 2 lesions
grade 0	4	0	0	1
grade 1	10	0	0	1
grade 2a or 2b	4	6	4	0
T2 hyperintense	3	0	3	1
T2 mixed	0	6	1	0
T2 hypo-intense	15	0	0	1
Contrast +	8	5	4	1
Contrast -	10	1	0	1

CT_{3m} Primary site	True negative	True positive	False positive	False negative
	of 19lesions	of 7 lesions	of 3 lesions	of 1 lesions
grade 0	17	0	0	1
grade 1	2	0	0	0
grade 2a or 2b	0	7	3	0
Contrast +	2	7	2	0
Contrast -	17	0	1	1

Table 2: Imaging appearance of primary site lesions showing later tumour recurrence or remission at the MRI_{3w} (upper table) and CT_{3m} (lower table)

Primary tumour	ΔADC	MRI	CT
Time point	3 weeks	3 weeks	3±1 months
TP	8	6	7
FN	0	2	1
FP	1	4	3
TN	21	18	19
Sens	100%	75%	88%
Spec	95%	81%	86%
Acc	97%	80%	87%
PPV	89%	60%	70%
NPV	100%	90%	95%

Table 3: Primary tumour: comparative accuracy between ΔADC_{post}, MRI_{3w} and CT_{3m}

7.3.3 Lymph node metastases

None of the perfusion parameters showed a statistically different value between lesions with later post-CRT recurrence compared to lesions with CR and were excluded of further evaluation (c-peak: recurrence : -0.045±0.5 vs. CR : 0.24±1.35 ; AS: recurrence : 0.027±1.5 vs. CR : -0.17±0.72 ; washout : recurrence : -1.26±1.51 vs. CR : 1.88±1.9 ; $p>0.1$). At 3weeks after the end of CRT, the ΔADC_{post} was significantly lower for lesions with post-CRT recurrence than with CR (-2.25±0.3 vs. 79.8±41;$p<0.0001$) (Figure 3).

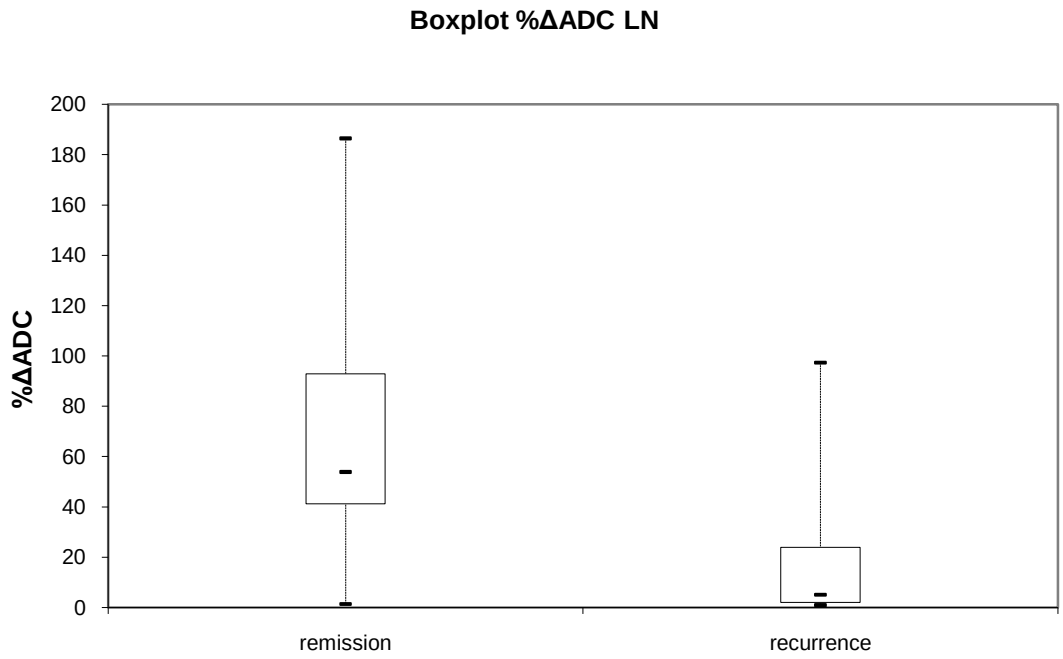

Figure 3: Comparison of ΔADC_{post} between adenopathies showing complete remission 2 years after the end of chemoradiotherapy and with recurrence. The ΔADC_{post} was significantly lower in lesions showing later recurrence. Box-whisker plots are presented with median (-), interquartile range (box) and minima/maxima (-).

For nodal differentiation at MRI_{3w}, nodal size was the main discriminative variable while intranodal heterogeneity showed no additional value for detecting small adenopathies. Overall, 33 lymph nodes were smaller than 1 cm, 8 lymph nodes had a diameter range between 1 and 1.5 cm, 9 lymph nodes were larger than 1.5 cm. Comparative sensitivity, specificity, accuracy, PPV and NPV for the ΔADC_{post} at the optimal threshold of 20% and MRI_{3w} and CT_{3m} per lymph node and neck side are shown in table 4. The ΔADC_{post} showed higher PPV and NPV per lymph node and neck side than MRI_{3w} and CT_{3m} for both the 1 cm and 1.5 cm threshold, improving the detection of persistent subcentimetre nodal metastatic

disease and improving the exclusion of residual tumoral disease in persistently enlarged lymphadenopathy.

Lymph node	ΔADC_{3w}	MRI_{3w} - 1 cm	MRI_{3w} - 1.5*	CT_{4m} – 1*	CT_{4m} – 1.5 cm
TP	7	6	3	5	3
FP	5	11	6	5	3
TN	36	30	35	36	38
FN	2	3	6	4	6
sens	78%	67%	33%	56%	33%
spec	88%	73%	85%	88%	92%
acc	86%	72%	76%	82%	82%
PPV	58%	35%	33%	50%	50%
NPV	95%	91%	87%	90%	86%

Neck side	ΔADC3w	MRI3w - 1 cm	MRI_{3w} - 1.5*	CT_{4m} – 1*	CT_{4m} - 1.5 cm
TP	8	6	3	5	3
FP	3	11	6	5	3
TN	24	16	21	22	24
FN	1	3	6	4	6
sens	88%	67%	33%	56%	33%
spec	89%	59%	77%	86%	89%
acc	89%	61%	67%	80%	75%
PPV	70%	35%	33%	50%	50%
NPV	96%	84%	79%	89%	80%

*Size threshold in cm – intranodal heterogeneity

Table 4: Lymph nodes: comparative accuracy for post-treatment evaluation between ΔADC, MRI_{3w} and $CT_{4m.}$ Per lymph node (upper table) and per neck side (lower table).

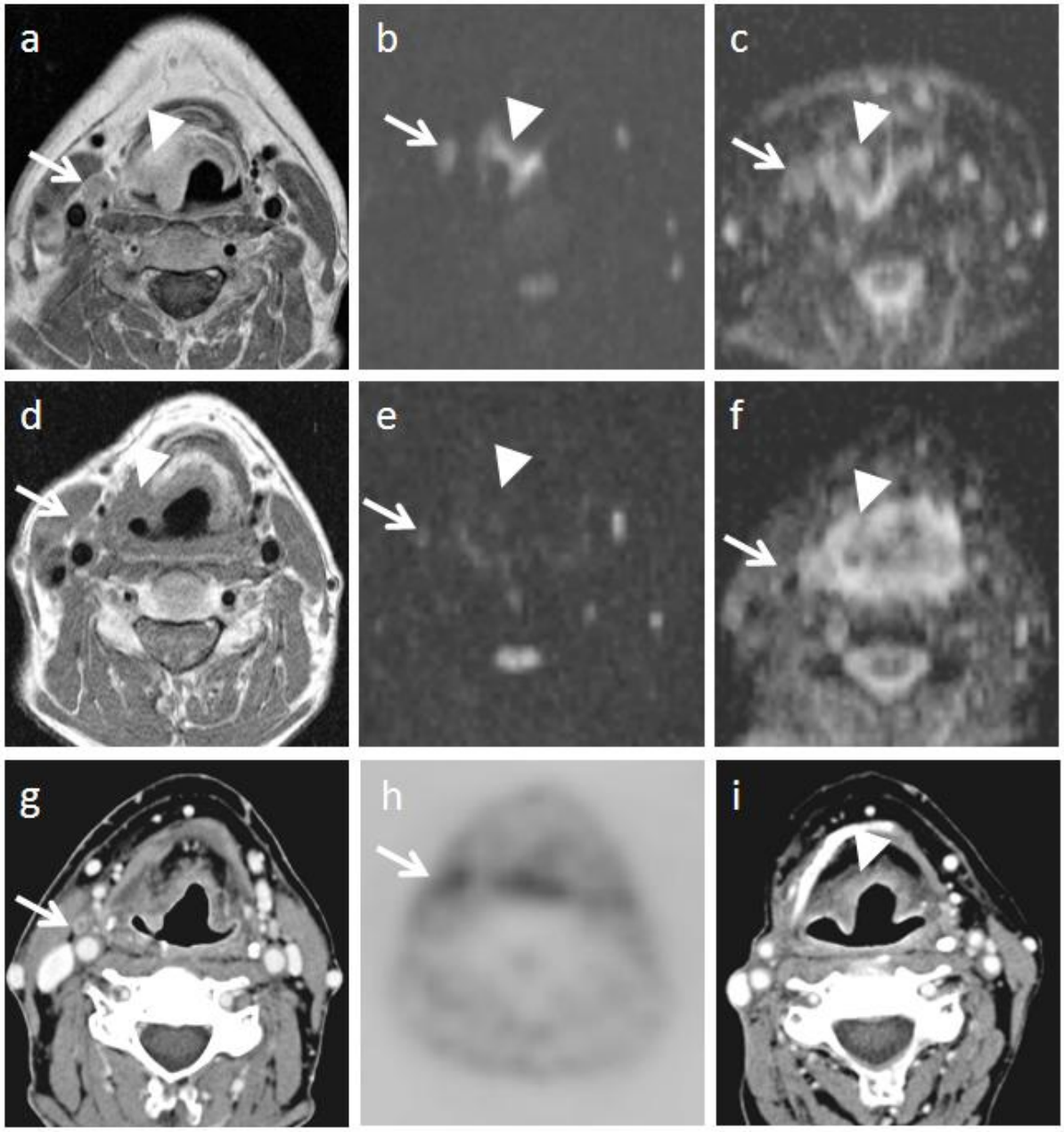

Figure 4: Upper row: (a) right supraglottic tumour (arrowhead) and right level 2 metastatic adenopathy are shown on contrast-enhanced T1-weighted turbo-spin echo (TSE) image, (b) b1000 diffusion-weighted image, and (c) ADC-map prior to therapy. Middle row: (d) Three weeks after the end of chemoradiotherapy, the primary tumour (arrowheads) shows slight asymmetry (grade I), shows complete loss of signal on the b1000 diffusion-weighted image and corresponds to (f) a ΔADC (in %) of 60, indicating complete tumour eradication. The lymph node (arrows) (d) shows no intranodal heterogeneity and a diameter of 0.8 cm. (e) Visualized as a hyperintense lesion on the b1000 diffusion-weighted image, it corresponds to (f) a ΔADC (in %) of 5, indicating persisting tumour. (g) CT scan at 8 months after completion of chemoradiotherapy shows necrotic adenopathy in right level 2, corresponding to (h) a hypermetabolic lesion on FDG-PET. Subsequent histological examination after neck dissection confirmed the presence of a recurrent nodal metastasis (arrows). Bottom row: (i) follow-up CT scan at 2 years after completion of chemoradiotherapy shows complete remission at the primary tumour site (arrowhead).

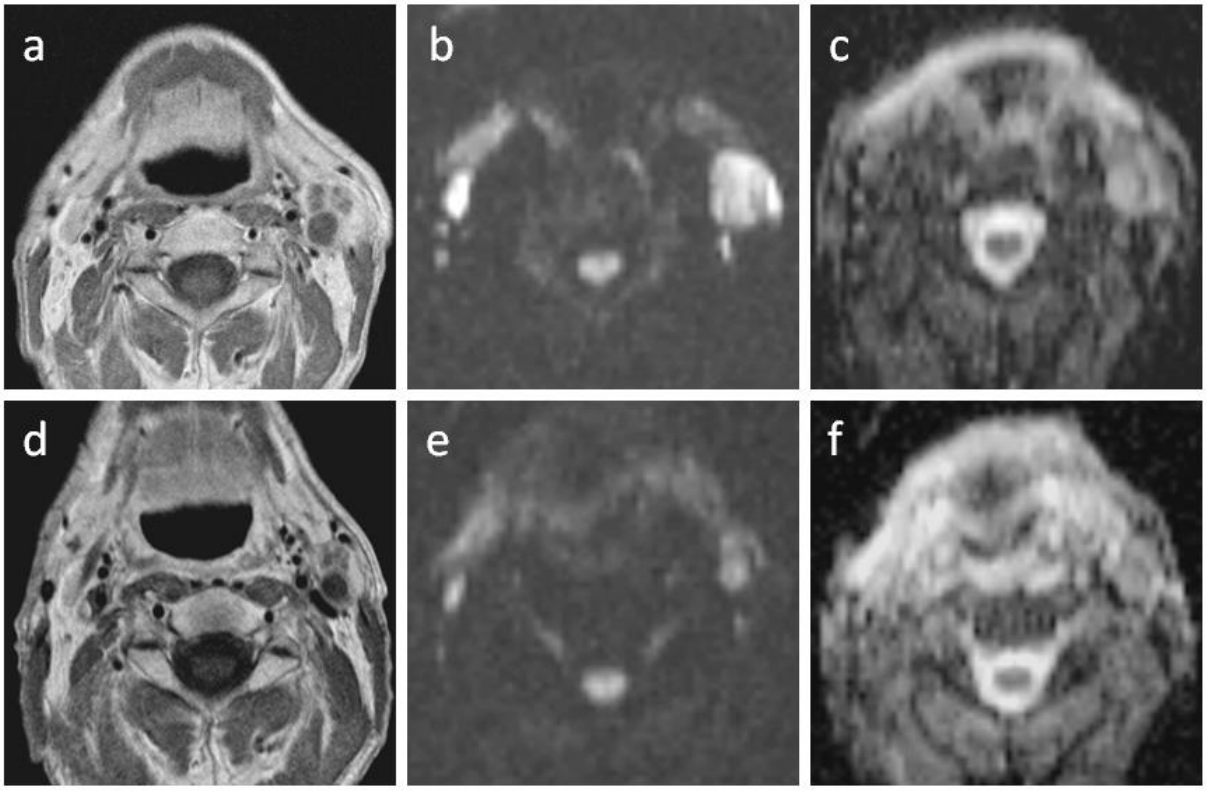

Figure 5: Upper row: patient with left tonsillar cancer (image not shown) presents with nodal metastasis in left level 2 on (a) contrast-enhanced T1-weighted TSE image, (b) b1000 diffusion-weighted image, and (c) ADC-map prior to therapy.

Bottom row: (d) Contrast-enhanced T1-weighted TSE image 3 weeks after completion of chemoradiotherapy shows persistent adenopathy > 1.5cm and with intranodal heterogeneity indicating necrosis. (e) the lymph node is hyperintense on the b1000 diffusion-weighted image and corresponds to a ΔADC (in %) of 50, indicating tumour eradication. Watchful waiting during 2 years after chemoradiotherapy showed regression of the lymph node with persistent complete remission.

7.4 Discussion

In this study, DWI with the ΔADC_{post} allowed for treatment assessment of the head and neck as early as 3 weeks after the completion of CRT. Primary tumoral sites and lymph nodes that lacked a substantial increase in ADC 3 weeks after completion of CRT compared to the baseline scan (primary tumours: less than 25%, adenopathies: less than 20%) correlated significantly with later tumour recurrence.

Prior studies have shown the value of DWI for detection of post-radiation or post-surgical tumour recurrence in the head and neck. At the time of clinical presentation or with suspect clinical examination, recurrent tumour showed a significantly lower ADC compared to post-treatment inflammation or necrosis (1,2). This lower ADC was histologically correlated to the dense microstructure of HNSCC of residual or recurrent tumour (1). Moreover, a recent study has suggested the value of DWI for early response assessment prior to, during and early after CRT for nodal metastases of HNSCC in correlation to histology or short period of follow-up (7).

In our study, DWI showed higher accuracy for both the evaluation of the treated primary site and nodal metastases, compared to conventional MRI at 3 weeks and the routinely implemented post-treatment CT, on average 3 months after CRT.

Remarkably, no substantial difference in accuracy was found between the MRI_{3w} and CT_{3m} for the post-treatment evaluation of the head and neck. Usually, the first CT is routinely performed at 3 to 4 months after the end of treatment for the evaluation of the primary site, while CT studies earlier in the time course of follow-up rather aim at assessing nodal status before planned neck dissection (8). The findings of this study indicate that earlier implementation of routine imaging follow-up may be feasible. This in concordance with the findings of a prior study where imaging 4 to 8 weeks after RT was useful in the early identification of local treatment failure (3). However, despite the relatively high sensitivity for early detection of residual or recurrent tumour at the primary site the specificity and PPV was low, similarly as reported in earlier studies (9,10). In the first 3 to 4 months oedema, tumour necrosis and acute or chronic inflammation can lead to anatomical distortion and signal changes that may be difficult to distinguish from persistent or recurrent tumour or that may obscure small persistent tumoral lesions (11). The PPV for the early identification of lesions at risk of recurrence was markedly improved by DWI compared to the MRI_{3w} and CT_{3m}. Although the limited patient population in this initial study prohibits to draw definite

conclusions, a number of benefits of early post-CRT imaging for the post-CRT management of primary lesions in the head and neck may be postulated. The high NPV and PPV of DWI for assessment of the primary lesion site may aid in the stratification of patients for early salvage surgery in patients with failed CRT. An increase in the success rate of early surgical salvage surgery may improve likelihood of survival (12). As previously shown, clinical evaluation and planned imaging or pathologic restaging of T3-T4 non-laryngeal primary tumours 1 to 2 months after RT may initiate early salvage surgery and improve local control and survival rates (3). The higher accuracy of DWI over anatomical imaging and the ability for early evaluation, may further increase the number of patients still eligible for salvage surgery.Additionally, the improved differentiation of persistent tumour from post-CRT inflammation and necrosis compared to anatomical imaging may help to obviate invasive diagnostic procedures in patients with a persistent suspect mass on serial imaging.

For the evaluation of lymph nodes, DWI substantially improved both PPV and NPV compared to the MRI_{3w} and CT_{3m} for differentiation of persistent nodal disease. DWI improved the detection of persistent disease in subcentimetre lymph nodes and allowed exclusion of remnant tumoral disease in lymph nodes that were persistently enlarged or showed internal focal abnormalities. This underscores the potential limitations of size-related and anatomical criteria inherently used by CT and conventional MRI; DWI has the advantage that, being a microstructural imaging modality, it is not significantly influenced by lesion size or by treatment-induced tissue distortion (fibrosis, necrosis) or inflammation (1,2,7).

The management of the post-radiotherapeutic neck remains controversial. Neck dissection performed 4 to 12 weeks after the completion of radiation treatment has been shown to improve regional control (13). Different studies have shown that patients with incomplete radiographic response on anatomical imaging showed higher neck control and cause-specific survival in patients when undergoing neck dissection (13,14). However, this improved survival comes at the cost of a high number of unnecessary performed surgical procedures and a significantly increased morbidity (15,16). In order to reliably avoid adjuvant neck dissection after CRT, imaging modalities need high sensitivity and high NPV. Liauw et al have reported a high NPV of CT performed at 4 weeks after the end of CRT for exclusion of persistent nodal metastatic disease and found only 1 neck recurrence in 32 necks with complete radiographic response (6). However, using the same imaging criteria, both MRI_{3w} and CT_{4m} did not achieve a similar NPV in this study. Moreover, these criteria have the evident drawback that they do not allow to exclude patients from neck dissection who still have enlarged lymph nodes after CRT (17).

The high sensitivity and NPV of DWI may be of additional use for the post-CRT management of the neck. DWI showed a particularly high NPV for the exclusion of persistent neck disease, most importantly in patients with persistently enlarged adenopathies. DWI was able to correctly downstage 6 patients presenting with persistently enlarged adenopathies on post-CRT conventional MRI at 3 weeks and in 5 patients at the time of the CT_{3m}. In these patients careful follow-up was performed and none required neck dissection.

Therefore, DWI may improve the risk assessment of patients and further safely reduce the number of elective post-CRT neck dissections. Nevertheless, it is currently unclear to what extent the early addition of DWI could decrease the number of imaging studies performed in the post-CRT phase. One persistent subcentimetric adenopathy was missed by both DWI and conventional imaging. A negative early DWI study should therefore not necessarily preclude further imaging follow-up during the first two years post-CRT in order to allow salvage surgery in initially missed metastatic adenopathies (6).

Additionally, the high sensitivity combined with the improved PPV of DWI compared to the MRI_{3w} and CT_{3m} for early nodal differentiation may aid in the timely selection of patients for neck dissection and maximize the chance for successful salvage neck dissection. DWI allowed for the additional detection of persistent nodal disease in 5 patients with complete radiological remission at repeated anatomical imaging.

However, an issue for further improvement appears to be the false positive findings produced by DWI, which occurred in 3 patients with complete nodal regression on conventional imaging. This may be explained by a number of factors. First, in this study, all lymph nodes were included regardless of post-CRT size and a number of lymph nodes may have reached the lower resolution limit of DWI producing falsely lowered ADC-values as a result of inadequate ROI-delineation. Currently, DWI appears to be limited to the evaluation of lesions with a diameter of 4 mm or larger (18). Furthermore, DWI may have effectively detected residual nodal metastatic disease further regressing during follow-up secondary to late radiation effects. It is not always clear whether residual disease in the post-RT neck represents viable tumour at risk of progressive disease. In a prior study, not all histologically proven persistent nodal metastases after adjuvant neck dissection showed proliferative capacity by Ki-67 staining (19). Evidently, further studies are required to determine the post-CRT management in patients with DWI positive subcentimetric lymph nodes; intensified imaging follow-up or US-FNAB may be of use for further work-up of these patients. In this context, as interest in integrated PET/MRI is rising, it may be of value to evaluate the combined use of DWI with novel PET-tracers, such as 3-deoxy-3-[18F]fluorothymidine (FLT). FLT-PET

correlates with pathology based proliferation, including the Ki-67 score but is severely limited in its application in head and neck cancer due to false-positivity in areas of infection and inflammation (20,21). Although significant technical considerations have to be taken into account, FLT-PET may help to identify proliferation capacity in DWI positive lymph nodes, while DWI can reduce false positive findings of FLT by excluding inflammatory tissue areas (1).

The time point where DWI allows for adequate post-CRT assessment in this study appears to be in agreement with the expected optimal timing of adjuvant neck dissection between 4-8 weeks after RT (22). Although further comparison with metabolic imaging is warranted in the future, FDG-PET has not been firmly shown to be reliable in this early post-treatment setting (23). Previous reports have shown optimal diagnostic results at 3 to 5 months after end of CRT for FDG-PET but this may be too late to adequately guide the management of the post-CRT neck (24).

7.5 Conclusion

DWI with the ΔADC is useful for early post-CRT assessment of the head and neck and shows higher accuracy than conventional MRI at 3 weeks and routine CT at 3 months after treatment for the detection of persistent HNSCC. A ΔADC higher than 20% for primary tumours and higher than 25% for nodal metastases is strongly indicative of tumour remission during the first 2 years of post-CRT follow-up and the high NPV may be useful to avoid invasive diagnostic procedures or exclude patients from adjuvant salvage surgery.

The improved early identification of treatment failure by DWI may be beneficial for the timely selection of patients with persistent tumoral disease at the primary site or neck lymph adenopathy for salvage surgery.

7.6 References

1. Vandecaveye V, De Keyzer F, Nuyts S, et al. Detection of head and neck squamous cell carcinoma with diffusion weighted MRI after (chemo)radiotherapy: correlation between radiologic and histopathologic findings. *Int J Radiat Oncol Biol Phys* 2007;67:960-971
2. Abdel Razek AA, Kandeel AY, Soliman N, et al. Role of diffusion-weighted echo-planar MR imaging in differentiation of residual or recurrent head and neck tumors and posttreatment changes. *Am J Neuroradiol* 2007;28:1146-1152
3. Yom SS, Machtay M, Biel MA, et al. Survival impact of planned restaging and early surgical salvage following definitive chemoradiation for locally advanced squamous cell carcinomas of the oropharynx and hypopharynx. *Am J Clin Oncol* 2005;28:385-392
4. Robbins KT, Medina JE, Wolfe GT, et al. Standardizing neck dissection terminology. Official report of the Academy's Committee for Head and Neck Surgery and Oncology. *Arch Otolaryngol Head Neck Surg* 1991;117:601-605
5. Ljumanovic R, Langendijk JA, Hoekstra OS, Knol DL, Leemans CR, Castelijns JA. Pre- and post-radiotherapy MRI results as a predictive model for response in laryngeal carcinoma. *Eur Radiol* 2008;18:2231-2240
6. Liauw SL, Mancuso AA, Amdur RJ, et al. Postradiotherapy neck dissection for lymph node-positive head and neck cancer: the use of computed tomography to manage the neck. *J Clin Oncol* 2006;24:1421-1427
7. Castelijns JA, van den Brekel MW. Imaging of lymphadenopathy in the neck. *Eur Radiol* 2002;12:727-738
8. Ojiri H, Mendenhall WM, Mancuso AA. CT findings at the primary site of oropharyngeal carcinoma within 6-8 weeks after definitive radiotherapy as predictors of primary site control. *Int J Radiat Oncol Biol Phys* 2002;52:748-754
9. Velázquez RA, McGuff HS, Sycamore D, Miller FR. The role of computed tomographic scans in the management of the N-positive neck in head and neck squamous cell carcinoma after chemoradiotherapy. *Arch Otolaryngol Head Neck Surg* 2004;130:74-77
10. Ojiri H, Mendenhall WM, Stringer SP, Johnson PL, Mancuso AA. Post-RT CT results as a predictive model for the necessity of planned post-RT neck dissection in patients with cervical metastatic disease from squamous cell carcinoma. *Int J Radiat Oncol Biol Phys* 2002;52:420-428

11. Lell M, Vaum U, Greess H, et al. Head and neck tumors: imaging recurrent tumor and post-therapeutic changes with CT and MRI. *Eur J Radiol* 2000;33:239-247
12. Lefebvre JL, Chevalier D, Luboinski B, Kirkpatrick A, Collette L, Sahmoud T. Larynx preservation in pyriform sinus cancer: preliminary results of a European Organization for Research and Treatment of Cancer phase III trial. EORTC Head and Neck Cancer Cooperative Group. *J Natl Cancer Inst* 1996;88:855-856
13. Brizel DM, Prosnitz RG, Hunter S, et al. Necessity for adjuvant neck dissection in setting of concurrent chemoradiation for advanced head-and-neck cancer. *Int J Radiation Oncology Biol Phys* 2004;58:1418-1423
14. Narayan K, Crane C, Kleid S, et al. Planned neck dissection as an adjunct to the management of patients with advanced neck disease treated with radiotherapy: for some or for all. *Head Neck* 1999;21:606-613
15. Morgan JE, Breau RL, Suen JY, Hanna EY. Surgical wound complications after intensive chemoradiotherapy for advanced squamous cell carcinoma of the head and neck. *Arch Otolaryngol Head Neck Surg* 2007;133:10-14
16. Grabenbauer GG, Rödel C, Ernst-Stecken A, et al. Neck dissection following radiochemotherapy of advanced head and neck cancer: for selected cases only? *Radiother Oncol* 2003;66:57-63
17. Ojiri H, Mancuso AA, Mendenhall WM, Stringer SP. Lymph nodes of patients with regional metastases from head and neck squamous cell carcinoma as a predictor of pathologic outcome: size changes at CT before and after radiation therapy. *Am J Neuroradiol* 2002;23:1627-1631
18. Vandecaveye V, De Keyzer F, Hermans R. Diffusion-weighted magnetic resonance imaging in neck lymph adenopathy. *Cancer Imaging* 2008;8:173-180
19. Wanebo H, Chougule P, Ready N, et al. Surgical resection is necessary to maximize tumor control in function-preserving, aggressive chemoradiation protocols for advanced squamous cancer of the head and neck (stage III and IV). *Ann Surg Oncol* 2001;8:644-650
20. Salskov A, Tammisetti VS, Grierson J, Veselle H. FLT: measuring tumor cell proliferation in vivo with positron emission tomography and 3'-deoxy-3'-[18F]fluorothymidine. *Semin Nucl Med* 2007;37:429-439
21. Troost EG, Bussink J, Ojen WJ, Kaanders JH. 18F-FDG and 18F-FLT do not discriminate between reactive and metastatic lymph nodes in oral cancer. *J Nucl Med* 2008;49:1053-1059

22. Lango MN, Myers JN, Garden AS. Controversies in surgical management of the node-positive neck after chemoradiation. *Semin Radiat Oncol* 2009;19:24-28
23. McCollum AD, Burrell SC, Haddad RI, et al. Positron emission tomography with 18F-fluorodeoxyglucose to predict pathologic response after induction chemotherapy and definitive chemoradiotherapy in head and neck cancer. *Head Neck* 2004;26:890-896
24. Kostakoglu L, Goldsmith SJ. PET in the assessment of therapy response in patients with carcinoma of the head and neck and of the esophagus. *J Nucl Med* 2004;45:56-68

Chapter 8:
Challenges in apparent diffusion coefficient-based quantitative analysis: inter- and intra-observer variability of region-of-interest assessment

8.1 Introduction

Among the potential applications of DWI in the head and neck, the differentiation of lymph nodes is probably most affected by issues concerning image interpretation. Contrary to the primary lesion site, native high b-value DWI images do not allow for differentiation of benign and malignant lymph nodes, and therefore, nodal differentiation relies heavily on ADC calculation (1,2,3). In order to reliably use ADC-based differentiation in clinical practice, it is necessary that a high reproducibility is found in serial measurements or measurements between separate readers. This reproducibility will be affected by technical acquisition factors, but also by the region-of-interest-based analysis and the method of ADC calculation (4).

The primary aim of this study was to determine intra- and interobserver variability of ADC values in the setting of ADC based differentiation of lymph nodes. Additionally, variability of ADC-quantification was compared between direct calculation of the ADC from the averaged ROIs on the native images and values calculated from the co-registered pixel-wise ADC-map, for delineations by the same observer.

8.2 Materials and Methods

8.2.1 Study design

Of the patients scheduled for surgery of biopsy-proven HNSCC, 10 were randomly included irrespective of clinical T-stage, N-stage, or tumour localization. None of the patients had previously been treated for head and neck cancer. The interobserver study was performed 6 months after completion of all prior studies of this thesis project, in order to avoid recall bias in the readers. A detailed timeline of the different steps is given in Figure 1. The DWI-images were read in a blinded fashion by two readers (Reader 1: 7 years of experience in oncologic DWI, including head and neck tumour imaging – Reader 2: 15 years of experience

in head and neck imaging, 5 years of experience in head and neck DWI). Reader 1 repeated imaging analysis after a time delay of at least one month between the initial and second series of measurements.

First, inter- and intra-observer variability was determined. Second, for the reader one delineations, the difference was compared between the direct calculation of the ADC from the averaged ROIs on the native images and values calculated from the co-registered pixel-wise ADC-map.

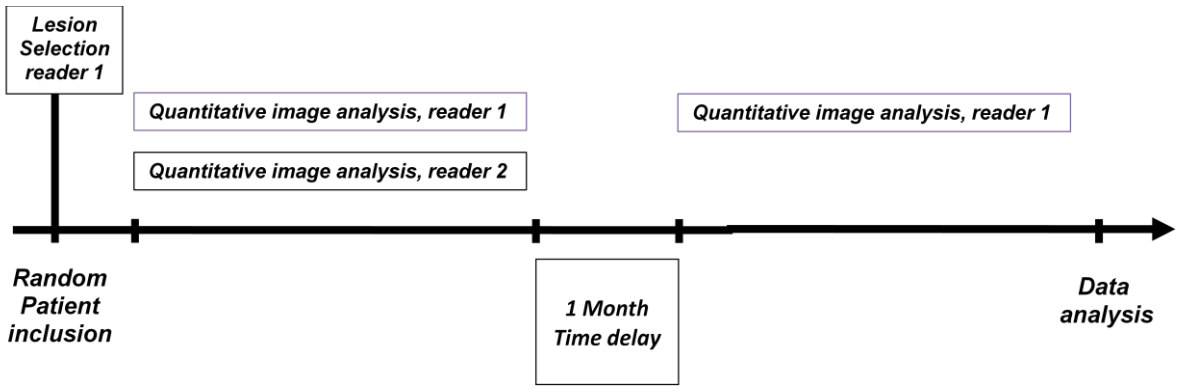

Figure 1: Timeline detailing the study concept and data processing.

8.2.2 Imaging technique

All patients underwent the standardized anatomical TSE-MRI, and functional DWI-sequences as described in chapter 3. MRI imaging covered the entire head and neck ranging from the base of skull to the thoracic outlet, and included all regional nodal stations (retropharyngeal space and neck levels).

8.2.3 Image analysis

DWI analysis was done on a PACS-workstation (Agfa-Gevaert, Mortsel, Belgium).

Observer 1 selected 10 study patients with histopathological confirmed neck nodal status and randomly indicated a maximum of 5 lymph nodes per patient for study analysis, irrespective of lesion size, level position in the neck and histological status (total 42 lymph nodes were selected, from which 6 were larger than or equal to 1 cm and 36 with a size range between 0.4

and 0.9 cm). The location according to the AAO-HNS classification and slice position of the selected lymph nodes were recorded for further analysis.

Quantitative analysis on the DWI was done as described in chapter 3.3.3. At first, quantitative analysis was done by a radiologist experienced for 7 years in head and neck DWI (observer 1), and by a subspecialty head and neck radiologist with 15 years of experience (observer 2). Both readers were blinded from each other and evaluated the recorded lesions. After a delay period of one month, observer 1 repeated the measurements in order to assess intra-observer agreement, using identical methodology.

Additionally, for reader one, the ROIs copied on the native images were copied on the co-registered pixel-wise ADC-map, in order to compare ADC calculations based on averaging native DWI signal intensities with averaging of pixel-wise calculated ADC values.

8.2.4 Data analysis

Mean ADC values ± SD were calculated for the lymph nodes for each single reader. Inter- and intra-observer variability of ADC calculations for lymph node measurements were determined as mean absolute difference (bias) and 95% confidence interval of the mean difference (limits of agreement), according to the method of Bland and Altman. Additionally, a spearman rank correlation and linear regression was used to correlate the inter- and intra-observer agreement of nodal ADC-values in correlation to the ROI-delineation. To illustrate the effect of variations of ADC-calculation on nodal differentiation based on the arbitrary determined threshold, inter- and intra-observer agreement was determined based on the previously determined threshold in this study population ($0.94x10^{-3}$; chapter 4) by means of agreement statistics (κ) (3). Linear-weighted kappa was used to determine inter- and intra-observer variability of the readers in correlation to the reference standard. To evaluate the difference between the co-registered pixel-wise ADC-map and the ADC calculated from the averaged ROIs on the native b-value images, the standard deviations of the difference between the 2 delineations in each setup were compared.

8.3 Results

8.3.1 Inter- and intra-observer agreement

Mean ADC of delineated lymph nodes were; for reader 1: 0.97 ± 0.17 x 10^{-3} (first interpretation session) and 0.97 ± 0.17 x 10^{-3} (second interpretation session). Mean ADC of delineated lymph nodes were; for reader 2: 0.99 ± 0.16 x 10^{-3}.

The mean biases and limits of agreement for inter- and intra-observer and corresponding Bland-Altman plots are depicted in Table 2 and Figure 2. Mean bias and limits of agreement for intra-observer comparison were slightly lower than for the inter-observer comparison.

Measurement	Mean bias (10^{-3} mm^2/s)	95% Limits of agreement (10^{-3} mm^2/s)
observer 1 vs. observer 2	0.011	-0.141 to 0.163
observer 1 repeated	-0.003	-0.119 to 0.113

Table 2: Inter-observer (upper row) and intra-observer (lower row) reproducibility of lymph node ADC values according to the Bland and Altman test.

Linear regression showed a high correlation for both inter- and intra-observer agreement with the latter showing slightly higher agreement (inter-observer agreement: $R^2 = 0.79$, slope=0.84; intra-observer agreement: $R^2 = 0.88$, slope=0.97) (Figure 3).

In correlation to the nodal characterization used in this study, the inter- and intra-observer variability showed excellent agreement (inter-observer: $\kappa = 0.81$, proportion of agreement = 0.91; intra-observer: $\kappa = 0.81$, proportion of agreement = 0.91).

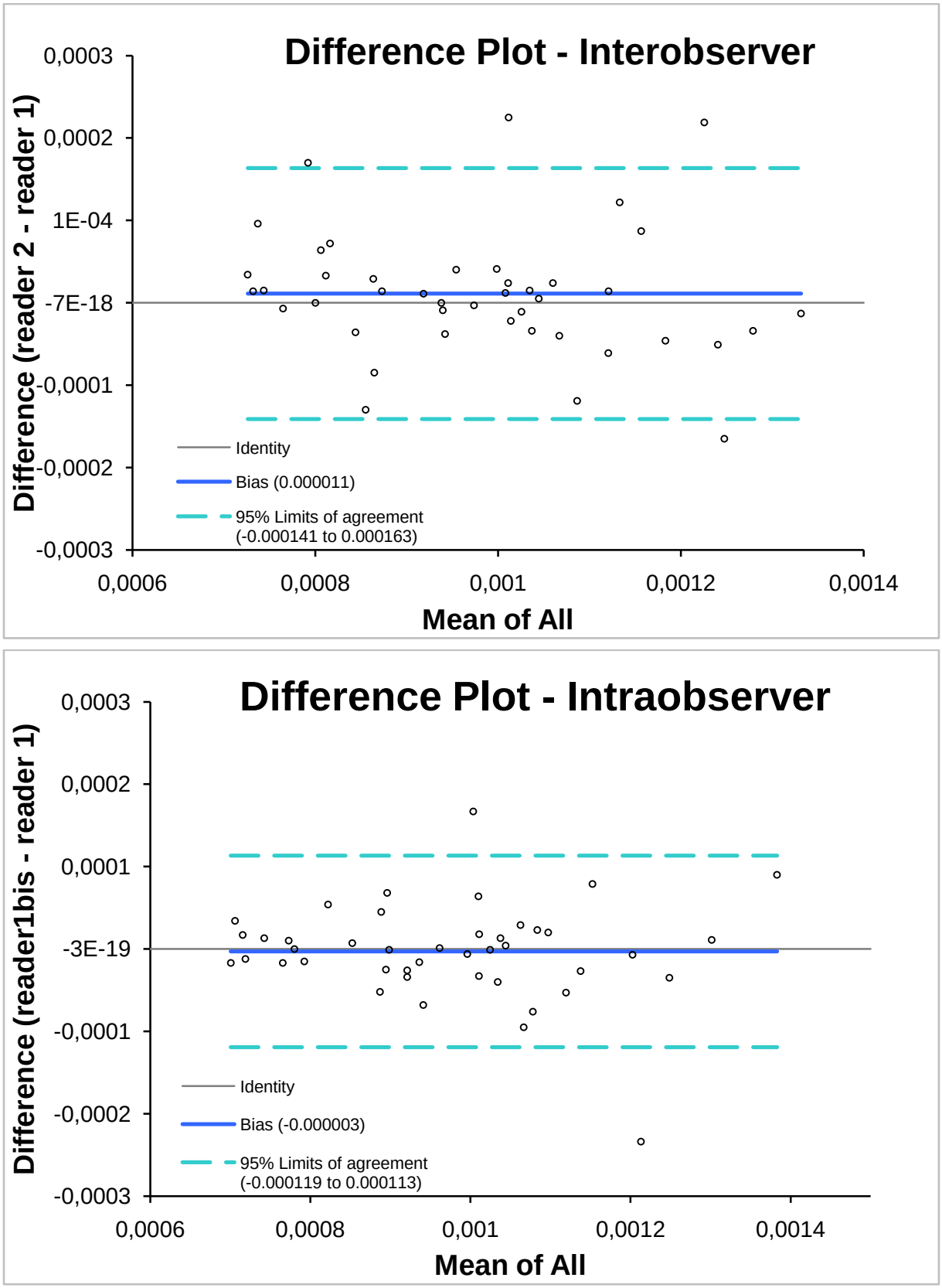

Figure 2: Upper plot shows inter-observer reproducibility, lower plot intra-observer reproducibility. The difference of ADC-measurements (y-axis) is plotted out against mean ADC measurement (x-axis), with depiction of mean absolute difference (bias) (continuous line) and 95% confidence interval of the mean difference (limits of agreement) (dashed lines).

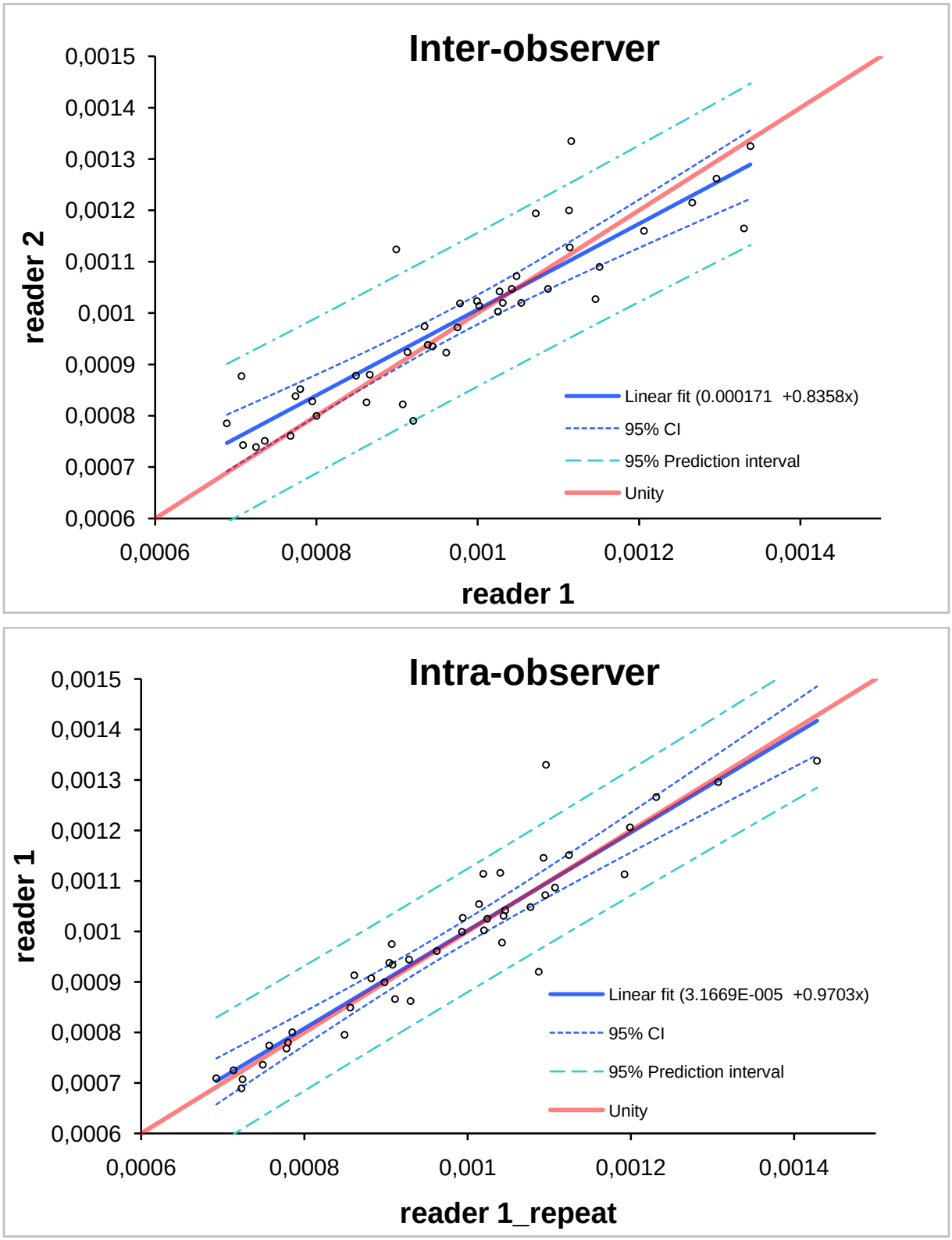

Figure 3: Linear regression analysis plots of inter- (upper graph) and intra-observer (lower graph) agreement. The ADC measurements of reader 1 are plotted out against ADC measurements of reader 2, respectively the repeated measurements of reader 1. Points clouds are approximated with the optimal linear fit (continuous blue line) and confidence intervals (dashed lines); unity line is provided as reference.

8.3.2 Intra-observer variance in correlation to ADC-methodology

The mean ADC of delineated lymph nodes, calculated from the averaged ROIs on the native b-value images (NATIVE group) were 0.97 ± 0.17 x 10^{-3} (first interpretation session) and 0.97 ± 0.17 x 10^{-3} (second interpretation session). Mean ADC of delineated lymph nodes, calculated from the co-registered pixel-wise ADC-map (ADCMAP group) were lower with 0.91 ± 0.17 x 10^{-3} (first interpretation session) and 0.91 ± 0.17 x 10^{-3} (second interpretation session). The standard deviation of the difference between the repeat measurements was 5.9 x 10^{-5} for the NATIVE group, while the standard deviation of the difference between the repeat measurements in the ADCMAP group was 39.6% higher (8.3 x 10^{-5}).

8.4 Discussion

The value of DWI for nodal staging in the head and neck has already been shown in several studies (1,2,3). The body background suppression inherent in DWI imaging allows much easier detection of small lymph nodes (high signal) from the black background compared to conventional imaging sequences (5). However, both benign and malignant lymph nodes express a certain degree of diffusion restriction and will appear hyperintense on native DW images, and a b1000 image will therefore not allow for accurate nodal differentiation (6). Hence, nodal characterization remains dependent of ADC-calculation, for which the ROI-analysis is likely to be influenced by observer related variations.

In this study, good inter- and intra-observer agreement was found for ROI based ADC evaluation of both malignant and benign lymph nodes. Most likely, the high reproducibility of DWI in this study is attributable to the high degree of standardization of imaging technique (same scanner hardware, imaging sequence and patient positioning) and image interpretation (on the same PACS imaging system) but also the level of experience of the readers.

The standardized analysis methodology in this study may have firmly contributed to the reproducibility. In our centre, ROI based analysis is performed on the native b-value images, with the ADC calculated only on the averaged signal intensities. A previous study in brain infarction has shown that native DWI-trace images were more reliable for quantification of final infarct volume compared to the pixel-wise ADC-map, anatomical sequences and magnetization transfer ratio (MTR) map (7). One of the possible reasons for this is the high image contrast on native DW images that might allow for improved lesion identification and delineation of lesion borders and probably facilitates a ROI-delineation with closer conformity to the true lesion volume compared to evaluation of ADC-maps alone. Also,

calculating ADC values based on the averaged native DWI-SI, instead of using the co-registered ADC map may have increased reproducibility. In this limited study group, higher standard deviation of the difference between the repeat measurements was found when using the co-registered ADC maps. ADC calculations of a single or a few pixels are likely to be more prone to inflate noise influences, leading to higher stochastic variability in calculated ADC values. Additionally, variability in ADC calculation through the ADC map may be increased by artifacts due to susceptibility or eddy currents. Both may cause errors in the calculation or misregistration of the ADC map compared to the native DWI images (8). As such, ROIs drawn on the native DWI images may not show an exact positional match on the ADC map exactly match when copied and produce erroneous ADC values.

In previous studies evaluating DWI for nodal staging in the head and neck, diverging results have been found for ADC values of benign and malignant lymph nodes (1,2,3,9,10,11). The most important cause for this variability in results can be attributed to the different choice of b-values to calculate the ADC. Other technical factors that influence the variability of ADC measurements, include, as previously mentioned susceptibility and eddy current related artifacts, and also movement artifacts, image noise, settings of diffusion gradient amplitudes, strength of the magnetic field and gradient calibration inaccuracy (8). Image artifacting is likely to be minimized by using combined head/neck coils as now routinely employed on most high-field MRI-systems, or by using more robust DWI-sequences such as Short Tau Inversion Recovery (STIR) DWI (5). Also, better gradients, or more optimal sequences with parallel imaging can be used to reduce sequence TE and reduce artifacts.

In this study setting, parallel imaging could not be used as the combination of a head coil with a dedicated neck coil prohibits its use to suppress potential artifacting. However, as previously described, manual shimming should be considered as an important factor to obtain optimal image quality and reduce fat-shift and distortion artifacts. A shim should cover the spine and muscles of the neck while avoiding large areas of air appears to provide best image quality (12).

So far, the lack of technical standardization has prohibited the routine application of DWI in the head and neck. However, as shown in recent studies investigating DWI for treatment follow-up, the stringent use of identical imaging protocols with identical technical parameters allowed for reproducible measurements and establishing fixed thresholds between different scanner types and field strengths (13,14).

This is reflected in three recent studies investigating DWI for nodal staging in HNSCC, where mainly subcentimetric lymph nodes were included (2,3,10). Similar ADC-values were reported for benign and malignant lymph nodes and the optimal thresholds for differentiating benign from malignant were similar. As these studies were performed using identical b-value settings, the slight variances may be explained by differences in the other technical parameters as detailed above, for which further standardization is probably required between different centres.

In a recent study, doubt was cast on the reproducibility of ADC measurements for nodal stages. When comparing ranges of ADC in normal lymph nodes found in their study, large variability was found with other studies and between different body regions (4).

While many discrepancies may be attributed to different settings of b-values and different method of ADC-evaluation, it can also be hypothesized that ADC-values and optimal thresholds may depend on the underlying tumour type and size of the lymph node. This could be important for the application of DWI in future studies incorporating several tumour tissue types and size thresholds. First, enlarged necrotic nodal metastases from HNSCC show high tendency for necrotic formation, which may falsely increase ADC-values. However, as reflected in the most recent papers, the consensus is to account for tissue heterogeneity when assessing necrotic adenopathies by delineating hyperintensities on native high b-value images to deal with this problem (1,2,3,10). Second, ADC-values for nodal characterization may vary according to the underlying histological subtype. As shown in previous studies, this may help to identify the underlying primary tumour type, thus helping in patient management (11). However, the development and implementation of DWI as a locoregional staging tool in head and neck tumours should probably be stratified according to the underlying primary tumour type. Therefore, for the further development of DWI, additional studies, including other head and neck tumour types like parotid tumours and thyroid cancers, may be required to further standardize image interpretation and characterization thresholds.

While interpreting the findings of this study, a number of limitations should be taken into account. First, the number of enlarged lymph nodes included for evaluation was limited. However, the inclusion of lymph nodes was done randomly and represents the ratio of sub- versus supercentrimetric lymph nodes in this patient group, in order to avoid selection bias. Also, as previously stated the additional clinical value of DWI lays in the detection of subcentimetric lymph nodes, which justifies the inclusion of a majority of subcentimetric lymph nodes in this study. Second, the readers in this study are experienced in evaluating head and neck MRI and DWI and the presented intra- and inter-observer variability therefore reflects only variability in personal assessment of lymph node boundaries and ROI delineations, not in training level. Generalizing these conclusions to advocate the widespread use of DWI may thus be premature, as currently the technique requires training and a minimal degree of expertise, currently limiting its use to centres with sufficient exposure to head and neck oncology. However, as the technique is easy to integrate in standard imaging protocols, continuous progression into widespread research should lead to further standardization and simplification of imaging interpretation.

8.5 Conclusion

Good inter- and intra-observer reproducibility was found for DWI for nodal staging of HNSCC between two experienced readers. Additionally, initial findings indicate that ADC-calculation from ROI-delineation on native b-value images may be more reproducible than values obtained from the pixel-wise ADC-map.

8.6 References

1. Razek A, Soliman N, Elkhamary S, Alsharaway M, Tawfik A. Role of diffusion-weighted MR imaging in cervical adenopathy. *Eur Radiol* 2006;16:1468-1477
2. De Bondt RB, Hoeberigs MC, Nelemans PJ, et al. Diagnostic accuracy and additional value of diffusion-weighted imaging for discrimination of malignant cervical lymph nodes in head and neck squamous cell carcinoma. *Neuroradiology* 2009;51:183-192
3. Vandecaveye V, De Keyzer F, Vander Poorten V, et al. Head and neck squamous cell carcinoma: value of diffusion-weighted MR imaging for nodal staging. *Radiology* 2009;251:134-146
4. Kwee TC, Takahara T, Luijten PR, Nievelstein RA. ADC measurements of lymph nodes: Inter- and intra-observer reproducibility study and an overview of the literature. *Eur J Radiol* 2009 Apr 15 [Epub ahead of print]
5. Takahara T, Imai Y, Yamashita T, Yasuda S, Nasu S, Van Cauteren M. Diffusion weighted whole body imaging with background body signal suppression (DWIBS): technical improvement using free breathing, STIR and high resolution 3D display. *Radiat Med* 2004;22:275-282
6. Kwee TC, Takahara T, Ochiai R, Nievelstein RA, Luijten PR. Diffusion-weighted whole-body imaging with background body signal suppression (DWIBS): features and potential applications in oncology. *Eur Radiol* 2008;18:1937-1952
7. Sibon I, Ménégon P, Orgogozo JM, et al. Inter- and intraobserver reliability of five MRI sequences in the evaluation of the final volume of cerebral infarct. *J Magn Reson Imaging* 2009;29:1280-1284
8. Tofts PS, Lloyd D, Clark CA, et al. Test liquids for quantitative MRI measurements of self-diffusion coefficient in vivo. *Magn Reson Med* 2000;43:368-374
9. Sumi M, Sakihama N, Sumi T, et al. Discrimination of metastatic cervical lymph nodes with diffusion-weighted MR imaging in patients with head and neck cancer. *Am J Neuroradiol* 2003;24:1627-1634
10. Perrone A, Guerrisi P, Izzo L, et al. Diffusion-weighted MRI in cervical lymph nodes: Differentiation between benign and malignant lesions. *Eur J Radiol* 2009 Aug 27 [Epub head of print]
11. King AD, Ahuja AT, Yeung DK, et al. Malignant cervical lymphadenopathy: diagnostic accuracy of diffusion-weighted MR imaging. *Radiology* 2007;245(3):806-813

12. Vandecaveye V, De Keyzer F, Hermans R. Diffusion-weighted magnetic resonance imaging in neck lymph adenopathy. *Cancer Imaging* 2008;8:173-180
13. Kim S, Loevner L, Quon H, et al. Diffusion-weighted magnetic resonance imaging for predicting and detecting early response to chemoradiation therapy of squamous cell carcinomas of the head and neck. *Clin Cancer Res* 2009;15:986-994
14. Koh DM, Blackledge M, Collins DJ, et al. Reproducibility and changes in the apparent diffusion coefficients of solid tumors treated with combretastatin A4 phosphate and bevacizumab in a two-centre phase I clinical trial. *Eur Radiol* 2009;19:2728-2738

Chapter 9:
Summary

The overall aim of the thesis was to evaluate in head and neck squamous cell carcinoma the potential value of DCE-MRI and DWI in nodal characterization, the differentiation of post-CRT necrosis and inflammation from tumoral recurrence, and early treatment prediction. While DWI was researched for nodal staging, differentiation of post-CRT recurrence and treatment prediction, DCE-MRI research was concentrated to its potential role in treatment follow-up and treatment prediction.

For pre-treatment nodal differentiation, 33 patients were included in the study and DWI was primarily compared to TSE-MRI. DWI with ADC-calculation showed significantly higher sensitivity than TSE-MRI using size-related and morphological criteria (per level: 94% vs. 57%, $p<0.0001$) with equal specificity (per level: 97% vs. 95%). Compared to TSE-MRI, DWI correctly changed nodal staging in 13 of 33 patients (39%). The main advantage of DWI was the detection of subcentimetric nodal metastases, as small as 4 mm in shortest transverse diameter, where DWI showed significantly higher sensitivity compared to TSE-MRI (per lymph node: 76% vs. 7%). In a smaller subpopulation (11 patients), DWI showed higher sensitivity than FDG-PET/CT for nodal characterization (per level: 96% vs. 67%). Although the main advantage of DWI is the detection of small nodal metastases, the spatial resolution limit of the technique did not allow to detect nodal micrometastatic deposits smaller than 4 mm. In the pre-operative setting, the technique may show additional value for contralateral neck staging in large tumours close to the midline, in order to determine the necessity for contralateral neck dissection or for the detection of skip metastases in oral cancer. For radiotherapy planning, the improved detection of nodal metastases may lead to closer conformity between the radiation target volume and the regional tumour extent, potentially improving regional tumour control and decreasing the treatment-induced side-effects.

In a second correlative study with histopathology in 26 patients, who underwent salvage surgery after chemoradiotherapy, DWI showed higher accuracy than DCE-MRI for the differentiation of tumour recurrence from necrosis and inflammation (primary tumour site: 97% vs. 82%; lymph nodes: 88% vs. 76%). The higher accuracy of DWI over DCE-MRI was explained by the lower false positive ratio secondary to inflammation and higher sensitivity of DWI, as the higher image contrast in the latter technique allows detection of small volume

disease. DWI provided complementary information to CT/TSE-MRI and FDG-PET, by reducing false positive results and excluding recurrent tumour in persistent ulcers or persistently enlarged lymph nodes more than 4 months after completion of CRT. Moreover, confirming the results of the nodal characterization study, DWI improved the detection of subcentimetric nodal metastases. The high sensitivity and negative predictive value of DWI may allow to avoid invasive diagnostic procedures surgery in persistent lesions. Additionally, the technique may be useful in the pre-operative staging of patients with a recurrent tumour, in order to determine the extent of neck dissection required.

Analysis with semi-quantitative parameters of DCE-MRI was less accurate in excluding recurrent tumour in persistent lesions after chemoradiotherapy. This limits the role of DCE-MRI as a standalone functional diagnostic tool in the post-CRT evaluation of the head and neck.

In the early treatment assessment, the value of imaging during treatment and imaging in the early post-treatment phase were separately investigated. Predictive imaging during CRT may help to tailor treatment to the individual patients response, while early post-CRT imaging mainly aims to timely select or exclude patients for salvage surgery. Thirty-one patients underwent DWI and DCE-MRI at 2 and 4 weeks during chemoradiotherapy for locally advanced HNSCC. DWI showed higher accuracy than serial volumetric measurements and DCE-MRI for the differentiation of responding and non-responding primary tumours and lymph nodes (primary tumour 2 weeks: DWI=94% vs. TSE-MRI=65% vs. DCE-MRI=87%; adenopathies 2 weeks: DWI=87% vs. TSE-MRI=56% vs. DCE-MRI=56%; primary tumour 4 weeks: DWI=94% vs. TSE-MRI=61% vs. DCE-MRI=72%; adenopathies: DWI=93% vs. TSE-MRI=63% vs. DCE-MRI=59%). While volumetric measurements showed a relatively high negative prediction value, and thus can reliable exclude lesions at risk of treatment failure, the low positive predictive value did not allow selection of patients for treatment intensification. The main contribution of DWI is early recognition of treatment response in lesions initially lacking significant volume regression, and thus improving the positive predictive value of imaging. DWI also enabled identification of non-responding lesions that did show early volume regression. DCE-MRI did not provide additional information in the early response assessment, which may be in part caused by the inflammatory changes induced by CRT.

In the multivariate analysis, DWI findings at 2 and 4 weeks was an independent predictor of LRC 2 years after treatment, while volumetric measurements and DCE-MRI were not. If treatment strategies such as dose escalation or systemic targeted agents and radio-sensitizers become clinically available, DWI may help selecting patients for such bio-adaptive treatment. Further research in a larger patient population is ongoing to confirm these preliminary findings and to investigate a correlation between per-treatment DWI-results and overall survival and disease free survival.

In a study on 29 patients, DWI and DCE-MRI were performed prior to and 3 weeks after completion of CRT and its accuracy was compared to TSE-MRI at the same time point, and a post-treatment CT study at 3 months after completion of CRT.

DCE-MRI failed to show any significant difference between lesions showing later recurrence and lesions with CR 2 years after completion of CRT.

DWI showed higher accuracy than TSE-MRI and CT for the assessment of treatment response at the primary tumour site (DWI=97% vs. TSE-MRI=80% vs. CT= 87%) and nodal disease (per neck side: DWI=89% vs. TSE-MRI=67% vs. CT=75%). For the primary tumour site, DWI mainly improved the positive predictive value compared to TSE-MRI and CT. DWI may be of use for the early identification of patients requiring salvage surgery. Timely selection for early salvage may improve local control and survival rates for T3-T4 non-laryngeal primary tumours. For the evaluation of lymph nodes, DWI both improved the PPV and NPV compared to TSE-MRI and CT. DWI showed a particularly high NPV, allowing exclusion of persistent tumour, most importantly, in patients with persistently enlarged adenopathies. Therefore, DWI may aid in the timely selection of patients for adjuvant surgical intervention and maximize the chance for successful salvage neck dissection. However, although positive predictive value was substantially improved by DWI in this setting, further optimization is still required to decrease false positive findings in subcentimetric lymph nodes.

In a final study, the inter- and intra-observer agreement regarding region of interest assessment for ADC-calculation was compared between two readers experienced in head and neck DWI. Statistical analysis showed a high correlation for both inter- and intra-observer agreement (inter-observer agreement: $R^2 = 0.79$, slope=0.84; intra-observer agreement: $R^2 = 0.88$, slope=0.97).

In addition, the direct calculation of ADC from the averaged ROIs on the native images (NATIVE group) was compared with the values obtained from the co-registered pixel-wise ADC-map (ADCMAP group), for variability of delineations by the same observer. In this limited group, the standard deviation of the difference between the repeat measurements was 5.9×10^{-5} for the NATIVE group, while the standard deviation of the difference between the repeat measurements in the ADCMAP group was about 40% higher (8.3×10^{-5}). This suggests that ADC-calculation from user-determined ROI's on native b-value images is more reproducible and reliable than values obtained from the pixel-wise calculated ADC-map.

These findings indicate that, although high inter- and intra-observer agreement is reached between experienced readers, strict standardization of image analysis will be necessary to further expand the use of DWI in the head and neck. Currently, DWI requires training and sufficient expertise, limiting its use to centres with a high throughput of oncologic head and neck pathology. As the technique can be integrated in standard imaging protocols without much burden for the patient, further research and standardization should permit easier interpretation and a more widespread application of this non-invasive imaging technique.

Hoofdstuk 10:
Samenvatting

Het globale doel van de thesis was om de waarde te evalueren van dynamische contrast- (DCE-MRI) en diffusiegewogen magnetische resonantie (DWI) in de karakterisatie van lymfeklieren, de differentiatie van post-radiotherapie necrose en inflammatie van tumorrecidief en de vroegtijdige voorspelling van het therapieresultaat in het spinocellulair carcinoom van het hoofd-halsgebied.

Terwijl DWI onderzocht werd voor lymfeklierstadiëring, differentiatie van het post-radiotherapie tumorrecidief en therapiepredictie, werd voor DCE-MRI de nadruk gelegd op therapie follow-up en -predictie.

Voor de pretherapeutische studie met betrekking tot lymfeklierdifferentiatie werden 33 patiënten geïncludeerd, voor wie DWI in de eerste plaats werd vergeleken met conventionele MRI. DWI, gekwantificeerd door de apparent diffusion coefficient (ADC), toonde een significant hogere sensitiviteit dan conventionele MRI voor de detectie van lymfeklier-metastasen (per nekzone: 94% vs. 57%, $p<0.0001$) met een gelijkaardige specificiteit (per nekzone: 97% vs. 95%). Hierbij maakte conventionele MRI gebruik van lymfeklierdiameter en morfologische klierafwijkingen ter differentiatie. Vergeleken met conventionele MRI veranderde DWI correct de lymfeklierstadiëring in 13 van de 33 patiënten (39%). Het grootste voordeel van DWI lag in de detectie van subcentimetrische lymfekliermetastasen tot een minimale diameter over de kortste as van 4 mm, waarbij voor DWI een significant hogere sensitiviteit werd bekomen in vergelijking met conventionele MRI (per lymfeklier: 76% vs. 7%). In een kleinere studiepopulatie van 11 patiënten toonde DWI een hogere sensitiviteit dan fluoro-deoxy-glucose positron emission tomography/computer tomografie (FDG-PET/CT) voor lymfeklierdifferentiatie (per nekzone: 96% vs. 67%). Hoewel DWI de differentiatie van kleine lymfeklieren als belangrijkste voordeel heeft, laat de spatiële resolutielimiet de detectie van metastatische deposities kleiner dan 4 mm - en dus micrometastasen - niet toe. De belangrijkste toegevoegde waarde van DWI in de pre-operatieve situatie lijkt de stadiëring van de contralaterale nek te zijn in tumoren die over of dicht op de midlijn uitbreiden en voor de detectie van “skip” metastasen in de lagere nekzones bij mondholtetumoren. In geval van radiotherapieplanning kan de verbeterde karakterisatie van lymfeklieren leiden tot een hogere conformiteit tussen het doelvolume van de bestraling en de regionale tumoruitbreiding. Dit

kan enerzijds leiden tot een verbeterde regionale tumorcontrole en anderzijds tot een daling van de therapie-geïnduceerde nevenwerkingen.

In een tweede correlatieve studie met histopathologie in 26 patiënten die chirurgie ondergingen voor een mogelijk recidief na chemoradiotherapie toonde DWI een hogere accuraatheid dan DCE-MRI voor de differentiatie van tumorrecidief met necrose en inflammatie (primaire tumoursite: 97% vs. 82%; lymfeklieren: 88% vs. 76%). De hogere accuraatheid van DWI t.o.v. DCE-MRI kon teruggebracht worden op lagere vals positieve ratio secundair aan inflammatie, en aan de hogere sensitiviteit van DWI als gevolg van het hogere beeldcontrast dewelke de detectie van kleine letsels toelaat. DWI leverde complementaire informatie aan CT en conventionele MRI en FDG-PET door de vals positieve ratio te verlagen en persisterende of recidief tumor uit te sluiten in ulceraties of vergrote adenopathieën meer dan 4 maand na het beëindigen van de chemoradiotherapie. Evenals in de eerste studie, verbeterde DWI de detectie van subcentimetrische lymfekliermetastasen. De hoge sensitiviteit en negatieve predictieve waarde van DWI kan behulpzaam zijn om invasieve diagnostische procedures te vermijden in persisterende letsels en om de locoregionale stadiëring te vervolledigen, meer bepaald de identificatie van lymfeklier-metastasen en dus het helpen bepalen van de uitbreiding van de geplande nekdissectie. Semi-kwantitatieve analyse van de DCE-MRI was minder accuraat dan DWI, vooral in het uitsluiten van tumoraal weefsel in persisterende letsels. Dit beperkt de rol van DCE-MRI als diagnostische techniek in de post-chemoradiotherapeutische evaluatie van het hoofd-halsgebied. Evenwel kan DCE-MRI nuttig zijn wanneer deze gebruikt wordt in combinatie met andere functionele technieken, zoals DWI.

De waarde van functionele MRI-technieken voor vroegtijdige therapie follow-up werd arbitrair opgedeeld in beeldvorming gedurende, respectievelijk vroegtijdig na chemo-radiotherapie. Predictieve beeldvorming gedurende chemoradiotherapie zou nuttig kunnen zijn om de therapie aan de individuele situatie van de patiënt aan te passen, terwijl beeldvorming vroegtijdig na chemoradiotherapie als doel heeft om vroegtijdig patiënten te selecteren die aanvullende chirurgie nodig hebben na het beëindigen van de chemoradiotherapie.

Bij eenendertig patiënten met lokaal gevorderd hoofd-hals spinocellulair carcinoom werd een DWI en DCE-MRI uitgevoerd op 2 en 4 weken gedurende de chemoradiotherapie. DWI was accurater dan seriële volumetrische metingen en DCE-MRI voor de differentiatie van therapiegevoelige en therapieresistente primaire tumoren en lymfekliermetastasen (primaire tumor 2 weken: DWI=94% vs. conventionele MRI=65% vs. DCE-MRI=87%; adenopathieën

2 weken: DWI=87% vs. conventionele MRI=56% vs. DCE-MRI=56%; primaire tumor 4 weken: DWI=94% vs. conventionele MRI=61% vs. DCE-MRI=72%; adenopathieën: DWI=93% vs. conventionele MRI=63% vs. DCE-MRI=59%). Terwijl volumetrische metingen een relatief hoge negatieve predictieve waarde vertoonden voor de exclusie van letsels met risico op ziekterecidief, belette de lage positieve waarde de vroegtijdige identificatie van patiënten die baat zouden kunnen hebben bij therapieaanpassing. De belangrijkste toegevoegde waarde van DWI was terug te brengen op het vroegtijdig herkennen van therapierespons in letsels die geen volumeafname vertoonden en dus het verbeteren van de positief predictieve waarde. Bovendien verbeterde DWI de identificatie van letsels die een onvolledige therapierespons hadden en tegelijkertijd toch een belangrijke doch onvolledige volumeafname vertoonden. DCE-MRI leverde geen toegevoegde informatie voor vroegtijdige evaluatie van therapierespons. Mogelijks is dit gedeeltelijk wijten aan de radiotherapie-geïnduceerde inflammatie.

Multivariaat analyse toonde dat DWI 2 en 4 weken gedurende chemoradiotherapie een onafhankelijke predictor was voor de 2-jaars locoregionale controle, terwijl dit niet het geval was voor volumetrie en DCE-MRI. Indien therapiestrategieën zoals dosisescalatie, weefselspecifieke systemische antitumorale geneesmiddelen of radio-sensibele medicatie beschikbaar komen, dan zou DWI kunnen helpen om patiënten uit te selecteren voor dergelijke bio-adaptieve therapieën. Verder onderzoek in een grotere patiëntengroep is bezig om de gevonden resultaten te bevestigen.

In een studie met 29 patiënten werd een DWI en DCE-MRI uitgevoerd vóór en 3 weken na het beëindigen van de chemoradiotherapie. De accuraatheid van beide functionele technieken werd vergeleken met conventionele MRI op 3 weken na het beëindigen van chemo-radiotherapie en met de routinematig uitgevoerde CT gemiddeld 3 maand na het beëindigen van de therapie. DCE-MRI kon geen significant verschil aantonen tussen letsels die een later tumorrecidief vertoonden en letsels met volledige remissie 2 jaar na het beëindigen van de chemoradiotherapie. DWI was accurater dan conventionele MRI en CT voor therapie-evaluatie van de primaire tumorlokalisatie (DWI=97% vs. TSE-MRI=80% vs. CT= 87%) en lymfekliermetastasen (per nekzijde: DWI=89% vs. TSE-MRI=67% vs. CT=75%). Voor de primaire tumorlokalisatie verbeterde DWI vooral de positieve predictieve waarde in vergelijking met conventionele MRI en CT. Als dusdanig kan DWI nuttig zijn voor de vroegtijdige selectie van patiënten met verhoogd risico op later tumorrecidief en die dus nood hebben aan bijkomende chirurgie. Tijdige selectie van patiënten voor vroegtijdige chirurgie kan leiden tot een verbeterde lokale controle en patiëntoverleving voor T3-T4 niet-laryngeale

tumoren. Voor de evaluatie van lymfekliermetastasen verbeterde DWI zowel de positieve als de negatief predictieve waarde in vergelijking met conventionele MRI en CT. DWI toonde een zeer hoge negatieve predictieve waarde dewelke op een betrouwbare wijze de uitsluiting van persisterende tumor toeliet, ook in patiënten met persisterende vergrote adenopathieën. Daardoor zou DWI nuttig kunnen zijn voor de selectie tussen patiënten die baat kunnen hebben van een bijkomende chirurgische nekdissectie of patiënten bij wie een afwachtende houding gewettigd is. Hoewel de positieve predictieve waarde van conventionele MRI en CT sterk werd verbeterd door DWI, is verdere oppuntstelling van de techniek nodig teneinde het aantal vals positieven in subcentimetrische lymfeklieren verder te beperken.

In een laatste studie werd de inter- en intraobserver variabiliteit van de manuele aflijningen voor ADC-berekening in lymfeklieren vergeleken tussen 2 observatoren met ervaring in hoofd-hals DWI. Statistische analyse toonde een hoge correlatie voor zowel de inter- als de intraobserver variabiliteit (inter-observer: R^2 = 0.79, slope=0.84; intraobserver: R^2 = 0.88, slope=0.97).

Ook werd de directe berekening van de ADC van de uitgemiddelde aflijningen op de natieve diffusiegewogen beelden (NATIVE groep) vergeleken met de waarden bekomen uit de gecoregistreerde pixelgebaseerde ADC-map (ADCMAP groep), voor variabiliteit tussen de aflijningen in 1 observator. Preliminaire resultaten duiden aan dat de standaarddeviatie van het verschil tussen de herhaalde metingen 5.9×10^{-5} was voor de NATIVE groep, terwijl de standaarddeviatie van het verschil tussen de herhaalde metingen in de ADCMAP groep ongeveer 40% hoger was (8.3×10^{-5}). Dit suggereert dat ADC-berekening van aflijningen op de natieve diffusiegewogen beelden meer reproduceerbaar en betrouwbaar zijn dan deze bekomen van de pixelgebaseerde ADC-map. Hieruit kan worden geconcludeerd dat, hoewel een hoge overeenkomst in observaties kan worden bekomen, strikte standaardisatie van de beeldinterpretatie nodig is om de toepassing van DWI verder uit te breiden in de hoofd-hals oncologie. Momenteel is voor hoofd-hals DWI training en een minimale expertise noodzakelijk; daardoor blijft het gebruik beperkt tot centra met een hoge doorstroming van hoofd-hals oncologische pathologie. Aangezien het vrij eenvoudig is de techniek te integreren in het standaard beeldvormingsprotocol zonder belasting van de patiënt, zou er een makkelijke toegang voor verder onderzoek moeten zijn. Verdere standaardisatie zou in de toekomst moeten leiden tot een makkelijker beeldinterpretatie en meer verspreid gebruik van deze niet-invasieve techniek.

Bibliography

Publications

- **Vandecaveye V**, Verswijvel G, Colla P, Verhelst H, Van Robaeys J, Palmers Y. Cystic insulinoma of the pancreas in a patient with myotonic dystrophy : correlation of imaging and pathologic findings. *JBR-BTR* 2003;85: 268-271
- Verswijvel G, **Vandecaveye V**, Gelin G, Vandevenne J, Grieten M, Horvath M, Oyen R, Palmers Y. Diffusion weighted MR imaging in the evaluation of renal infection : preliminary results. *JBR-BTR* 2002;85: 100-103
- De Wever W, **Vandecaveye V**, Lanciotti S, Verschakelen JA.: Multidetector CT-generated virtual bronchoscopy: an illustrated review of the potential clinical indications. *European Respiratory Journal* 2004;23:776-782
- Harriet C. Thoeny, Frederik De Keyzer, Feng Chen, **Vandecaveye V**, Erik K. Verbeken, Bisan Ahmed, Xihe Sun, Yicheng Ni, Hilde Bosmans, Robert Hermans, Allan van Oosterom, Guy Marchal, Willy Landuyt. Diffusion-Weighted Magnetic Resonance Imaging Allows Noninvasive *In Vivo* Monitoring of the Effects of Combretastatin A-4-Phosphate After Repeated Administration. *Neoplasia* 2005;7:779-787
- Harriet C. Thoeny, Frederik De Keyzer, **Vandecaveye V**, Feng Chen, Xihe Sun, Hilde Bosmans, Robert Hermans, Eric K. Verbeken, Chris Boesch, Guy Marchal, Willy Landuyt, Yicheng. Comparison of Dynamic Contrast-Enhanced MRI and Diffusion-Weighted MRI for Monitoring the Effect of a Vascular Targeting Agent on Tumors: a Study in Rodents. *Radiology* 2005;237:492-499
- Lewi L, Jani J, Cannie M, Robyr R, Ville Y, Hecher K, Gratacos E, Vandecruys H, **Vandecaveye V**, Dymarkowski S, Deprest J. Intertwin anastomoses in monochorionic placentas after fetoscopic laser coagulation for twin-to-twin transfusion syndrome: is there more than meets the eye? *Am J Obstet Gynecol* 2006;194:790-795
- Chen F, Sun X, De Keyzer F, Yu J, Peeters R, Coudyzer W, **Vandecaveye V**, Landuyt W, Bosmans H, Van Hecke P, Marchal G, Ni Y. Liver tumourmodel with implanted rhabdomyosarcoma in rats: MR imaging, microangiography, and histopathologic analysis. *Radiology* 2006;239:554-562

- **V. Vandecaveye**, MD, F. De Keyzer, V. Vander Poorten, K. Deraedt, H. Alaerts, W. Landuyt, S. Nuyts, R. Hermans. Evaluation of the Larynx for Tumour Recurrence by Diffusion-Weighted Magnetic Resonance Imaging after Radiotherapy: Initial Experience in Four Cases. *Br j Radiol* 2006;79:681-687
- Roels S, Duthoy W, Haustermans K, Penninckx F, **Vandecaveye V**, Boterberg T, De Neve W. Definition and delineation of the clinical target volume for rectal cancer. *Int J Radiat Oncol Biol Phys* 2006 Jul 15;65:1129-42
- **Vandecaveye V**, De Keyzer F, Nuyts S, Deraedt K, Dirix P, Hamaekers P, Vander Poorten V, Delaere P, Hermans R. Detection of head and neck squamous cell carcinoma with diffusion weighted MRI after (chemo)radiotherapy: correlation between radiologic and histopathologic findings. *Int J Radiat Oncol Biol Phys* 2007;67:960-971
- Chen F, De Keyzer F, Wang H, **Vandecaveye V**, Landuyt W, Bosmans H, Hermans R, Marchal G, Ni Y. Diffusion weighted imaging in small rodents using clinical MRI scanners. *Methods* 2007;43:12-20
- Hermans R, **Vandecaveye V**. Diffusion-weighted MRI in head and neck cancer. *Cancer Imaging* 2007;7:126-127
- Hermans R, **Vandecaveye V**. Diffusion-weighted MRI in head and neck cancer. *JBR-BTR* 2007;90:264-267
- Jeunen G, Desloovere C, Hermans R, **Vandecaveye V**. The Value of Magnetic Resonance Imaging in the Diagnosis of Residual or Recurrent Acquired Cholesteatoma After Canal Wall-Up Tympanoplasty. *Otol Neurotol* 2008 Jan;29:16-18
- **Vandecaveye V**, De Keyzer F, Dymarkowski S. Imaging and targeted agents in GI cancers: overview on perfusion- and diffusion-weighted MRI and angiogenesis inhibitors. *Targeted oncology* 2008;3:101-110
- Dirix P, De Keyzer F, **Vandecaveye V**, Stroobants S, Hermans R, Nuyts S. Diffusion-weighted magnetic resonance imaging to evaluate major salivary gland function before and after radiotherapy. *Int J Radiat Oncol Biol Phys* 2008; 71:1365-1371
- **Vandecaveye V**, De Keyzer F, Dymarkowski S. Perfusion-and diffusion-weighted imaging of hepatocellular carcinoma. *JBR-BTR* 2007;90:492-496
- **Vandecaveye V**, De Keyzer F, Hermans R. Diffusion-weighted magnetic resonance imaging in neck lymph adenopathy. *Cancer Imaging* 2008; 8:173-180
- Wang H, Sun X, Chen F, De Keyzer F, Yu J, Landuyt W, **Vandecaveye V**, Peeters R, Bosmans H, Hermans R, Marchal G, Ni Y. Treatment of rodent liver tumourwith

combretastatin A4 phosphate: Noninvasive therapeutic evaluation using multiparametric magnetic resonance imaging in correlation with microangiography and histology. *Invest Radiol* 2009;44:44-53.

- **Vandecaveye V**, De Keyzer F, Vander Poorten V, Dirix P, Verbeken E, Nuyts S, Hermans R. Head and neck squamous cell carcinoma: value of diffusion-weighted MR imaging for nodal staging. *Radiology* 2009;251:134-146
- Roels S, Slagmolen P, Nuyts J, Lee JA, Loeckx D, Maes F, **Vandecaveye V**, Stroobants S, Ectors N, Penninckx F, Haustermans K. Biological Image-Guided Radiotherapy in Rectal Cancer: Challenges and Pitfalls. *Int J Radiat Oncol Biol Phys* 2009;75:782-790
- **Vandecaveye V**, De Keyzer F, Verslype C, Op de beeck K, Komuta M, Topal B, Roebben I, Bielen D, Roskams T, Nevens F, Dymarkowski S. Diffusion-weighted MRI provides additional value to conventional dynamic contrast-enhanced MRI for detection of hepatocellular carcinoma. *Eur Radiol* 2009;19:2456-2466
- De Keyzer F, **Vandecaveye V**, Thoeny H, Chen F, Ni Y, Marchal G, Hermans R, Nuyts S, Landuyt W, Bosmans H. Dynamic contrast-enhanced and diffusion-weighted MRI for early detection of tumoral changes in single-dose and fractionated radiotherapy: evaluation in a rat rhabdomyosarcoma model. *Eur Radiol* 2009;19:2663-2671
- Dirix P, **Vandecaveye V**, De Keyzer F, Stroobants S, Hermans R, Nuyts S. Dose painting in radiotherapy for head and neck squamous cell carcinoma: value of repeated functional imaging with (18)F-FDG PET, (18)F-fluoromisonidazole PET, diffusion-weighted MRI, and dynamic contrast-enhanced MRI. *J Nucl Med* 2009;50:1020-1027
- Dirix P, **Vandecaveye V**, De Keyzer F, Op de Beeck K, Poorten VV, Delaere P, Verbeken E, Hermans R, Nuyts S. Diffusion-Weighted MRI for Nodal Staging of Head and Neck Squamous Cell Carcinoma: Impact on Radiotherapy Planning. *Int J Radiat Oncol Biol Phys* 2009;76:761-766
- Maleux G, van Malenstein H, **Vandecaveye V**, Heye S, Vaninbroukx J, Nevens F, Verslype C. Transcatheter chemoembolization of unresectable hepatocellular carcinoma: current knowledge and future directions. *Dig Dis* 2009;27:157-163
- **Vandecaveye V**, Dirix P, De Keyzer F, Op de Beeck K, Vander Poorten V, Roebben I, Nuyts S, Hermans R. Predictive value of diffusion-weighted magnetic resonance imaging during chemoradiotherapy for head and neck squamous cell carcinoma. Eur Radiol 2010; Epub ahead of print.

Chapter in book

- Hermans R, De Keyzer F, **Vandecaveye V**

"Chapter 3. Imaging Techniques"In : Hermans R, (ed). Head and Neck Cancer Imaging Springer-Verlag 2006.

Invited lectures

- 3D-CT congres, november 2003 Rome - Italy : Virtual bronchoscopy: a correlation with real time fiberoptic bronchoscopy
- Oncologic seminar, March 2005 Maastricht - The Netherlands: The potential of Diffusion weighted MR-Imaging in blood vessel related anticancer treatments
- Oncologic seminar; May 2005 Leuven - Belgium: Diffusion Weighted Magnetic Resonance Imaging in experimental and clinical oncology: From physico-biological basis to potential applications
- High field symposium, September 2005 Seoul - South-Korea: High field-strength imaging at 3Tesla : Whole body applications in conventional MRI and diffusion weighted imaging
- High field symposium, September 2005 Seoul - South-Korea: Applications of neuroradiology at 3 Tesla
- Teaching symposium on targeted therapy, May 2006 Utrecht - the Netherlands: role of functional MRI techniques in staging and treatment follow-up of solid tumors
- Teaching symposium on anti-angiogenetic treatment, October 2006 and 2007 leuven - Belgium: role of radiology in diagnosis of colorectal cancer
- Symposium on latest developments in hepatocellular carcinoma, October 2006 leuven - Belgium: Application of functional MRI-techniques in the diagnosis and treatment follow-up of hepatocellular carcinoma
- MRI-symposium high field imaging, November 2006 Muscat - Oman : Full-body Diffusion-MRI at 3T: applications in oncological imaging
- Diffusie-MRI symposium, march 2007 Wilrijk - Belgium: Basic principles of diffusion-weighted MR imaging
- Diffusion-MRI symposium, march 2007 Wilrijk - Belgium : Advanced applications of diffusion-weighted MRI in oncology

- La diagnostica per immagini nella pratica clinica. "PET-TC ed Imaging integrato in Oncologia – national Italian national convention, June 2007 Trani - Italie: Full-body Diffusion-MRI at 3T: applications in clinical oncology
- Annual meeting of the international cancer imaging society, October 2007 Bruges - Belgium: Diffusion-weighted MRI in neck lymph adenopathy
- Annual meeting of the international cancer imaging society, October 2007 Bruges - Belgium: Diffusion-weighted MRI in extrahepatic abdominal tumors
- Symposium of the Royal Belgian Radiological Society, November 2007, Antwerp - Belgium: CT Perfusion and MR Diffusion of hepatic and pancreatic lesions
- Preceptorship on anti-angiogeneic treatment in gastro-intestinal tumours, October 2007 Leuven - Belgium: Role of functional MRI-techniques in the diagnosis and treatment follow-up of gastro-intestinal cancers.
  Repeated in 2008, 2009 and 2010
- Novara Whole Body Workshop, September 2008 Novara - Italy: Value of whole body diffusion-weighted MRI compared to PET/CT.
- Clinical teaching session, annual meeting of the International Society for Magnetic Resonance in Medicine (ISMRM), May2009 Honolulu - USA: Additional value of Diffusion-weighted MRI for the detection of abdominal tumors.
- Annual meeting of the European Society of Head and Neck Radiology (ESHNR), September 2009 Verona - Italy: The ultrasound negative neck: value of diffusion-weighted magnetic resonance imaging.
- Annual meeting of the European Society of Head and Neck Radiology (ESHNR), September 2009 Verona - Italy: Diffusion-weighted magnetic resonance imaging in head and neck cancer: the integration of the engineer and radiologist experience. (Co-presentation with engineer Frederik De Keyzer).
- Liver imaging workshop, educational course of the European society of gastrointestinal and abdominal radiology (ESGAR), November 2009 Antwerp - Belgium: Diffusion-weighted imaging in hepatic imaging
- Whole body MRI symposium (F Lecouvet), December 2009 Brussels - Belgium: Beyond the skeleton: one step imaging of the brains, liver, lungs?
- ERASMUS course MRI of the head and neck, Februari 2010, Brugge – Belgium: Diffusion-weighted MRI in the head and neck: basic principles and clinical applications

- Diffusion-weighted MRI work-shop: body and head and neck applications, February 2010 Kuwait city – Kuwait: Various lectures on head and neck and body diffusion-weighted MRI, hands on image analysis training (cooperation with engineer Frederik De Keyzer)
- Neuro-imaging Council, March 2010 Boston – 2010: Diffusion-weighted imaging for post-radiotherapy assessment in head and neck cancer
- Oncologic round, department of radiology, Brighams and Women's hospital Boston, March 2010 Boston – USA: Diffusion-weighted MRI, general applications in body oncology
- EORTC head and neck cancer group meeting, March 2010 Brussels – Belgium: Diffusion-weighted imaging for post-radiotherapy assessment and treatment prediction in head and neck cancer

Abstracts (scientific presentations)

- **Vandecaveye V**, Thoeny HC, De Keyzer F, Cheng F, Landuyt W, Hermans R, Marchal G, Ni Y, Thys M. Early effects of vascular targeting agents on rhabdomyosarcomas: Evaluation with power Doppler and histopathologic correlation.
  Eur Radiol, Suppl 2, Vol 14, p278 (A 681), ECR 2004.
  European Congress of Radiology, ECR 2004, Vienna, Austria.
- Thoeny HC, De Keyzer F, **Vandecaveye V**, Chen F, Ni Y, Hermans R, Marchal G, Landuyt W. Value of dynamic contrast-enhanced MRI (DCE-MRI) and diffusion-weighted MRI (DW-MRI) for the monitoring of the effect of a vascular targeting agent on rodent tumors.
  Proc Intl Soc Magn Reson Med 11, p1998, 2004
  International Society on Magnetic Resonance in Medicine, ISMRM 2004, Kyoto, Japan.
- De Keyzer F, **Vandecaveye V**, Thoeny HC, Chen F, Sun X, Ni Y, Hermans R, Boesch C, Marchal G, Landuyt W, Bosmans H. Noninvasive Assessment of the effect of a Vascular Targeting Agent on Rodent Tumors with Diffusion-Weighted and Dynamic Contrast-Enhanced MRI. MAGMA, Suppl 1, Vol 17, p301 (A 514), ESMRMB 2004.
  European Society for Magnetic Resonance in Medicine and Biology, ESMRMB 2004, Copenhagen, Denmark.

- Thoeny HC, De Keyzer F, **Vandecaveye V**, Chen F, Verbeken EK, Boesch C, Ni Y, Landuyt W, Marchal G, Hermans R. Monitoring the effect of a vascular targeting agent on rodent tumors: dynamic contrast-enhanced MRI or diffusion-weighted MRI?
  International Cancer Imaging Society, ICIS 2004, Sestri Levante, Italy.
- **Vandecaveye V**, De Keyzer F, Landuyt W, Thoeny HC, Sun X, Chen F, Marchal G, Thys M, Ni Y, Hermans R. Early effects of a vascular targeting agent on rat tumors: evaluation by power Doppler ultrasound.
  International Cancer Imaging Society, ICIS 2004, Sestri Levante, Italy.
- **Vandecaveye V**, Cannie M, De Keyzer F, Lewi L, Jani J, Deprest J, Dymarkowski S. Assessing the potential role of diffusion-weighted MR imaging in the evaluation of placental changes before and after laser - treatment in twin-to-twin transfusion syndrome : pilot study.
  14th World Congress on Ultrasound in Obstetrics and Gynecology, ISUOG 2004, Stockholm, Sweden. Ultrasound in Obstetrics and Gynecology 2004; 24(3):318.
- De Keyzer F, **Vandecaveye V**, Thoeny HC, Chen F, Ni Y, Hermans R, Boesch C, Marchal G, Landuyt W, Bosmans H. Noninvasive in vivo assessment of vascular targeting effects on rodent tumors with diffusion-weighted and dynamic contrast-enhanced magnetic resonance imaging.
  European Society for Therapeutic Radiology and Oncology, ESTRO 2004, Amsterdam, The Netherlands.
- **Vandecaveye V**, Landuyt W, De Keyzer F, Chen F, Sun X, Marchal G, Thys M, Hermans R, Ni Y. Early assessment of vascular targeting effects in tumors with contrast-enhanced sonography: predictive value for treatment-induced necrosis on diffusion MRI with histopathologic correlation.

European Society for Therapeutic Radiology and Oncology, ESTRO 2004, Amsterdam, The Netherlands.

- **Vandecaveye V**, Cannie M, De Keyzer F, Lewi L, Deprest J, Dymarkowski S. Diffusion-weighted MR imaging in the evaluation of placental changes before and after laser coagulation treatment in twin-to-twin transfusion syndrome: preliminary results.
  Radiological Society of North America, RSNA 2004, Chicago, USA.
- Thoeny HC, De Keyzer F, **Vandecaveye V**, Chen F, Verbeken EK, Boesch C, Ni Y, Landuyt W, Marchal G, Hermans R. Monitoring the Effect of a Vascular Targeting Agent on Rodent Tumors: Dynamic Contrast-Enhanced MRI or Diffusion-Weighted MRI?

European Congress of Radiology, ECR 2005, Vienna, Austria.

- Chen F, Sun XH, De Keyzer F, Yu J, **Vandecaveye V**, Landuyt W, Bosmans H, Hermans R, Marchal G, Ni Y. TumourVascular Targeting Therapy in Rodent Models of Liver Metastases: Noninvasive Monitoring with Advanced MRI. Proc. Acta Gastro-enterologica Belgica, Fasc. 1, 2005XVII Belgian Week of Gastroenterology.
- **Vandecaveye V**, De Keyzer F, Landuyt W, Bosmans H, Chen F, Sun X, Ni Y, Thys M, Hermans R. Assessment of early vascular targeting-induced changes with contrast-enhanced sonography as a predictive parameter for induced necrosis formation on diffusion MRI.

  International Society on Magnetic Resonance in Medicine, ISMRM 2005, Miami Beach, Florida, USA.
- De Keyzer F, Thoeny HC, **Vandecaveye V**, Chen F, Sun X, Ni Y, Hermans R, Marchal G, Landuyt W, Bosmans H. In Vivo Monitoring of the Effect of Repeated Administration of Combretastatin A-4-Phosphate by Diffusion-Weighted Magnetic Resonance Imaging.

  International Society on Magnetic Resonance in Medicine, ISMRM 2005, Miami Beach, Florida, USA.
- Lewi L, Cannie M, **Vandecaveye V**, Jani J, De Keyzer F, Dymarkowski S, Deprest J. Feasibility of magnetic resonance imaging as a preoperative guidance tool for laser coagulation in twin-twin transfusion syndrome.

  15th World Congress on Ultrasound in Obstetrics and Gynecology, ISUOG 2006, September 25 - 29, Seoul, Korea.
- De Keyzer F, Eckelmans J, **Vandecaveye V**, Chen F, Peeters RR, Ni Y, Hermans R, Nuyts S, Landuyt W, Bosmans H. Use of functional MRI techniques for early detection of radiotherapy-induced tumoral changes in a rat rhabdomyosarcoma model.

  European Society for Magnetic Resonance in Medicine and Biology, ESMRMB 2005, Basel, Switzerland.
- **Vandecaveye V**, Nuyts S, Vander Poorten V, De Keyzer F, Delaere P, Hermans R. Assessment of post-radiotherapeutic tumour recurrence in head and neck squamous cell carcinoma by diffusion-weighted MRI: a feasibility study.

  European Society of Head and Neck Radiology, ESHNR 2005, Oxford, United Kingdom.
- **Vandecaveye V**, De Keyzer F, Nuyts S, Vander Poorten V, Delaere P, Hermans R. Diffusion-weighted MRI-based differentiation of tumour recurrence after radiotherapy for head and neck squamous cell carcinoma.

International Cancer Imaging Society, ICIS 2005, Amsterdam, The Netherlands.

- **Vandecaveye V**, De Keyzer F, Vander Poorten V, Nuyts S, Hermans R. Diffusion-weighted magnetic resonance imaging for discrimination of malignant and benign lymph nodes in primary head and neck squamous cell carcinoma: preliminary results.
  Radiological Society of North America, RSNA 2005, Chicago, USA.
- **Vandecaveye V**, De Keyzer F, Landuyt W, Bosmans H, Sun X, Chen F, et al. Predictive value of early perfusion changes on contrast-enhanced doppler ultrasound for vascular targeting-induced necrosis on diffusion MRI: study in a rat tumourmodel.

Radiological Society of North America, RSNA 2005, Chicago, USA.

- **Vandecaveye V**, De Keyzer F, Op De Beeck K, Nijs E, Bielen D, Vanbeckevoort D, Dymarkowski S. Differentiating hepatic lesions with diffusion-weighted magnetic resonance imaging in patients with extrahepatic primary tumor: Initial Experience.
  XVIIIth Belgian Week of Gastroenterology, BWG 2006, Feb 9-11, Oostende, Belgium.
- De Keyzer F, **Vandecaveye V**, Eckelmans J, Chen F, Peeters RR, Hamaekers P, Ni Y, Hermans R, Nuyts S, Landuyt W, Bosmans H. Difference in early intratumoral changes induced by single dose and fractionated radiotherapy in rat rhabdomyosarcoma measured with diffusion- and perfusion-weighted magnetic resonance imaging.
  International Society on Magnetic Resonance in Medicine, ISMRM 2006, May 6-12, Seattle, Washington, USA.
- Ni Y, Sun X, Chen F, De Keyzer F, **Vandecaveye V**, Landuyt W, Van Hecke P, Bosmans H, Marchal G. Comprehensive Magnetic Resonance Monitoring of Tumoricidal Effect of a Vascular Targeting Agent in a Rodent Liver Metastatic Model.
  International Society on Magnetic Resonance in Medicine, ISMRM 2006, May 6-12, Seattle, Washington, USA.
- **Vandecaveye V**, De Keyzer F, Nuyts S, Dirix P, Vander Poorten V, Hermans R. Characterizing nodal metastases in primary head and neck cancer with diffusion-weighted MRI: preliminary report.
  19th Congress of the European Society of Head and Neck Radiology, ESHNR/ICHNR 2006, Sep 28-30, Budapest, Hungary.
- **Vandecaveye V**, Nuyts S, De Keyzer F, Dirix P, Vander Poorten V, Hermans R. Detection of persistent or recurrent head and neck squamous cell carcinoma with diffusion weighted MRI after radiotherapy: correlation between radiologic and histopathologic findings.

Meeting of the European Society for Therapeutic Radiology and Oncology, ESTRO 2006, Oct 8-12, Leipzig, Germany.

- **Vandecaveye V**, De Keyzer F, Nuyts S, Dirix P, Vander Poorten V, Hermans R. Detecting nodal metastases in primary head and neck cancer with diffusion-weighted MRI: Initial experience.

  Society Meeting and 6th Annual Teaching Course of the International Cancer Imaging Society, ICIS 2006, Oct 16-18, Dublin, Ireland.

- Dirix P, Nuyts S, Hermans R, **Vandecaveye V**, De Keyzer F, Van den Bogaert W. Retropharyngeal nodes in squamous cell carcinoma of oropharynx: incidence, localization, and impact on prognosis.

  Society Meeting and 6th Annual Teaching Course of the International Cancer Imaging Society, ICIS 2006, Oct 16-18, Dublin, Ireland.

- Ni Y, Chen F, Sun X, De Keyzer F, Yu J, **Vandecaveye V**, et al. Monitoring tumorocidal effects of a vascular targeting agent using multiparametric MR in a rodent liver tumourmodel.

  92nd Scientific Assembly and Annual Meeting of the Radiological Society of North America, RSNA 2006, Nov 26-Dec 1, Chicago, Ill, USA.

- Nuyts S, Dirix P, **Vandecaveye V**, De Keyzer F, Van den Bogaert W, Hermans R. Diffusion weighted (DW) MRI to evaluate salivary gland function before and after RT.

  International Meeting on Innovative Approaches in Head and Neck Oncology, EHNS-ESTRO 2007, Feb 22-24, Barcelona, Spain.

- De Keyzer F, Chen F, **Vandecaveye V**, Wang H, Ni Y, Nuyts S, Hermans R, Landuyt W, Bosmans H. Comparison of diffusion-weighted with necrosis avid contrast agent – enhanced MRI for the assessment of spontaneously developed necrosis in a rat rhabdomyosarcoma model.

  15th Scientific Meeting and Exhibition of the International Society for Magnetic Resonance in Medicine, ISMRM 2007, May 19-25, Berlin, Germany.

- **Vandecaveye V**, De Keyzer F, Roebben I, Roskams T, Verslype C, Dymarkowski S. Assessing cirrhotic nodules with diffusion-weighted MRI: predictive value for malignant differentiation or lesion progression. International cancer imaging society October 2007, Bruges, Belgium

- Dirix P, **Vandecaveye V**, De Keyzer F, Op de beeck K, Vander Poorten V, Delaere P, Verbeken E, Hermans R, Nuyts S. Diffusion-weighted (DW) magnetic resonance imaging

(MRI) for nodal staging of locally advanced head and neck squamous cell carcinoma (HNSCC): impact on radiotherapy (RT) planning. Forum of the Leuvens Kankerinstituut (Oncoforum LKI) 2008, Februari 15, Leuven, Belgium.

- **Vandecaveye V**, De Keyzer F, Roebben I, Roskams T, Verslype C, Dymarkowski S. Diffusion-weighted MRI for detection of hepatocellular carcinoma: a correlation to histology and imaging follow-up. Belgian Week of Gastroenterology (BWG) 2008, Feb 21-23, Antwerpen, Belgium.
- **Vandecaveye V**, De Keyzer F, Dirix P, Verbeken E, Vander Poorten V, Nuyts S, Hermans R. Diffusion-weighted MRI for nodal staging in patients with head and neck squamous cell carcinoma: a comparison with conventional MRI in correlation to histopathology. European Congress of Radiology (ECR) 2008, Mar 9-11, Vienna, Austria.
- Dirix P, **Vandecaveye V**, De Keyzer F, Op de beeck K, Vander Poorten V, Delaere P, Verbeken E, Dirix LY, Hermans R, Nuyts S. Diffusion-weighted (DW) magnetic resonance imaging (MRI) for nodal staging of locally advanced head and neck squamous cell carcinoma (HNSCC): impact on radiotherapy (RT) planning. 99th Annual Meeting of the American Association for Cancer Research (AACR) 2008, Apr 12-16, San Diego, CA, USA.
- Dirix P, **Vandecaveye V**, Slagmolen P, De Keyzer F, Stroobants S, Hermans R, Nuyts S. Biological image-guided radiotherapy with repeated FDG-PET, FMISO-PET, DCE-MRI and DW-MRI in head and neck cancer. 27th Annual Meeting of the European Society for Therapeutic Radiology and Oncology (ESTRO) 2008, Sep 14-18, Göteborg, Sweden.
- **Vandecaveye V**, Dirix P, De Keyzer F, Op de beeck K, Vander Poorten V, Delaere P, Verbeken E, Hermans R, Nuyts S. Accuracy of diffusion-weighted MRI for nodal staging and radiotherapy planning of head and neck squamous cell carcinoma. 27th Annual Meeting of the European Society for Therapeutic Radiology and Oncology (ESTRO) 2008, Sep 14-18, Göteborg, Sweden.
- De Keyzer F, Roebben I, **Vandecaveye V**, Marchal G, Bosmans H. Monte Carlo simulations indicate the need for ADC correction for diffusion-weighted MR imaging of low signal-to-noise scans. 25th Annual Meeting of the European Society for Magnetic Resonance in Medicine and Biology (ESMRMB) 2008, Oct 2-4, Valencia, Spain.
- **Vandecaveye V**, Dirix P, De Keyzer F, Vander Poorten V, Roebben I, Nuyts S, Hermans R. Additional value of diffusion-weighted MRI to conventional MRI for predicting treatment outcome in chemoradiotherapy (CRT) of head and neck squamous cell

carcinoma: preliminary results. 94th Scientific Assembly and Annual Meeting of the Radiological Society of North America (RSNA) 2008, Nov 30-Dec 5, Chicago, Ill; USA.

Grants and scientific prizes

- **2005 – 2010** : Chair Prof. Dr. A. L. Baert: Oncologic applications for MRI.
- **2005** : Grant of the Belgian federation against cancer: "Improved Definition of the Anatomical and Biological Target in Radiotherapy of Head and Neck Squamous Cell Cancer by Magnetic Resonance Imaging"

  Cooperation between departments of radiology and radiotherapy, University Hospitals Leuven.
- **2004** : First price for best poster presentation (presented by Jacques Jani): **Vandecaveye V**, Cannie M, De Keyzer F, Lewi L, Jani J, Deprest J, Dymarkowski S. Assessing the potential role of diffusion-weighted MR imaging in the evaluation of placental changes before and after laser - treatment in twin-to-twin transfusion syndrome : pilot study. 14th World Congress on Ultrasound in Obstetrics and Gynecology, ISUOG 2004, Stockholm, Sweden. Ultrasound in Obstetrics and Gynecology 2004; 24(3):318.
- **2005** : Second price for best oral presentation : **Vandecaveye V**, Nuyts S, Vander Poorten V, De Keyzer F, Delaere P, Hermans R. Assessment of post-radiotherapeutic tumour recurrence in head and neck squamous cell carcinoma by diffusion-weighted MRI: a feasibility study. European Society of Head and Neck Radiology, ESHNR 2005, Oxford, United Kingdom.
- **2007** : First price for best oral presentation: **Vandecaveye V**, De Keyzer F, Roebben I, Roskams T, Verslype C, Dymarkowski S. Assessing cirrhotic nodules with diffusion-weighted MRI: predictive value for malignant differentiation or lesion progression. International cancer imaging society 2007, Bruges, Belgium
- **2008**: First price for best oral presentation: **Vandecaveye V**, De Keyzer F, Dirix P, Verbeken E, Vander Poorten V, Nuyts S, Hermans R. Diffusion-weighted MRI for nodal staging in patients with head and neck squamous cell carcinoma: a comparison with conventional MRI in correlation to histopathology. European Congress of Radiology (ECR) 2008, Mar 9-11, Vienna, Austria.